Person Authentication based on Palm-print Recognition

THESIS

Submitted in partial fulfillment
of the requirements for the degree of
DOCTOR OF PHILOSOPHY
by

Poonam Poonia

2017PHXF0016P

Under the Supervision of

Prof. Pawan Kamalkishor Ajmera

BITS Pilani
Pilani | Dubai | Goa | Hyderabad

BIRLA INSTITUTE OF TECHNOLOGY AND SCIENCE, PILANI
2023

Dedication

This work is completely dedicated to my respectful parents and beloved husband without whose constant support this thesis work was not possible. They always inspire me.

BIRLA INSTITUTE OF TECHNOLOGY AND SCIENCE PILANI – 333031 (RAJASTHAN), INDIA

CERTIFICATE

This is to certify that the thesis entitled **"Person Authentication based on Palm-print Recognition"** submitted by **Poonam Poonia,** ID No. **2017PHXF0016P** for the award of Ph.D. of the institute embodies original work done by him under our supervision.

_____

Signature of the Supervisor

Name:

Designation:

Date:

Acknowledgments

I would like to acknowledge the contribution of all those people who have assisted me in my dissertation work. I would like to thank my guide and mentor Prof. Pawan K. Ajmera, Assistant professor, Department of Electrical and Electronics Engineering, Birla Institute of Technology and Science, Pilani, Rajasthan, for their supervision. They steered me through this journey with their invaluable advice, positive criticism, simulating discussions and consistent encouragement.

I also express my deep gratitude to my DAC members Prof. K. K. Gupta and Dr. Puneet Mishra and Prof. Ananthakrishna Chintanpalli. They provided me continuous help and guidance to complete my thesis.

I wish to express my humble gratitude to the Vice Chancellor, Prof. V. Rangopal Rao, Director Prof. Sudheer Kumar Barai, for providing me the opportunity to pursue doctoral studies. I express my gratitude to Dr. S. K. Verma, Dean of Administration, Prof. Shamik Chakraborty, Associate Dean AGSRD, Prof. Navneet Gupta, HOD-EEE, for their official support and encouragement. I extend my thanks to SRCD, AGSRD, EEE Department and Library staff for their support.

Above all, I would like to offer my heartiest thanks to God for encouraging me to the best throughout the entire span of my studies and in every aspect of my life.

Poonam Poonia

Abstract

There was a time when biometrics was looked upon as the science of the future. It has featured prominently in various science fiction movies as an advanced security measure used to safeguard important documents, buildings etc. With the help of fast paced technological innovation, today, this is not far from reality. Biometrics is increasingly being used for secure authentication of individuals and making its presence felt in our lives. It uses an individual's physical or behavioral traits to identify them. The decision of which biometric is to be used for a particular application is a complex function of the people's security needs, ease of use and size of the enterprise. People can now see biometrics-based security checks at airports that use iris and hand geometry-based authentication and at ATMs using fingerprint and hand veins for authentication. The stage is now set for the use of biometric recognition in commercially viable civilian applications. A biometric authentication is basically a pattern recognition problem which makes a personal identification decision on specific physiological or behavioral features. An easy-to-capture biometric modality that could work well with a commodity camera is palm-print. It has coarse lines which can be easily detected using a low-resolution camera and it is easy to present due to the free mobility of our palm. Besides these, palm-print exhibit unique attribute such as color, clarity, position, continuity, length and variation in thickness which can be characterized as palm features and computed in the presence of wrinkles, ridges and creases of human palm. On most surveys, hand (palm-print) as a biometric modality rate high on user acceptance. For these reasons, palm-print would be an ideal choice for person recognition.

A number of algorithms have been proposed to extract efficient and accurate features. The performance of existing techniques for palm-print authentication falls considerably, when the camera is not aligned with the surface of the palm.

Palm-print variations such as scale, rotation, and illumination also create immense concern in developing efficient palm-print recognition method. Therefor considering all these variations, extracting robust palm-print features is vital for efficient palm-print recognition systems. The extracted significant palm-print features must be discriminative for dissimilar subjects and invariant to different palm-print variations.

In this thesis, we address some of the challenges of palm-print recognition such as variation in scale, rotation, and illumination by enhancing the representation of texture descriptors.

Primarily, a palm-print recognition algorithm is developed using Gabor filter with kernel-based full space Fisher Discriminant Analysis (FDA) and neural network to improve the performance of existing texture descriptors. Gabor filter was designed using the parameter estimation and a kernel-based FDA is applied for dimension reduction. Proposed method yields a high recognition rate of 98.34% and least equal error rate of 0.051% on PolyU database. Further, energy featured were extracted by replacing Gabor filter bank by a single optimal Gabor filter. A two-stage hybrid Particle Swam Optimization (PSO) with artificial neural network is applied to optimize the filter parameters. The proposed method attains better fitness results and prevent premature convergence. The method obtains 98.79% recognition rate.

Further, palm-print recognition algorithm, using Local Binary Pattern (LBP) based methods is proposed to improve the performance of existing texture descriptors. In Multi Scale Edge Angles LBP (MSEALBP) we combine edge operator and multi-scale uniform patterns, which extracts texture patterns at different angular space and spatial resolution. This makes the extracted uniform patterns less sensitive to the pixel level values. The method yields an Equal Error Rate (EER) of 0.2% and classification accuracy of 98.52% on PolyU database. Additionally, two robust operators for multi feature representation are designed. The descriptors represent the palm-images in a rotation and illumination invariant way. The proposed method makes the learned multi features discriminative and complementary in an unsupervised manner. We evaluated the performance using CASIA, IIT-Delhi, Tongji and REST contactless palm-print databases.

At the end a secure and cancellable palm-print biometric recognition system is proposed. The suggested method combines Convolution Neural Network (CNN) and feature transform structure for mapping palm-prints to random base-n codes. SHA-3 is used for storage of templates, which is non-invertible, and hence, there's no scope for an intrusion. The good separability between genuine and impostor dataset generates uncorrelated transformed templates. The proficiency of the proposed approach has been tested on PolyU, CASIA and IIT-Delhi palm-print datasets. The evaluations and experiments show high GAR of 99.05% with an EER of 0.62% irrespective of the base and length of labels. Hence, any enterprise can choose the specified bit length for a tunable level of security.

Table of Contents

List of Figures

List of Tables

List of Symbols

μ_g	Mean of genuine
μ_i	Mean of imposter
σ_g	Variance of genuine
σ_i	Variance of imposter
σ	Standard deviation
μ	Frequency
ϕ	Orientation
a_1, a_2	Accelerating coefficients
f	Evolutionary factor
G_x	Sobel horizontal operator
G_y	Sobel vertical operator
$\|G\|$	Gradient magnitude
θ	Angle direction
H	Entropy
m_p	Mean
Δ	Step size

List of Abbreviations

PIN	Personal Identification Number
ID	Identification
DNA	Deoxyribonucleic Acid
ATM	Automated teller Machine
APIS	Automated Palm Print Identification System
FAR	False Acceptance Rate
FRR	False Rejection Rate
CMC	Cumulative Match Characteristic
ROC	Receiver Operating Characteristics
GAR	Genuine Acceptance Rate
ROI	Region Of Interest
DR	Dimensionality Reduction
FDA	Fisher Discriminant Analysis
LFDA	Local FDA
KFDA	Kernel FDA
BRBPC	Bidirectional Representation Based Pattern Classification
PCA	Principal Component Analysis

SRC	Sparse Representation-based Classification
KSR	Kernel trick based Sparse Representation
FSC	Fast Sparse Coding
2DPCA	Two-Dimensional PCA
MFRAT	Modified Finite Radon Transform
BOCV	Binary Orientation Co-occurrence Vector
E-BOCV	Expand BOCV
DOC	Double Orientation Code
2DLDA	Two-Dimensional Linear Discriminant Analysis
2DLPP	Two-Dimensional Locality Preserving Projection
BDOC	Block Dominant Orientation Code
HOG	Histogram of Oriented Gradients
BHOG	Block-based HOG
NHD	Normalized Hamming Distance
ANN	Artificial Neural Network
LBP	Local Binary Pattern
DP	Directional Patterns
TP	Texture Patterns

WHOG-LSP	Weighted HOG for Locally Selected Pattern
MSEALBP	Multi-scale edge angles LBP
ULBP	Uniform LBP
NCC	Normalized Correlation Coefficient
LMTrP	Local Micro-structure Tetra Pattern
MPNN	Modified Probabilistic Neural Network
HM-LBP	Hierarchical Multiscale LBP
WACS-LBP	Weighted Adaptive Center Symmetric LBP
HMS-CLBP	Hierarchical Multi-Scale Complete LBP
WSRC	Weighted SRC
OLOF	Orthogonal Line Ordinal Feature
BTP	Biometric Template Protection
SVM	Support Vector Machine
IoM	Index-of-Max
LSH	Locality Sensitive Hashing

MVD	Minutia Vicinity Decomposition
CV	Coefficient of Variation
PSO	Particle Swarm Optimization
OL	Orientation Level
RD	Ridge Density
LDP	Line Directional Pattern
LLDP	Local Line Directional Pattern
ICA	Independent Component Analysis
CDFB	Complex Directional Filter Bank
SIFT	Scale Invariant Feature Transform
LSC	Locality Sampled Code
SHA	Secure Hash Algorithm
CNN	Conventional Neural Network
DR	Dimensionality Reduction
ER-KDA	Eigenspectrum-based Regularised KDA

BNF	Bottle Neck Features
CLAHE	Contrast Limited Histogram Equalization
RBF	Radial Basis Function
VGG	Visual Geometry Group
GSA	Genetic Search Algorithm
HOL	Histogram Of Oriented Lines
DGLBP	Directional Gradient LBP
COVID-19	Corona Virus Disease of 2019
IoU	Intersection over Union
FRLD	Full Ranking Local Descriptor
FMR	False Match Rate
FNMR	False Non-Match Rate

Chapter 1

Introduction

1.1. Biometric

The advancement of the information society has increased the demand for secure identity systems in a wide range of applications, including financial transactions, forensics, border control, computer security, and law enforcement. Human authentication has traditionally relied on knowledge-based systems (passwords, PIN) and token-based schemes (ID cards, passports). Despite the widespread usage of such validation procedures in society, these identity systems do not offer adequate security against identity fraud [1]. Biometrics is an alternative method for accurate and trustworthy authentication in a highly networked society. In next-generation technologies, human factors are becoming increasingly crucial, necessitating the adoption of biometric technology for person validation. Biometrics is the science of using behavioural (gait, keystroke, signature, etc.) and physiological (face, ear, finger, palm-print, DNA etc.) attributes to validate an individual's identity [2]. The special attributes on which the biometric recognition system is developed are known as modalities or identifiers. The images of the various biometric traits are shown in Figure 1.1. A trait can be used as a biometric characteristic if it satisfies the following properties [3]:

- **Uniqueness:** It establishes the extent to which a biometric system can distinguish a user from a set of users.

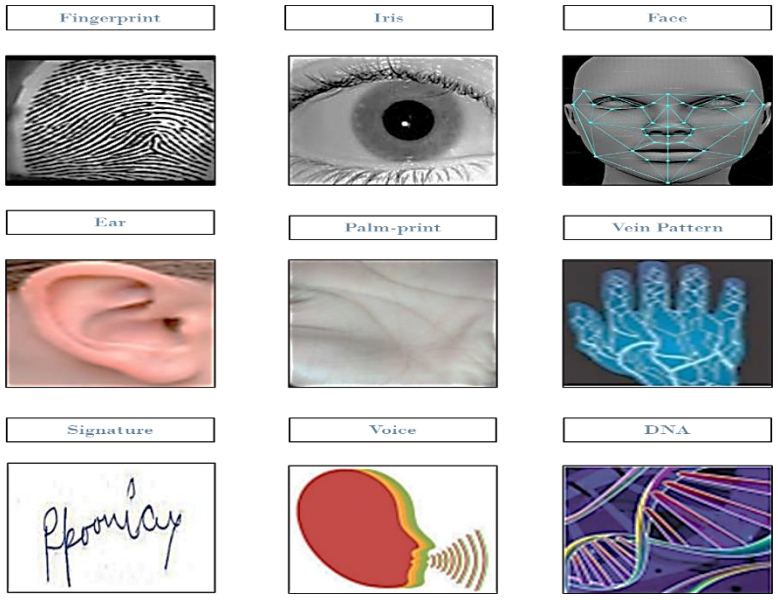

Figure 1.1: Representation of different biometric traits.

- **Universality:** Each individual has a unique biometric trait.
- **Circumvention:** It has to do with the system's capacity to endure fraud.
- **Performance:** It specifies the required resources' acceptable recognition accuracy, reliability, and stability.
- **Acceptability:** It specifies the level of acceptance of a specific biometric characteristic in everyday life.
- **Permanence:** It means that a personal trait must remain consistent in the database for a sufficient period.
- **Collectability:** It refers to how easily a person's trait may be acquired, quantified, and processed.

  The comparison of various traits in terms of different properties is listed in Table 1.1.

Table 1.1: Comparison of biometric traits [3].

Biometric Trait	**Properties**						
	Uniqueness	**Universality**	**Circumvention**	**Performance**	**Acceptability**	**Permanence**	**Collectability**
Face	Low	High	High	Low	High	Medium	High
Fingerprint	High	Medium	Medium	High	Medium	High	Medium
Iris	High	High	Low	High	Low	High	Medium
Ear	Medium	Medium	Medium	Medium	High	High	Medium
Palm-print	High	Medium	Medium	High	Medium	High	Medium
Signature	Low	Low	High	Low	High	Low	High
Voice	Low	Medium	High	Low	High	Low	Medium
Vein Pattern	Medium	Medium	Low	Medium	Medium	Medium	Medium
DNA	High	High	Low	High	Low	High	Low

Biometric system components are image processing, pattern recognition, and statics. In image processing, image enhancement techniques are employed to increase the quality of the acquired images. Pattern recognition employs feature extraction algorithms. The statics parameter includes the final choice and thresholding. Figure 1.2 shows the general framework of a biometric system.

Biometric authentication systems generally have two modes of operation [4]:

- **Enrollment mode:** During this mode, a sensor captures a biometric trait and stores it in the templates database. To make authentication easier, these templates are labelled with the user's identity. The block diagram of the different components of enrollment mode can be seen in Figure 1.3.

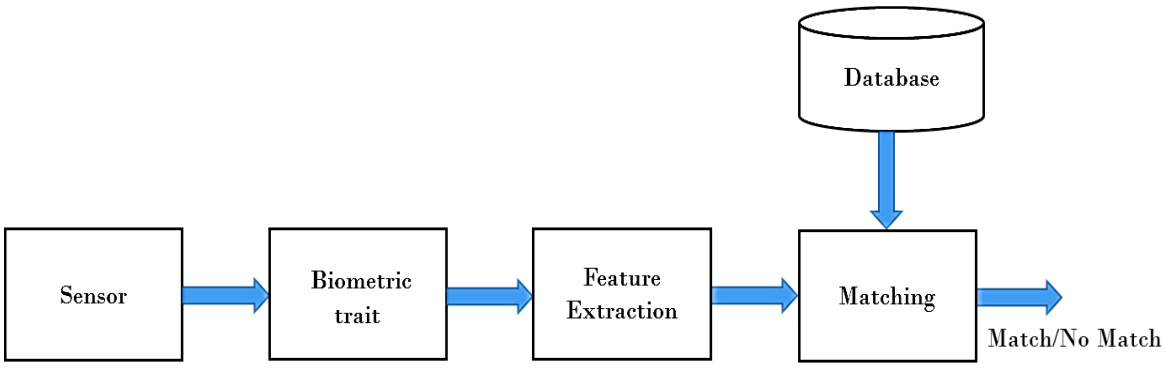

Figure 1.2: General framework of a biometric system.

- **Authentication mode:** Authentication mode is further classified in two categories such as identification mode and verification mode.

  1) **Identification mode:** Identification mode attempts to identify unknown individual by comparing the captured biometric to a database, i.e., one to many. Figure 1.4 illustrates the different components of identification mode.

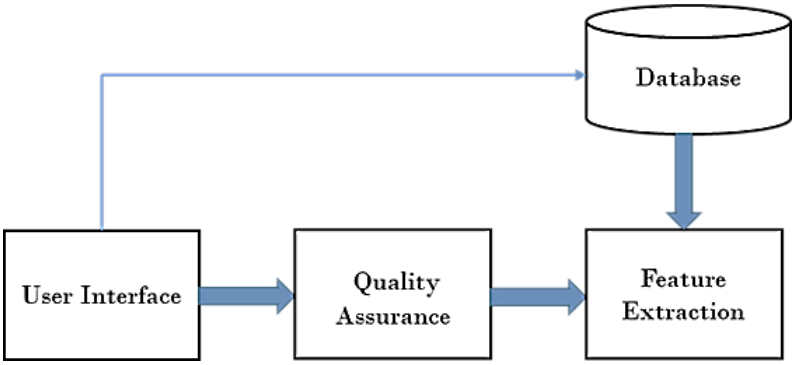

Figure 1.3: Block diagram of the different components of enrollment mode.

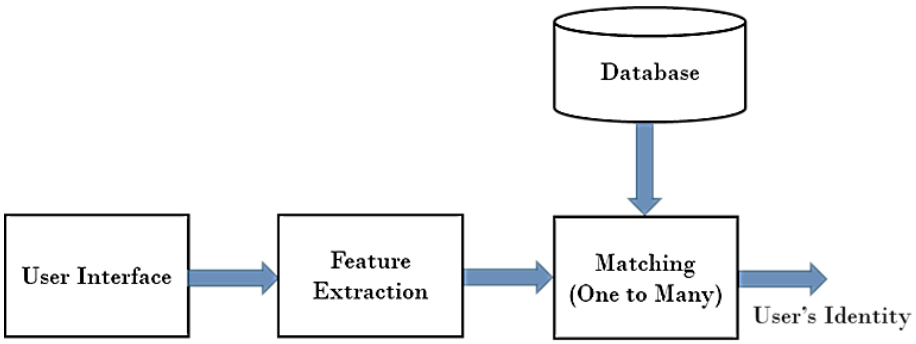

Figure 1.4: Block diagram of the different components of identification mode.

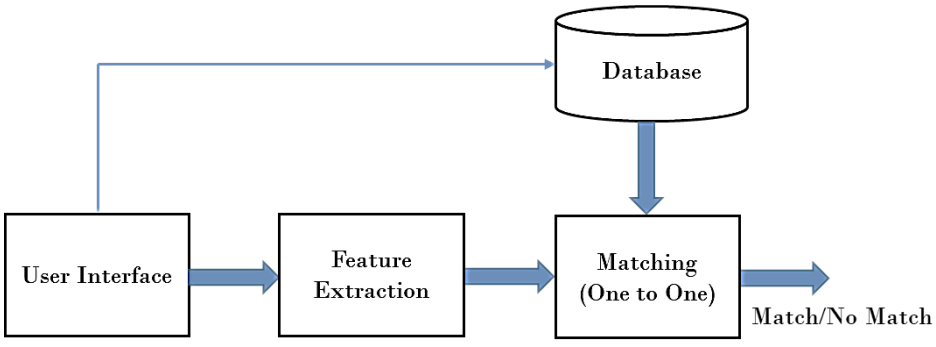

Figure 1.5: Block diagram of the different components of verification mode.

2) **Verification mode:** In verification mode, the biometric system verifies a person's stated identity by comparing it to the stored dataset. Figure 1.5 illustrates the different components of verification mode.

1.2. Performance measures

The performance of biometric system has become a major issue because of the massive development in their use in our daily lives. Researchers have proposed a number of evaluation measures for performance measurement of biometric systems. Accurate feature extraction is the key to raising the effectiveness of a biometric system; performance is not just reliant on the biometric algorithm. Many genuine and imposter attempts have been made to collect information of false acceptance and false rejections during the measuring performance of a biometric system. Genuine attempts are efforts by an individual to compare with his/her stored template, whereas imposter attempts are attempts to match with the biometric template with another person. Genuine attempts are used to count false acceptances, whereas imposter attempts are used to count false rejections. The following are the performance measures:

- **False Acceptance Rate (FAR):** FAR is the proportion of imposter samples that are mistakenly identified as that of the claimed identity. It is the ratio of false acceptance to the number of imposter attempts. The cost of a system is frequently measured in terms of FAR. A high FAR tends to make a system highly accessible, but it also makes it completely vulnerable because it allows imposters to use it [4]. FAR is defined as given in equation (1.1),

$$FAR = \frac{FA}{IA} \tag{1.1}$$

FA stands for false acceptance and IA is number of imposter attempts.

- **False Rejection Rate (FRR):** The term "false rejection rate" refers to the incorrect recognition of a genuine user as an imposter. FRR is a commonly used metric for determining the security of an authentication process. A system with a high FRR is totally secure, but it is inconvenient for legitimate users. For improved performance of a biometric system, one must be minimal FAR/ FRR and the other should be reasonable FAR/FRR [1].
  FRR is defined as given in equation (1.2),

$$FRR = \frac{FR}{GA} \tag{1.2}$$

  Where FR stands false rejection and GA is number of genuine attempts.

- **Equal Error Rate (EER):** EER is the error rate at which both the false acceptance and false rejection rates are equal. EER should be kept to a minimum. EER should ideally be zero. It is commonly used to compare the performance of different biometric systems.

- **Cumulative Match Characteristic (CMC):** The curve depicts the identification rate as a component of rank.

- **Genuine Acceptance Rate** (**GAR):** GAR is the number of genuine samples that are accepted appropriately. It assesses the reliability of biometric systems. GAR is defined as given in equation (1.3),

$$GAR = 1 - FRR \tag{1.3}$$

- **The Receiver Operating Characteristics (ROC) Curve:** ROC graphically depict the plot of FAR versus FRR according to various threshold levels. As a

result, the trade-off between FAR and FRR translates into a security-versus-convenience trade-off. The area under the ROC curve is a metric for assessing the performance of a system.

- **Verification Rate:** It evaluates how well the biometric system performs when operating in verification mode. It measures how quickly trustworthy users are accurately confirmed.

- **Identification Rate:** It shows how well a biometric system performs in identification mode. It denotes how frequently an already-enrolled user is successfully matched with the real user.

- **Decidability index** $(\boldsymbol{d})$**:** The decidability index is a measure of the degree of separation between genuine and imposter populations [5]. It is defined as given in equation (1.4),

$$d = \frac{|\mu_g + \mu_i|}{\sqrt{\frac{\sigma_g^2 + \sigma_i^2}{2}}} \tag{1.4}$$

  Where, μ_g and μ_i are mean of genuine and imposter respectively. σ_g and σ_i are variance of genuine and imposter respectively.

- **Sensitivity:** The percentage of true positives that are correctly identified is used to determine sensitivity. The ability of the test to identify positive outcome is relevant.

$$Sensitivity = tp/(tp + fn) \tag{1.5}$$

- **Specificity:** The degree of negatives that are correctly recognized serves as the basis for the specificity evaluation. It has to do with how well the test can identify unfavorable outcomes.

$$Specificity = tn/(tn + fp) \tag{1.6}$$

- **Accuracy:** The proportion of total tp and tn to total data determines how accurate the suggested method is. Accuracy is defined as given in equation (1.7),

$$Accuracy = tp + tn/(tp + tn + fp + fn) \tag{1.7}$$

Here, tn is true negative, tp is true positive, fp is false positive, and fn is false negative.
In the literature, various biometric frameworks have already been introduced, among them, systems that use biometric traits like fingerprints, iris, face, voice, signature and palm-prints are the most common [6-10].
Face recognition is quite possibly the most adaptable biometric methodology, working in any event, when subject is uninformed of being scanned. Face biometric has been restricted by the issues related with appearances, posture and light [8]. Iris as a biometric is widely used, however its image capturing is difficult and expensive [9]. Fingerprint as a biometric is broadly utilized because of its simple and inexpensive data capturing. Fingerprint verification has been restricted by the troubles, for example, that manual workers and aged individuals fail to give adequate quality fingerprints [7]. In recent years, palm-print that may be a giant space of hand proves to be smart answer for varied identification issues.

1.3 Palm-print as biometric

Recently, research in hand biometrics has shifted to examining the value of palm-prints in real-world contexts such as smartphones, ATMs, and notebooks [11, 12].

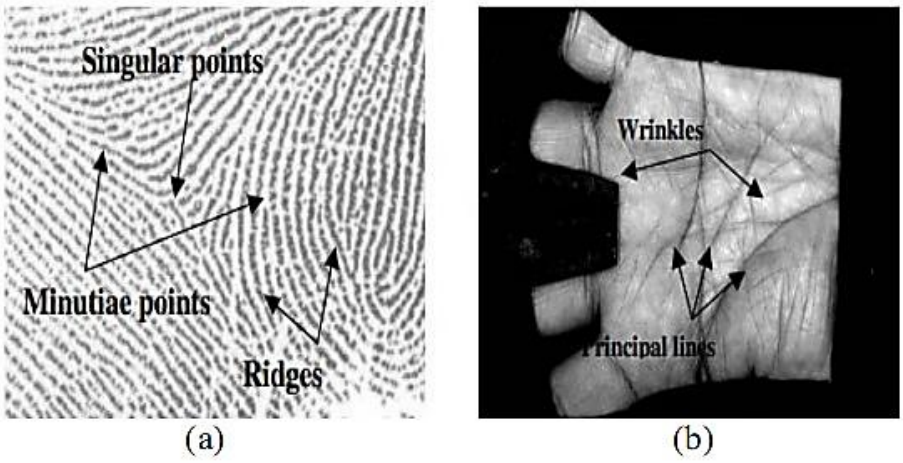

Figure 1.6: Sample images (a) High resolution image, (b) Low resolution image.

Users prefer biometric systems that rely on palm-print features because they are straightforward and nonintrusive to gather [13]. The characteristics of a human palm are rather unique and consistent. The palm-prints of monozygotic twins differ significantly. Even a low-resolution camera can retrieve biometric features of the palm-print easily because to its larger field of vision. Around the world, the Biolink APIS [14] has been employed in forensic case studies and law enforcement. Palm-print research using with a image resolution of 400 dpi or above is adequate for forensic and legal applications [15]. Low-resolution images are those with a resolution of less than 150 dpi and are better suited to civil and commercial uses [16, 17]. As seen in Figure 1.6, high resolution images have significant ridges, minutia, and singular features, whereas low resolution images have primary lines, texture, and wrinkles. Palm print has rich features as discussed below:

- **Geometry features:** The width, length, and area of a palm are primarily determined by its shape. A low-resolution and low-quality image can be used to extract these features.

- **Line features:** The heart line, head line, and life line are the most notable principle lines. The placement and shape of these lines are crucial physiological

criteria for identifying and verifying individuals since they show less fluctuation over time.

- **Wrinkle features:** The minor creases/wrinkles of the inner palm are finer and more uneven than the main lines. These features are classified as coarse wrinkles and fine wrinkles.

- **Delta points:** Delta point characteristics are extracted from high resolution images and are positioned in the centre of a delta-like section in the palm. The finger-root region and the outer portion of the palm are the most common locations for these.

- **Minutia points:** Minutiae features similar to the finger print type feature displayed in Figure1.6(a), which is employed as a critical measure in individual verification/identification. Only high-quality, fine-resolution images have been used to create these palm features.

As shown in Figure 1.7, a traditional palm-print identification system consists of the following sections: image acquisition, pre-processing, feature extraction, database, and classifier.

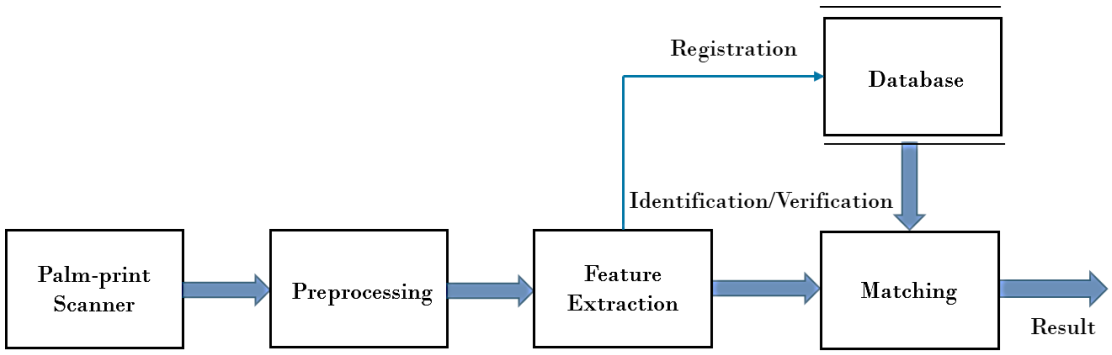

Figure 1.7: Block diagram of palm-print recognition system.

The palm-print acquisition part includes a scanner/camera that collects palm-print samples of various characteristics for later recognition. The extraction of Region Of Interest (ROI), which extracts only important sample properties using standard coordinate methods, is at the heart of the pre-processing stage. Effective features can be extracted from high-quality ROI samples for feature extraction. Based on a specified classifier, the matching method adopted the extracted features to those stored in the database. Fusion is applied in case of multimodal biometrics where; more than one biometric modality features are extracted.

1.4 A review of earlier work

Numerous advancements have been reported in various factors of palm print recognition, and researchers have presented a number of useful views to improve its performance [18, 19]. Various palm-print recognition methods have indeed been presented in the recent past, and they can be categorized broadly into the following categories [14]:

- Holistic based methods
- Structural based methods
- Hybrid methods
- Deep learning-based methods

1.4.1 Holistic based methods

The holistic method tries to process the entire palm-print image. They are divided into two types: (1) Subspace-based and (2) Representation-based methods.

1) **Subspace-based methods:** Subspace-based methods are suggested to treat a palm-print image as a high-dimensional vector and map it to a lower-

dimensional vector. These methods don't require any knowledge of palm prints beforehand. The subspace's coefficients are regarded as features. PCA was suggested by Lu et al. [20] as a method of preserving spatial structure data for palm-print recognition. A group of orthogonal basis vectors are discovered. It explains the key differences between the training images. Only pair-wise linear correlations between pixels may be distinguished using PCA.

Sang et al. [21] proposed a palmprint recognition method based on two-dimensional PCA (2DPCA). The PolyU database was used in the trials, along with a distance classifier. Especially for short training data, the 2DPCA technique outperforms PCA in terms of recognition accuracy and processing efficiency. In parallel, other application systems have conducted research on threshold selection.

Pan and Ruan [22] propose a Gabor feature-based (2DPCA) for palmprint recognition. Initially, Gabor features are retrieved from the data at various scales and orientations. The feature space is then dimensionally reduced in both the row and column directions using (2DPCA). Finally, classification is done using distance measure and the k nearest classifier. The approach is unaffected by illumination and rotation. Experimental findings show that the proposed strategy is efficient in terms of the both speed and efficiency.

Wang et al. [23] proposed a palmprint recognition method based on sparse representation. 2DPCA is used to extract features from the palm-print image in order to obtain training samples, which will help with sparse representation. Due to its greater data dimension, the 2DPCA approach not only overcomes the PCA method's inability to perform complex calculations, but also keeps the original image's data structure in order to provide superior features. The classification is achieved by representation coefficient and sparse concentration. The method reduces the spatial and temporal complexity because of the sparsity of the representation coefficient. The experimental

findings on the PolyU multispectral database demonstrate that the method's rate of recognition is notably higher than that of the conventional method.

Wu et al. [24] proposed a palmprint recognition method i.e., Fisherpalms. In order to more effectively distinguish between the palm-prints from the various palms. Fisher's linear discriminant has been used to projected palm-prints from the high-dimensional initial palmprint space to a notably lower dimensional space. The proposed technique has shown high accuracy results, and it operates quickly enough to detect palm prints in real-time.

Du et al. [25] fuses bidirectional 2D linear discriminant analysis (2DLDA) with Gabor filters. Applying horizontal and vertical 2DLDA will first let you extract two different types of features from Gabor-based images. A distance-based adaptive technique is created to combine these two types of features. Experimental results on the PolyU database show that the suggested approach produces several desired results that use the Gabor-palms of a slightly higher dimension, which means minimal computing cost.

Independent component analysis (ICA) method for palmprint identification is presented by Lu et al. [26]. ICA representation is capable of capturing both the structure and key elements of the palm-print images. In addition, the palm-prints have a variety of features that can be classified as multi-scale features, including texture, wrinkles, primary lines, and minutiae points. Therefore, it makes sense for us to combine the ICA and multi-resolution analysis to represent the features of a palm-print. The outcomes of the experiment demonstrate that the integrated approach is more effective than the ICA algorithm.

Hu et al. [27] proposed 2D locality preserve projection (2DLPP) for palm-print representation and recognition. The primary advantage of 2DLPP over LPP is that the former's image representation bases have significantly lower dimensionality than the latter, resulting in a more accurate approximation of

the original images and the potential to avoid the drawbacks of the latter's PCA+LPP algorithm. The efficiency of the suggested strategy is demonstrated by experimental findings on images of PolyU palm-prints. The proposed technique here is thought to encourage the employment of LPP based methods on a much larger scale. The Fisher discriminant analysis (FDA) approach was first put forth by Fukunaga in 1990 [28]. Whereas if sample in a class create a few distinct groups or clusters, FDA typically produces unsatisfactory results. To address the problem of FDA, Sugiyama [29] presented a linear supervised technique called local FDA. The FDA and LPP structures are integrated in this method. Computing a general eigenvalue problem makes it simple to handle the LFDA arrangement. When there are only a few marked samples available, LFDA performance can suffer.

Wang and Ruan [30] proposed Kernel FDA (KFDA) to represent palmprint features. PCA and FLDA are not vulnerable to rising order statistics of data and only consider the 2-order statistics of palmprint image pixels. In process of extracting higher order interactions between palm-print images for prospective recognition, KFDA is utilized. The experimental findings show that KFDA performs better than eigenpalms and fisherpalms, particularly when employing a limited amount of training data.

2) **Representation based methods:** The query image is projected in this method as a weighted sum of all training images. Bidirectional representation method-based pattern classification (BRBPC) was used by Cui et al. [31] to identify palm-prints. The BRBPC approach takes into account not only using training data to describe the test sample but also presenting the test sample to training examples. Experimentation on PolyU multispectral database and 2D and 3D palmprint databases show that the proposed method works better than the conventional palm-print recognition algorithms.

In the Sparse representation-based classification (SRC) approach of collaborative representation, training images are used directly as a sparse representation dictionary [32]. This method offers great accuracy and a good capacity to discriminate. Performance is significantly influenced by the quality of training data. SRC seeks out significant inter-class differences, which misclassifies the new test sample.

Li [33] proposed kernel trick based sparse representation (KSR) algorithm for palmprint recognition. The algorithm can capture elements in palm-print images that are nonlinearly similar. KSR has a strong ability to improve the performance of sparse coding and effectively decrease feature quantization error. Fast sparse coding (FSC) is employed to speed up the sparse coding process. The FSC model has a faster rate of convergence than the current SC model. It solves the $L1-$regularized least squares issue and the $L2-$constrained least squares problem iteratively. KSR can be successfully done by using the Gauss kernel function and taking into account various feature dimensions.

1.4.2 Structural based methods

The structural or local feature approaches rely on the extraction of the stable palm-print features such as palm lines and texture. These approaches can be further divided into three sub-categories: (1) Line-based, (2) Coding based, and (3) Texture based methods.

1) **Line based methods:** Line based methods extract line information from palm-print images [34, 35]. These line features are either matched directly or represented in other formats.

   A set of line detectors for palm-print lines was developed by Wu et al. [36]. One of the two parameters determines how smooth the lines are, while the other determines how wide they are. Corresponding direction

detectors identify the lines in various directions, which are subsequently combined into one edge image. The Hausdorff distance is used to match the lines.

Canny edge operator is used by Wu et al. [37] to retrieve line information of palm images. In order to represent the edge points in four separate directions, four membership functions are fed with the edge points and their corresponding orientations. Euclidean distance is also calculated for matching.

To obtain the slope of the palm-prints, Diaz et al. [38] adopt Sobel masks and the morphologic operator as two distinct feature extractors.

A palm-line extraction method with both global and local filtering was proposed by Wang and Ruan [39]. To extract rough palm lines and determine approximative orientations, steerable filters are first applied. Additionally, steerable filters in nearby regions retrieve palm lines and re-join damaged palm lines.

Huang et al. [40] suggest a cutting-edge principle line-based palm-print verification method. The primary lines are efficiently and successfully extracted using the modified finite Radon transform. A matching method based on pixel-to-area comparison is created to determine how similar two palmprints are, and it has demonstrated good stability for minor palmprint rotations and translations.

Without employing edge detection, Zia et al. [41] suggested a new strategy to retrieve principal lines in two stages. Preprocessing procedures are part of the first stage, followed by morphological operations and the removal of unwanted components in the second stage.

2) **Coding based methods:** Coding based methods improve and extract the phase and directional aspects of palm-prints by using a set of filters.

Zhang et al. [42] proposed Palm Code that extracts the phase information from the palm-print using Gabor filter. Bitwise hamming distance has been used to compare Palm Codes after the phase has been quantified in bits. Because palm-print identification performance of the system is affected by the high correlation of palm code aspects, originality of palm codes may be further degraded.

Kong et al. [43] proposed Fusion Code based technique that addresses the Palm Code's correlation issue. Multiple circular Gabor filtering with different angle is used in this technique to retrieve the phase information from palm-print images. The features are combined further to create a separate feature vector known as the Fusion Code. The final decision is made using a dynamic threshold rather than a fixed threshold.

A method for extracting palm features using competitive coding with angular matching is proposed by Kong and Zhang et al. [44]. Using several Gabor filters, competitive coding extracts orientation data from palm lines. A feature vector called Competitive Code contains the orientation data. The respective Competitive Codes are compared using additional angular matching.

Sun et al. [45] proposed a palmprint representation method i.e., orthogonal line ordinal features. The method determines line-like image patches that are orthogonal in orientation and provide one bit feature codes on a qualitative level. Numerous ordinal feature codes are used to represent a palm-print pattern. The method improves accuracy and reduces the equal error rate by 42% while halving the complexity of feature extraction.

Jia et al. [46] proposed robust line orientation code for palm-print verification. Initially, a modified finite Radon transform (MFRAT) is employed to more correctly retrieve the orientation feature and address the sub-sampling issue. Furthermore, we build a larger training set to address

the issue of huge rotations brought on by faulty preprocessing. Finally, a matching technique based on pixel-to-area comparison that is more error tolerant has been developed. The presented method has a greater recognition performance and a lower response time according to experimental data from the PolyU database.

To represent various orientations for a small location, Guo et al. [47] presented a feature extraction method called binary orientation co-occurrence vector (BOCV). The regional orientation features can be better described by the BOCV, and it is more resistant to image rotation. The suggested BOCV beats the Comp Code, POC, and RLOC by significantly reducing the EER, according to experimental findings on the public palmprint database.

By appropriately adding fragile bits information, Zhang et al. [48] expand BOCV to E-BOCV. When compared to other cutting-edge palmprint verification techniques, experiments show that E-BOCV can reach the best verification accuracy. The study exploring on the fragile bits of coding-based palmprint recognition methods.

Fei et al. [49] suggested a method based on double half-orientation for palmprint recognition. The method defines a bank of half-Gabor filters for retrieval of a palm-print in half-orientation. The double half-orientations could quite accurately define the overall directional feature of a palm-print as compared to the single dominant orientation. Extensive testing is done on three distinct types of palm-print databases, and the findings demonstrates that the suggested method performs superior to the existing methods.

Fei et al. [50] proposed double-orientation code (DOC) with nonlinear angular matching for palm-print recognition. The orientation component of palmprints is represented by DOC. Angular matching assesses whether

similar the DOCs seem to be. In compared to earlier approaches, experiments using palmprint databases show that the suggested method performs excellently.

A discriminative and robust competitive code-based technique for palm-print authentication was proposed by Xu et al. [51]. The technique represents palmprint images with a more precise dominant orientation. In addition, we suggest weighting the orientation data of a nearby region to enhance the discriminative and stable dominant orientation code's accuracy and stability. The efficiency of the suggested strategy has been tested using palm-print datasets and a noisy dataset.

A double-layer direction extraction approach for palm-print recognition was proposed by Fei et al. [52]. Initially, the apparent direction is extracted from a palmprint's surface layer. The inherent orientation information from the energies single map of the apparent orientation is then further exploited. Finally, the apparent and latent direction components are combined for palmprint recognition with the multiplication and addition techniques. For the recognition of noisy palmprint images, the latent energy orientation feature in particular exhibits a promising performance.

3) **Texture based methods:** Many different types of images largely depend on texture. Due to large texture patterns and ambiguous imaging conditions, retrieving discriminative yet robust texture characteristics is challenging [53, 54].

Line Directional Pattern (LDP), a novel texture descriptor that is presented, acts in gradient space as opposed to intensity space, is comparable to the LBP approach in that it functions in intensity space

[55]. Local line directional pattern (LLDP) [56], a texture descriptor that constructs feature vectors in the local line geometry space, is defined.

Hong et al. [57] proposed a hierarchical approach based on Block dominant orientation code (BDOC) and Block-based histogram of oriented gradient (BHOG) for multispectral palm-print recognition. In the suggested approach several features gathered from various bands are fused to increase recognition precision. Additionally, it can further enhance the state-of-the-art performance attained by certain approaches that are based on the PolyU multispectral database.

For robust palm-print recognition, Hong et al. [58] presented weighted histogram of oriented gradient for locally selected pattern (WHOG-LSP). It is used to the structure layer of images of blurred palm-prints to extract some strong features. The low performance concerns with translational and rotational in palm-print recognition can be solved using these derived characteristics. Finally, the suggested recognition method compares the similarities of palm-print features using the normalized correlation coefficient (NCC). The performance and real-time validation of the proposed recognition method have been validated by extensive trials on the PolyU and the blurred PolyU palmprint databases.

Li and Kim [59] presented the local micro-structure tetra pattern (LMTrP) as a local descriptor for palm-print recognition. The descriptor uses the direction of local descriptors in a similar way to how thickness does. To changes in translation, rotation, and blurriness, the technique is least susceptible.

Personal authentication frequently uses the Local binary pattern (LBP), a potent local image descriptor that extracts uniform patterns [60].

For palm-print recognition, Tamrakar and Khanna [61] proposed uniform LBP (ULBP). It provides a consistent appearance with little

discontinuities. The images are categorized as occluded or non-occluded based on the assumption of average entropy. The technique is adaptable enough to manage occlusion up to 36%.

To derive the directional response of the palm-print, Michael et al. [62] used a gradient operator. To retrieve the textural representation of the palm pattern in various directions, the LBP is used. Further, matching is done by the Modified probabilistic neural network (MPNN).

A feature extraction approach was given by Mu et al. [63] employing shiftable Complex directional filter bank (CDFB) transform, uniform LBP, and Fisher linear discriminant analysis (FLDA). The shiftable CDFB transform, which produces sub-band coefficients controlled by the uniform LBP, decomposes the palm-prints. Additionally, the LBP mapping sub-blocks are performed using statistical histograms. Finally, the histogram feature representation is used to train the FLDA classifier for palm-print authentication.

The hierarchical multiscale local binary pattern (HM-LBP), a unique collaborative representation paradigm for palm-print identification, was put out by Guo et al. [64]. It is possible to extract useful information from non-uniform patterns. The feature dimension is minimized using principal component analysis. A collaborative classification with HM-LBP is then provided in order to effectively employ the discriminating information. The suggested methodology is validated on the PolyU database to demonstrate its viability and performance. The outcomes demonstrate that the algorithm works better in terms of recognition accuracy than current methods. This approach allows for the reduction of illumination, rotation, and grey scale.

Zhang et al. [65] proposed a palm-print recognition method by combining weighted adaptive center symmetric LBP (WACS-LBP) and weighted

sparse representation-based classification (WSRC). One of the main rationales of this method is that it reasonably makes the classification problem become a simpler one with fewer classes. In the proposed method, five parameters are decided empirically by the cross-validation strategy. The method is limited by parameter selection. The descriptor based on edge gradient will give preferable recognition performance because the edge gradient is more consistent than the pixel intensity. Hence, the edge gradient will give better outcomes over unique LBP for face and expression acknowledgment [66].

Tarhouni et al. [67] proposed a variant of LBP constructed from Pascal's coefficients and referred to as a multiscale local binary pattern. Multiple characteristic subsets were created via random sampling. The method integrates oriented gradient pyramid histograms and LBP, in which the characteristics are concatenated for classification. Extensive tests on the PolyU database demonstrate the suggested approach's superiority to state-of-the-art methods.

The combination of ULBP with sparse representation was presented by Wang et al. [68]. The results of the studies show that the suggested method is effectively robust to rotation and noise, and that the total recognition rate has clearly increased. The recognition rate has increased by 8.8% and 6.8%, respectively, as compared to the conventional PCA and 2DPCA approaches.

Zhang et al. [69] proposed a combination of hierarchical multi-scale complete local binary pattern (HMS-CLBP) and weighted sparse representation-based classification (WSRC). The optimization problem based on the $l1$ norm is then solved to implement the sparse decomposition of test samples, and the palmprints are identified by the

minimum residuals. The suggested approach has good rotation, illumination, and inherits the benefits of WSRC and CLBP.

1.4.3 Hybrid methods: In this approach, both holistic and structural features are used to represent palm-print image.

Kumar and Zhang [70] integrate texture, line, and appearance-based features for palm-print recognition. The work also compares the abilities of the PCA, line detector, and Gabor filter. The distance measure used to calculate the matching distance, which is the matching criteria, has a significant impact on the performance. The suggested use of several palm-print representations, especially when using a peg-free, non-contact imaging setup, yields favorable results and shows the strength of the method.

For contactless palm-print identification, Morales et al. [71] recommend combining Scale invariant feature transform (SIFT) with Orthogonal line ordinal feature (OLOF). The weighted sum method was used to create the integrated similarity score of SIFT and OLOF characteristics.

A nonlinear rank-level fusion technique to personal recognition is suggested by Kumar and Shekhar [72]. The comparative analysis of rank-level fusion techniques, which can be helpful in combining multibiometric fusion, is also investigated in the present study. The detailed experimental findings given in this work further imply that the suggested nonlinear rank-level technique surpasses the rank-level combination approaches.

1.4.4 Deep learning-based methods: Recent advances in biometric approaches have shown promise for deep learning-based systems. These techniques are capable of accurate contactless image identification and information extraction from voluminous data [73–75].

Svoboda et al. [76] suggested palm-print recognition with a CNNs architecture. Get a superior genuine/impostor score distribution separation than past methods with less training data because the network's training process uses a novel loss function connected to the d-prime index. On publicly available palm-print datasets from IIT-Delhi and CASIA, our method produces cutting-edge results without the need for time-consuming parameter tuning.

An introduction study for the verification of new-borns is presented by Ramachandra et al. [77]. In two separate sessions, collected a fresh library of contactless palm-print images from 50 new-borns. The data for the first session is recorded between 6 and 8 hours after the birth, while the data for the second session is recorded between 28 and 36 hours. By adjusting the pre-trained AlexNet architecture, further suggest a fresh approach based on transfer learning that would boost verification precision.

Genovese et al. [78] proposed a novel CNN i.e., PalmNet for contactless palm-print recognition. The technique uses PCA and Gabor responses to tune palm-print specific filters without the need for class labels during training. PalmNet uses Gabor filters in a CNN to extract highly discriminative palmprint features. The findings of experiments on databases of contactless palm-prints obtained with various devices. The achieved recognition accuracy was better than that of the existing approaches.

Minaee and Wang [79] presents a deep scattering network for palm-print recognition. The layout and filters of a scattering network are predetermined wavelet transforms. The features in the first layer of the scattering transform are comparable to SIFT descriptors. PCA is used to minimize the dimensions of the scattering features. Finally, two distinct classifiers, multi-class SVM and a distance classifier are used to perform the recognition. The proposed approach was tested on palm-print datasets and achieved higher accuracy rates.

For multispectral palm-print recognition, Meraoumia et al. [80] developed a novel feature extraction technique named PCANet deep learning. Research was done using the PolyU and CASIA databases.

Dian and Dongmei [81] propose a CNN based palm-print recognition approach. Initially, the improved fuzzy enhancement technique is used to pre-process palm-print images. After that, feature extraction is done using AlexNet's eight-layer network structure. Finally, compare the characteristic to the hausdorff distance. In comparison to the existing approaches, the proposed method obtains the best EER of 0.044 % on three publicly accessible databases under various conditions.

A contactless palm-print recognition system relying on the CNN approach is presented by Jalali et al. [82]. Because discriminant features are created by consecutive layers of the CNN method, the correction and alignment operations of the samples to same fixed orientation and spatial position are partially eliminated. Multi-scale instead of using the usual, subjective and time-consuming selection approach, the feature selection process is carried out using a self-taught learning procedure. The approach is unaffected by translation, rotational changes, stretching, and deformation.

Using CNN and transfer learning, Izadpanahkakhk et al. [83] suggested a palm-print verification model. A feature extractor is first employed, which is a pre-trained CNN architecture. The application of a machine learning classifier continues. The model proved competitive with existing hand-crafted descriptors. For the PolyU palm-print database, an intersection over union (IoU) score of 93% and an EER of 0.0125 % were attained.

1.5 Security aspects of palm-print biometric

The EU general data protection regulation (2016/679) has characterized biometric information as sensitive information [84]. Therefore, the security of biometric templates

is a fundamental and vital issue [85]. The biometric framework offers different preferences over the customary framework, yet the biometric framework itself is vulnerable to numerous identity threats [86, 87].

Similar to other biometric modalities, the increasing use of palm-print recognition has raised privacy concerns significantly [88, 89]. Biometric template protection can be categories into two classes (a) biometric cryptosystems, and (b) cancelable biometrics.

In these days, cryptography is one of the best ways to improve the biometric security. Biometric cryptosystems can be categories as key-generation and key binding scheme [91]. In key-generation the secret is generated directly from the biometric feature and in key-binding the secret is secured using biometric feature.

Juels and Wattenberg [92] proposed a fuzzy commitment scheme that is capable of protecting biometric data. The fuzzy commitment schemes suffer from drawbacks such as impracticable assumptions, restricted length of keys and restricted error correcting capability. To overcome the limitations of fuzzy commitment schemes a new approach called fuzzy vault schemes [93] have been investigated in the past. Fuzzy vault algorithm i.e., a traditional algorithm in key-binding strategy that can connect the fuzziness of biological features with the accuracy of key algorithm. The fundamental issues in the fuzzy vault are lack of reusability and cross-match attack.

Dodis et al. [94] proposed more generalized framework i.e., fuzzy extractors and demonstrate that secure sketches imply fuzzy extractors. They also give different enhancements and expansions to previous schemes. Fuzzy extractors only concern about the strength of the secret key extracted. They cannot straightforwardly guarantee that privacy is preserved. In recent years, cancelable biometrics has become an active research area as it provides good recognition accuracy and strong security [95, 96]. The concept of cancelable biometrics was proposed by Ratha et al. [97] to ensure the security and privacy of the biometric templates. It refers to the irreversible transform.

Connie et al. [98] proposed PamHashing which addresses the non-revocable biometric issue. The method uses a set of pseudo-random keys to attain a unique code i.e.,

palmhash which can be stored in portable devices (tokens, smartcards) for verification. In addition, PalmHashing offers several advantages such as zero EER occurrences and isolated genuine-imposter populations. The security and secrecy of the transmitted templates is enhanced by using encryption and data hiding techniques.

Khan et al. [99] presents a novel content based chaotic secure hidden transmission scheme. Biometric images are used to generate secret keys and these are used as the initial condition of the chaotic map. Each transaction session has different secret keys to protect from the attacks. For the encryption, two chaotic maps are integrated that further resolve the finite word length effect. The method also enhances the system's resistance against attacks. But the templates are not cancelable during verification stage.

Umer et al. [100] suggested a feature learning approach to generate cancelable iris templates. The method extended the existing BioHashing scheme in two token scenarios such as subject-specific and subject independent.

Jin et al. [101] proposed an Index-of-Max (IoM) hashing based on ranking-based locality sensitive for biometric template protection. The hashing is more robust against biometric feature variation as it is insensitive to the feature magnitude. The magnitude-independence trait makes the hash codes being scale-invariant, which is critical for matching and feature alignment. In [102] a dual-key-binding cancelable cryptosystem was developed to improve the security needs of palm-print biometrics. Dual-key-binding scrambling not only has more robustness to resist against chosen plain text attack, but also enhances the secure requirement of non-invertibility.

Liu et al. [103] generates cancelable palm-print templates by using the chaotic high speed stream cipher. The palm-print features having multiple orientations are encoded in a phase coding scheme. The method fails to satisfy irreversibility property. To balance the conflict between security and verification performance cancelable palm-print coding schemes are proposed in [104]. The method also reduces computational complexity and storage cost, by extending the coding framework from one dimension to two dimensions.

The irreversible projections (2DHash and 2DPhasor) projections ensured the irreversibility.

Teoh et al. [105] proposed BioHashes that are straightforwardly revoked and reissued (via refreshed password or reissued token) if compromised. BioHashing furthermore enhances recognition effectiveness by using the random multi-space quantization of biometric and external random inputs.

Sadhya and Raman [106] proposed a cancelable IrisCode i.e., Locality sampled code (LSC) based on the concept of Locality sensitive hashing (LSH). The method provides security guarantees and also gives satisfactory system performance. Recently, Bloom filter have also been extensively researched for biometric template protection. Bloom filter is extensively used in database and network applications.

Bringer et al. [107, 108] develop Bloom filter-based iris biometric template protection scheme. They performed a brute force attack for each block of the code words successfully and analyzed the unlinkability and irreversibility of the biometric template [109]. Therefore, some randomized bloom filter biometric template protection schemes have emerged [110, 111]. Rathgeb et al. [112] proposed an adaptive Bloom filter to generate cancelable iris templates. Bloom filter-based representations of iris-codes enable an efficient alignment-invariant biometric comparison. Although the original bloom filter scheme claimed of satisfying the irreversibility, but the scheme was shown to be vulnerable to cross-matching attacks. In recent past, random projection is extensively used for generating revocable biometric templates to ensure the security of the biometric data [113-115]. These methods use many-to-one mapping to protect the biometric templates. The original feature vector is projected into a newer feature vector which having lower dimensions. With the help of user-specific key, the projection is guided to ensure the security [116].

To overcome the issue of changing quality of biometric sample a sector based random projection method is proposed by Pillai et al. [117]. When the random projection is applied to the entire iris image, then the low-quality region tends to corrupt the data of

the good-quality region. The negative impact of the low-quality region is confined locally by partitioning the sample into numerous areas and applying random projection to every area separately.

Pillai et al. [118] presents random projection and sparse representation-based method for iris recognition. Random projection along with random permutation is utilized to empower revocability, while sparse representation is utilized for image selection. Jin et al. [119] proposed a two-dimensional random projection method called minutia vicinity decomposition (MVD) for generating cancelable fingerprint templates. Trivedi et al. [120] generates the non-invertible fingerprint templates by utilizing Delaunay triangulation. The extracted minutia features are secured through arbitrary binary string (key). The generated template is revocable and another template can be made simply by changing the random binary string (key).

Block remapping and image warping strategies are used to produce cancelable iris templates [121]. The iris image is separated into arbitrary squares and exposed to random permutation. The method can restore the 60% of the original template when the permutation key and stolen template are accessible [122]. The method achieved a comparable performance in contrast to the existing methods. Li et al. [123] proposed cancelable palm-print template based on randomized cuckoo hashing and minHash. Initially, palm-print features are extracted by utilizing anisotropic filter and further secured by randomized cuckoo hashing. To additionally improve the unlinkability, minHash is applied to the transformed template. The method achieved a comparable performance in contrast to the existing methods.

1.6 Research Gap identified

With increase in use of digital mode for regular needs like financial transaction, important file and personal information, access to interface devices is critical issue. Palm print biometric access makes it more safe and spoofing proof.

Following research gaps were identified for the research work:

1) The majority of the research that has been published in the literature has made use of contact-based palm-print databases. The contactless database includes posture, translation, and scale variations, making palm-print detection more understandable and reliable. Therefore, there is potential for employing contactless palm-print databases to improve performance metrics.
2) The majority of texture descriptors are concerned with encoding local intensity variations between a center pixel and its sample points. Also, they can't explain the intensity ordering between adjacent sample points. They can't detect long-range pixel relationships outside of a compact region. The issue of learning robust and discriminative characteristics for palm-print recognition remains a fascinating and demanding topic.
3) The majority of research for designing biometric systems has been done in the field of single feature extraction (subspace based, coding based, structural based and hybrid based) techniques. The key elements of a palm-print image are precisely described by multiple feature vectors, which can offer more feature-specific details for joint feature learning. Therefore, a multiple feature extraction approach can be more helpful in improvising the system accuracy.
4) The biometric framework offers numerous advantages over the customary framework, yet the biometric framework itself is vulnerable to numerous identity threats. The increasing use of palm-print recognition has raised privacy concerns significantly. Therefore, the security of palm-print templates is a fundamental and vital issue.

1.7 Objective of the work

1) A comparative study and analysis of various feature extraction and classification techniques of palm print authentication on various databases.
2) Design of robust feature extraction algorithm for palm-print recognition.

3) Design of robust multiple feature extraction algorithm based on texture description.

4) Designing of a robust palm-print security framework.

1.8 Outline of the Thesis

The thesis is organized in the following manner:

Chapter 1: This chapter introduces the fundamentals of the biometrics, and palm-print specifically. This chapter also includes a comprehensive overview of the related literature that has already been published. The evaluation takes into account several approaches, including holistic, structural, hybrid, and deep learning-based methods.

Chapter 2: This chapter discusses the design of Gabor filter and explains the texture feature extraction methods using the Gabor filter. The first section elaborates on the construction of the Gabor filter for palm-print recognition using a kernel-based full space FDA. To further illustrate the effectiveness of the Gabor filter with kernel-based full space FDA technique, the experiment is conducted on contact-based palm-print datasets. In the next section, the design of Gabor filter with neural network is explained. Furthermore, the experiments performed on contactless palm-print databases are described.

Chapter 3: In this chapter, the first section explains the implementation of the proposed multi scale edge angles LBP (MSEALBP). Initially, Sobel gradient operator in both vertical and horizontal directions produce directional angle images and then passed through multi-scale LBP to produce uniform patterns of palm-prints. Further, uniform images are divided into non-overlapping blocks of size 5×5 pixels. Finally, the feature vector is fed as an input into the ANN. Next section elaborates the implementation of LBP with multi feature learning for palm-print recognition. Two complementary robust

operators, one with dominating directional pattern (DP) and the other with the texture patterns (TP), extract multi feature information simultaneously. Further, we learn feature mapping to project the multi data into hash codes. Furthermore, the experiments performed on contactless palm-print databases are described.

Chapter 4: In this chapter, we discuss the implementation of a non-invertible palmprint template for secure authentication. Proposed CNN and transformation scheme in a single mechanism is explained further. Experimental results on palm-print databases are described and consequently generated ROC curves are discussed.

Chapter 5: In this chapter, we provide a comparative examination of our different proposed methods such as Gabor filter with kernel-based full space FDA, Gabor filter with neural network, MSEALBP, LBP with multi feature learning, and non-invertible template, and CNN and transformation method. Two independent experiments are performed. The first compares the recognition performance on contact-based methods. The second experiment discusses the efficacy of the proposed methods on contactless databases. Finally, discusses the main findings of the thesis work and the direction to future work.

Chapter 2

Structure based Palm-print recognition: Gabor filter-based approach

2.1 Introduction

Palm-print biometric has many special benefits like stable and unique features, fewer distortions and straightforward self-positioning. Additionally, it may also get high recognition rate (RR) with fast processing speed [12].

Texture as an important feature of palm-print was obtained by wavelet and transform methods [42]. The Gabor filter has been perceived as a useful tool in computer vision and image processing applications. It is capable of providing a precise depiction of most spatial qualities of basic receptive fields [124].

Li et al. [125] uses morphological operator and Gabor filter with different orientations for texture extraction. The technique is a decent answer for turn variety in palm images. To recover the phase information of palm-prints using the Gabor filter, Zhang et al. [42] used palm code. The resulting features are highly correlated that may reduce the individuality of palm codes. The bitwise Hamming distance is used for comparing two palm codes. Zhang et al. [126] proposed a Gabor filters-based double-orientation code and nonlinear matching method for palm-print recognition. Lunk et al. [49] proposed palm-print recognition approach based on Gabor filter. To extricate the half-direction a bank of half-Gabor channels is characterized.

2.2 Gabor filter

In the biometric literature, Gabor filter is successfully applied to exploit biometric modalities like iris [127], face [128], fingerprints [129] and palm-prints [20]. A circular 2D Gabor filter is a Gaussian modulated by complex oriented sinusoidal function which capture the spatial and frequency information simultaneously [124].

Circular 2D Gabor filter is expressed as follows:

$$G_{\sigma,\mu,\phi}(x,y) = gu_{\sigma}(x,\mathrm{y}).exp[2\pi j\mu(x\,cos\,\phi + y\,sin\,\phi)] \tag{2.1}$$

Where, $gu_{\sigma}(x,\mathrm{y})$ is Gaussian function defined as $gu_{\sigma}(x,\mathrm{y}) = \frac{1}{2\pi\sigma^2}exp[-(x^2+y^2)/2\sigma^2]$, $j = \sqrt{-1}$, σ is standard deviation, μ is frequency and ϕ is the orientation [0°-180°]. The complex form of Gabor filter $G_{\sigma,\mu,\phi}(x,y)$ can be decomposed in terms of real part $R_{\sigma,\mu,\phi}(x,\mathrm{y})$ and imaginary part $I_{\sigma,\mu,\phi}(x,\mathrm{y})$ as given in Eq. (2.2) -(2.4).

$$G_{\sigma,\mu,\phi}(x,y) = R_{\sigma,\mu,\phi}(x,\mathrm{y}) + jI_{\sigma,\mu,\phi}(x,\mathrm{y}) \tag{2.2}$$

$$R_{\sigma,\mu,\phi} = gu_{\sigma}(x,\mathrm{y}).cos[2\pi\mu(x\,cos\,\phi + y\,sin\,\phi)] \tag{2.3}$$

$$I_{\sigma,\mu,\phi} = gu_{\sigma}(x,\mathrm{y}).sin[2\pi\mu(x\,cos\,\phi + y\,sin\,\phi)] \tag{2.4}$$

To make the illumination response insensitive, the DC component of the Gabor filter is removed as given in Eq. (2.5),

$$\overline{G}_{\sigma,\mu,\phi}(x,\mathrm{y}) = G_{\sigma,\mu,\phi}(x,\mathrm{y}) - \frac{\sum_{i=-k}^{k}\sum_{j=-k}^{k}G_{\sigma,\mu,\phi}(i,\mathrm{j})}{(2k+1)^2} \tag{2.5}$$

Finally, Gabor transform with robust illumination is defined as

$$O(x, \mathrm{y}; \sigma, \mu, \phi) = I(x, \mathrm{y}) \otimes \overline{G}_{\sigma,\mu,\phi}(x, \mathrm{y}) \tag{2.6}$$

Where, k scales the magnitude of Gaussian envelope and $(2k+1)^2$ denotes the size of the Gabor filter. $I(x, \mathrm{y})$ is the ROI and symbol $\otimes$ is convolution operator.

2.3 Motivation

1. Gabor filter gives high recognition performance at the expense of speed and memory [130]. Therefore, dimensionality reduction methods can be utilized to obtain a low-dimensional illustration of high-dimensional data samples.
2. It is significant to develop the contactless palm-print recognition algorithm, as it is effectively adequate in real-world applications because of its high ease of use.
3. To combine the traditional methods with the deep learning seems to be a fascinating and significant direction for developing the robust algorithm for both contact-based and contactless palm-print recognition.

2.4 Database

The performance of palm-print biometrics is estimated using certain publicly accessible databases. The databases were captured using different heterogeneous devices and acquisition procedures which are briefly explained as follows:

2.4.1 PolyU palm-print database [132]

In the PolyU database, there are 386 different palms represented by a total of 7,752 grayscale palm-prints from 193 participants. It is a contact-based palm-print database.

In two separate sessions, 16 images of each individual with 256 grey levels and a 75dpi resolution were collected. Before 2003, researchers explored employing digital cameras, scanners, and hand-drawn drawings to gather information about palm-prints. These devices collect palm-prints, but the quality of the images they produce is very inconsistent and not satisfactory. As a result, a large-scale palm-print database was created and a real-time palm-print capturing device was developed.

2.4.2 CASIA palm-print image database [133]

This database includes the left and right palms of 312 distinct participants who were captured using a self-made device. There are 5,502 palm-print images in the 8-bit JPEG format. This database is kept on a device without pegs. As a result, several postures and palm positions are used to capture the images. The database is publicly available for the users.

2.4.3 IIT-Delhi touchless palm-print database [134]

This database includes 3,290 palm-prints that were gathered from 235 students of Indian Institute of Technology Delhi. It is a large touchless database that was set up in 2007. Seven images of each subject, taken with varied hand poses on the left and right hands, are collected. Each image has a bitmap format and is 800×600 pixels. The database also provides access to 150×150 pixel automatically cropped images. Pose, translation, and scale variations in this database allow more dependable and user-friendly palm-print identification. The database is publicly available for the users.

2.4.4 PolyU multispectral palm-print database [135]

This multispectral palm-print database contains 6,000 palms from 250 volunteers for one illumination. In the 20–60 year age range, there are 195 men and 55 women. The samples

are collected over the duration of two distinct sessions, with an average time gap of roughly nine days between them. Each volunteer provides 24 palm images for each illumination. A more discriminating set of data was obtained using this database. The correlation between various spectral bands is used to strengthen the antispoof capacity.

2.4.5 REgim Sfax Tunisia (REST) database [136]

It measures 2048×1536 and contains 1945 images. The images are taken indoors with natural light and a digital camera [124]. This database was collected by research groups in intelligent machines of Sfax university. The hand repeatedly shifted in position and orientation. 358 persons, ages ranging from 6 to 70.

2.4.6 Tongji database [137]

It measures 800×600 and contains 6,000 images. 600 Tongji university students between the ages of 20-50. Each user had to put his or her hand within an enclosure to complete the acquisition process. The hand may move within a rather narrow area while not being in contact with any surfaces. The hand orientation and illumination patterns are roughly the same across all samples. Compared to the restrictions used to establish the CASIA and IIT-D databases, the acquisition criteria were less restricted.

2.5 Palm-print recognition using Gabor filter with kernel-based full space FDA method

For palm-print recognition, the Gabor filter is a popular texture-based technique that offers good recognition performance at the cost of speed and memory. As a result, DR methods are used to produce low-dimensional representations of high-dimensional data samples. These methods preserve the ‘inherent information’ contained in the original data. The previous decades have seen the rapid improvement in DR methods [138, 139].

The most notable DR methods are principal component analysis (PCA) [140] and Fisher discriminant analysis (FDA) [141] due to their simplicity and proficiency. In supervised learning scenarios, FDA is a well-known method for DR [28]. It has been observed that PCA and FDA only examine the global Euclidean structure of data, so they cannot oblige to the data with complex nonlinear structures. Hence, some kernel-based nonlinear strategies have been proposed, for example, kernel FDA (KFDA) [142], kernel PCA (KPCA) [143] and eigenspectrum-based regularised KDA algorithm (ER-KDA) [144]. These methods do not explicitly study the local structure of the data, which is vital for classification [145].

2.5.1 Proposed methodology

This section elaborates the proposed palm-print recognition framework as illustrated in Figure 2.1. Initially, the pre-processing is applied that gives a stable and aligned region of interest (ROI) image. The work also describes quality estimation and enhancement module which improvise the recognition results. After making the quality estimation the features are extracted by utilizing Gabor filter with five scales and eight different orientations. To make full use of the discriminant information in the full space of the within-class scatter a kernel-based full space FDA method is proposed. The method uses the discriminant information in the null space and non-null space of the within-class scatter for better recognition performance. The feature vector dimension is reduced which further reduces the computational complexity of the proposed approach. Finally, matching is finished by normalized Hamming distance (NHD).

1) **Pre-processing:** Pre-processing is an important step that updates the general quality and contrast of the image. Palm-print, i.e., the deformable area that causes unsure extending and reflections. So, it is utilized to lessen the impacts of these factors and also extract aligned and stable ROI. It is the area of hand that contains

significant features of palm-prints. ROI extraction is a step-by-step process as illustrates in Figure 2.2. Initially, the hand image is converted into binary format (0 or 1). As discussed in [146], the bearings of the five fingertips and four finger valleys are gotten by following the restriction of the palm using the binary image. The use of finger valleys and the centroid makes the image rotation invariant.

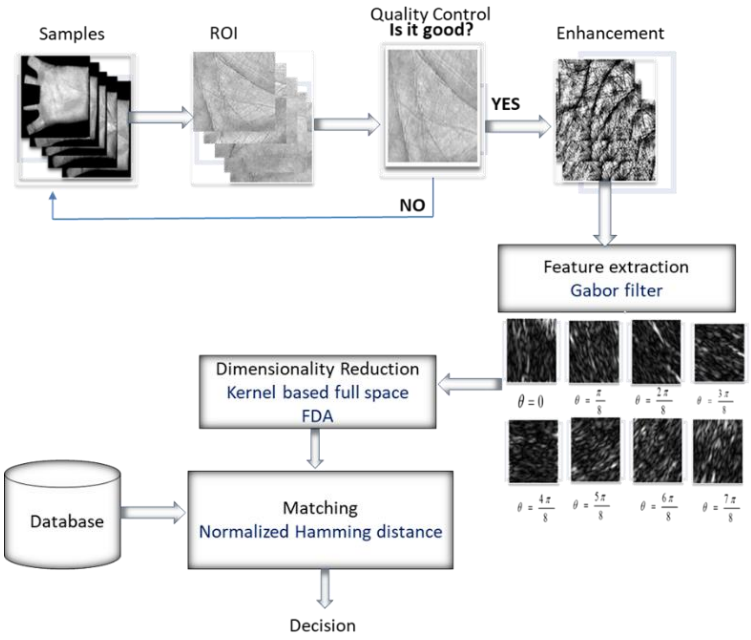

Figure 2.1: Work flow representation of the proposed method.

- **Quality analysis:** The bad or poor-quality images yield spurious or false features which diminishes the performance of the biometric framework. The blurred principal lines, edges and wrinkles reduce the characteristics of palm-print images. The orientation level (OL) of ridges and ridge density (RD) parameters are figured for the quality estimation. The

algorithm restores a scalar value 1 for good quality images and 0 for bad quality images. The fusion of individual quality attributes produces an aggregate quality score. The resulting quality score is represented as scalar value (1 or 0). If the quality score is greater than the threshold value, images are considered in the good quality category otherwise considered in the class of bad quality. Further, good quality images are fed to the next module. The bad quality images are recovered consistently till the satisfying quality level is accomplished. After that, support vector machine (SVM) is trained by palm-prints (having individual quality levels).

The image quality is defined as:

$$image\ Quality = f(OL, RD) \tag{2.7}$$

Where f is a function of OL and RD.

Orientation level: OL is an important parameter which requires directional features for evaluating the image quality [147]. The covariance matrix (C) is processed for an image block. From the covariance matrix, greatest two eigenvalues (e_1, e_2) are selected to compute the OL as given in equation (2.8):

$$OL = 1 - \frac{e_2}{e_1} \tag{2.8}$$

The bad quality ROI (low contrast and effected by noise) shows a low OL. In contrast, a good quality ROI having unambiguous straight lines separated by small wrinkles shows a high OL.

Ridge density: It is the measure of ridge blocks existing in the good quality palm-prints. The acquired OL info has been used to categories the given ridge block into good and bad classes. Higher number of ridge blocks improves the image quality. A sum of 2,100 images taken from the palm-print databases are utilized to train the SVM classifier. The two quality classes (good and bad) and two quality parameters (OL and RD) are used as input to train the SVM. When the classifier obtains a new test image than the quality parameters (OL, RD) are normalized to (0, 1). Further, the result is passed to the SVM which gives the quality class comparing to the ROIs.

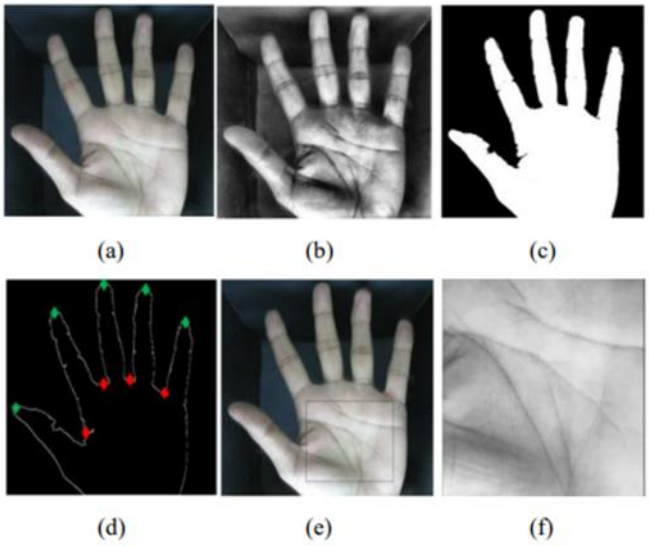

Figure 2.2: ROI location approach, (a) original image (b) filtered image (c) binary image (d) locating finger valleys and fingertips (e) ROI area using the maxima and minima (f) extracted ROI.

Finally, contrast limited histogram equalization (CLAHE) is applied as an enhancement module, which produces robust features against the image quality.

2) **Feature extraction:** In the pre-processing step, the size of ROI is normalized to 128×128 pixels. After that, the ROI is segmented into 8×8 non-overlapping sub-blocks, which conclude Gabor parameters independently. The literature demonstrated that Gabor filter provides the accurate recognition when filter parameters (orientation, variance, center frequency) are suitably chosen [145]. Therefore, this work proposes ROI image segmentation into $m \times m$ non-overlapping sub-blocks and then determines optimal Gabor parameters. The small value of 'm' can introduces noise in some smooth areas and larger value of 'm' may enhance the anti-noise capability of the block. The block cannot reflect the detailed variation of the image if we select too large value of 'm'.

- **Estimation of orientation:** The orientation is an intrinsic property of a Gabor filter and represented as $'\phi'$. The orientation analysis is done to compute the local direction at every block of ROI image. The direction operators is represented by local direction pattern (LDPs) with eight different orientations $\left(\frac{n\pi}{8}, where\ n = 0, 1, 2, \dots, 7\right)$. The displacement range (most local orientation determined) is restricted within a mask pattern of 3×3 pixels. The designed LDP generates eight features which represents the different direction characteristics more closely. These features are generated by summing up the pixel intensities of corresponding blocks. Lastly, the maximum value of the direction intensity is selected as the optimal direction in each block. Each pixel of an image is considered as the center of mask pattern. The direction intensity corresponding to each pixel is denoted as D_p, where $p = 1, 2, \dots, 8$.

  The feature value is computed as given in Eq. (2.9),

$$D_p(i,j) = \sum_{u=-1}^{1} \sum_{v=-1}^{1} \left| P(i+u, j+v) * L_p(u,v) \right| \qquad (2.9)$$

$$D_p = \sum_{j=1}^{m} \sum_{i=1}^{n} \left| D_p(i,j) \right| \qquad (2.10)$$

where, m and n are the height and width of the block respectively, $P(i, j)$ is the pixel value, and D_p denotes local patterns.

- **Estimation of standard deviation:** The standard deviation (σ) is associated with the breadth of the Gaussian that modulates the Gabor filter. A smaller value of (σ) gives more ridge features, but the result has greater noise. In distinction, Gabor filter is a lot of sturdies to noise once employing a larger value of σ , however the filter can lose ridge details [145]. Within the proposed methodology, the value of σ is decided by measure the native region variance of the ROI image $V(I(i,j))$. We decide a distinct value of σ by measure the degree of ridge detail altogether sub-regions. In the proposed method, the optimal value of standard deviation is $1, \sqrt{2,}$ and $2\sqrt{2}$. The image deviation is defined as follows:

$$M(I(i,j)) = \frac{\sum_{i=1}^{m} \sum_{j=1}^{n} I(i,j)}{m \times n} \qquad (2.11)$$

$$V(I(i,j)) = \sqrt{\frac{\sum_{i=1}^{m} \sum_{j=1}^{n} \left(I(i,j) - E(I(i,j)) \right)^2}{m \times n}} \qquad (2.12)$$

Where, $M(I(i,j))$ and $V(I(i,j))$ is the mean value and image deviation of sub-blocks respectively.

- **Estimation of frequency:** So as to discover appropriate frequency, each block of the ROI image is isolated according to standard deviation value $(\sigma = 1, \sqrt{2}, 2\sqrt{2})$. Further, the subsequent qualities (0, 0.12 and 0.8) are doled out to every frequency block. The assessment of central frequency (μ) is finished utilizing the standard deviation esteem as given in Eq. (2.13),

$$\mu = \begin{cases} 0, & if \ \ \sigma = 1 \\ 0.12, & if \ \ \sigma = \sqrt{2} \\ 0.8, \ \text{if} \ \sigma = 2\sqrt{2} \end{cases} \tag{2.13}$$

For a local window, having a size $u \times u$ for $u = 2k + 1$, the real part $\left(GR_{\sigma,\mu,\phi}(x, y)\right)$ and imaginary part $\left(GI_{\sigma,\mu,\phi}(x, y)\right)$ of the image were registered by discrete convolution.

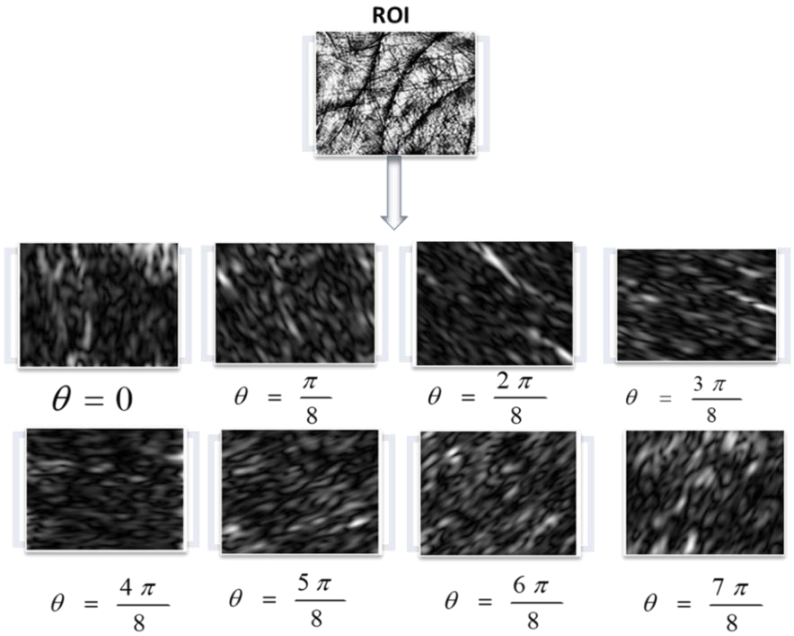

Figure 2.3: Gabor filter response with eight different orientations.

Each sub-square will be convolved with Gabor channel until the entire ROI picture was navigated [130].

$$GR_{\sigma,\mu,\phi}(x,y) = \sum_{i=-k}^{k} \sum_{j=-k}^{k} I(x+i, y+j) \cdot R_{\sigma,\mu,\phi}(x,y) \tag{2.14}$$

$$GI_{\sigma,\mu,\phi}(x,y) = \sum_{i=-k}^{k} \sum_{j=-k}^{k} I(x+i, y+j) \cdot I_{\sigma,\mu,\phi}(x,y) \tag{2.15}$$

In the proposed approach we design a Gabor filter having 5 scales and 8 orientations in order to extract more effective features. So, the bank of 40 (scale=5, orientation=8) Gabor filter is used to filter the images. Figure 2.3 shows the Gabor filter response with eight different orientations. Finally, feature vector $X = \{X_1, X_2, \ldots, \mathrm{X}_N\}$ is constructed by the individual Gabor matrices of training samples.

3) **Dimensionality Reduction:** In the proposed approach, kernel-based FDA method is employed for dimensionality reduction [148]. In the proposed method, the size of ROI is 128×128 pixel and the dimension of Gabor feature is $(H \times W \times m \times n)$. In order to reduce the dimension of Gabor features (high-dimensional), a down sampling scheme is applied and the Gabor coefficients are normalized (mean=0, variance=1).

   Suppose a down sampling factor is d and further a Gabor feature set $\left(f^d\right)$ is computed by concatenating all the individual coefficients $f_{a,b}^d$.

$$f^d = \left(\left(f_{0,0}^d\right)^t, \left(f_{0,1}^d\right)^t, \ldots \left(f_{2,3}^d\right)^t\right)^t \tag{2.16}$$

The full space includes both the null space and non-null space. The proposed method has the ability of fully using the discriminant information in the full space of the within-class scatter as discussed below.

Initially take the Gabor feature set (X) and non-linear projection $\varphi(.)$.

The Kernel matrix (km) is computed as given in equation (2.17):

$$km(a_i, a_j) = exp\left(-\frac{\| a_i, a_j \|^2}{\sigma^2}\right) \tag{2.17}$$

Now, we compute the non-null space (φ) step by step:

Initially an eigenvector (E_t) is computed with respect to $\left(\phi_t^{\phi}\right)^T \phi_t^{\phi}$, which produces $\left(\phi_t^{\phi}\right)^T E_t$.

After that, we compute the projection of the training samples X^{ϕ} on non-null space (φ)

$$Z = \left(\phi_t^{\phi} E_t\right)^T X^{\phi} \tag{2.18}$$

Z can be represented as $Z = E_t^T.\left(km - \frac{1}{N}.I_{N\times N}.km\right)$.

The following two matrix are computed:

(a) between-class scatter matrix $\left(sc_b^{\phi}\right)$

(b) within-class scatter matrix $\left(sc_w^{\phi}\right)$

The null space $(\overline{\psi})$ and non-null space $(\overline{\psi}_1)$ is composed of the eigenvectors (E_{sw}) and $E^1{}_{sw}$ respectively. Now, the optimal discriminant vectors is computed according to the Fisher criterion as given below:

Now a total scatter matrix $\left(sc_t^{\phi}\right)$ is computed form the feature space as given below

$$sc_t^{\phi} = \sum_{i=1}^{c} \sum_{j=1}^{n_i} \left(\phi(a)_j^i - v^{\phi}\right)\left(\phi(a)_j^i - v^{\phi}\right)^T = \phi_t^{\phi} \left(\phi_t^{\phi}\right)^T$$

Where $\phi_t^{\phi} = span\{(\phi(a)_1^1 - v^{\phi}), \ldots, (\phi(a)_{n_1}^c - v^{\phi})\}$

We can represent $\left(\phi_t^{\phi}\right)^T \phi_t^{\phi}$ as given below

$$\left(\phi_t^{\phi}\right)^T \phi_t^{\phi} = \frac{1}{N}\left(km - \frac{1}{N}\left(km.I_{N\times N} + I_{N\times N}.km + \frac{1}{N^2}.I_{N\times N}.km.I_{N\times N}\right)\right) \quad (2.19)$$

$(\overline{\psi}_1)$ is composed of the eigenvectors (E_{sw}) and $E^1{}_{sw}$ respectively.

Now, the optimal discriminant vectors is computed according to the Fisher criterion as given below:

Initially project $\left(sc_b^{\phi}\right)$ and $\left(sc_w^{\phi}\right)$ into the non-null space $(\overline{\psi}_1)$

$$\overline{sc_b^{\phi}} = E_{sw}^T S_b^{\varphi} E_{sw} \text{ and } \overline{sc_w^{\phi}} = E_{sw}^T S_w^{\varphi} E_{sw}.$$

In the null space $(\overline{\psi})$, project $\left(sc_b^{\phi}\right)$

$$\overline{sc_b^{\phi}} = (E_{sw}^1)^T S_b^{\varphi} E_{sw}^1$$

Further, we compute the Eigen vectors E_{wb} and E_{sb} corresponding the largest Eigen value l and t respectively.

$$\overline{sc_w^{\phi}}^{-1} \overline{sc_b^{\phi}} X = \lambda X$$

$$\overline{sc_b^{\phi}} X = \lambda X$$

Finally, the optimal discriminant vectors are computed as in the non-null space and null space respectively. $E_1 = E_{sw}E_{wb}$ and $E_2 = E_{sw}^1 E_{sb}$. The final optimal discriminant projection matrix is generated by combining the optimal vectors E_1 and E_2 as

$$E = [E_1, E_2]^T \tag{2.20}$$

Finally, the feature vector Y is extracted as $Y = EZ$. After dimensionality reduction the matching is performed. The normalized bitwise Hamming distance was utilized that produces invariant matching to translation and rotation [149].

The NHD is as given in equation (2.21),

$$HD_n = \frac{\sum_{i=max(1,1+g)}^{min(L,L+h)} \sum_{j=max(1,1+h)}^{min(L,L+h)} [P(i+g,j+h) \otimes Q(i,j)]}{2H(g)H(h)} \tag{2.21}$$

P is the stored ROI and Q is the tested ROI. Symbol $\otimes$ denotes Boolean XOR operator. g is offset (maximum) in horizontal direction, h is offset (maximum) in vertical direction.

2.5.2 Experimental results and discussion

Three palm-print databases, PolyU, IIT-Delhi and CASIA were utilized to evaluate the performance of the proposed framework. During the experiment, five images from each subject are randomly selected for training and the remaining images are used for testing. Figure 2.4 shows the sample hand images of PolyU database.

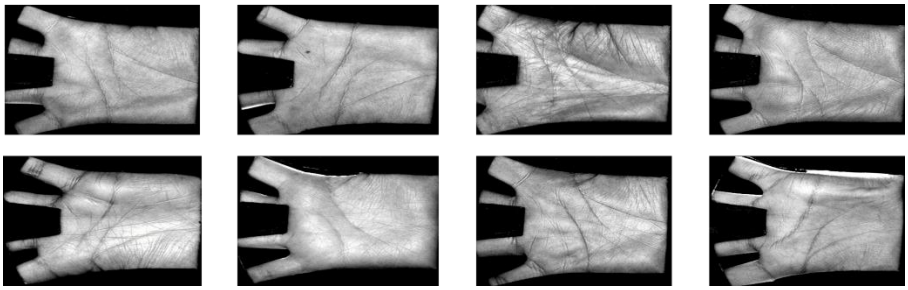

Figure 2.4: Hand images from PolyU palm-print database.

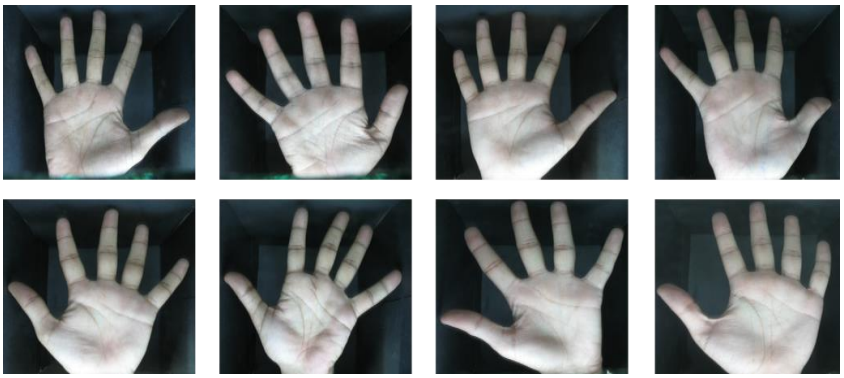

Figure 2.5: Hand images from IIT-Delhi palm-print database.

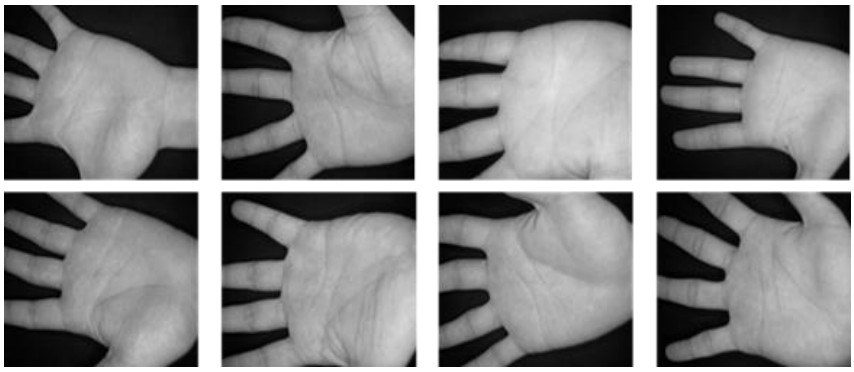

Figure 2.6: Hand images from CASIA palm-print database.

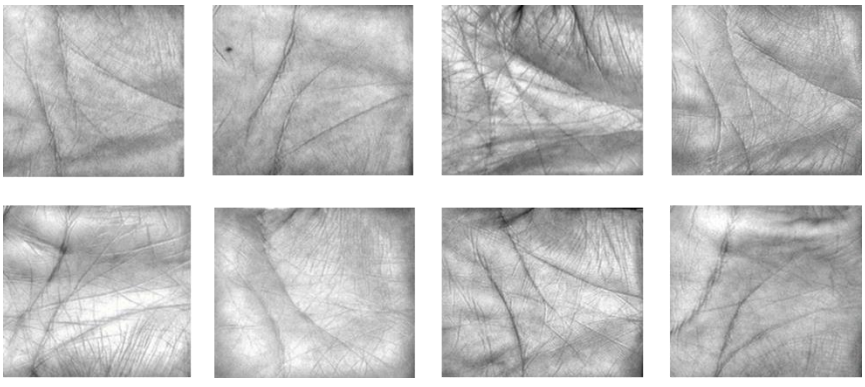

Figure 2.7: ROI images of PolyU palm-print database.

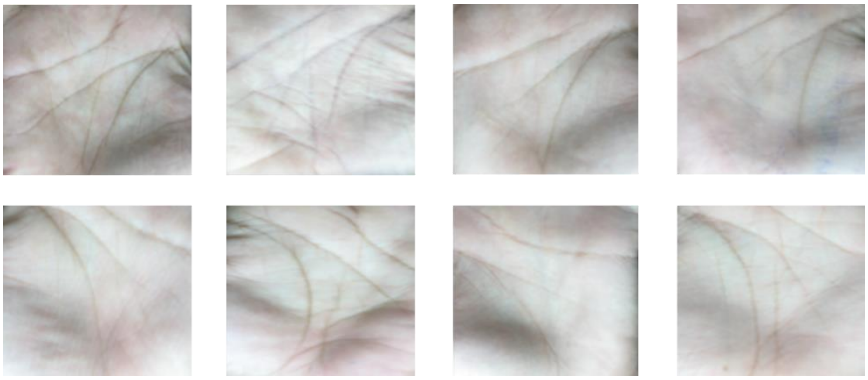

Figure 2.8: ROI images of IIT-Delhi palm-print database.

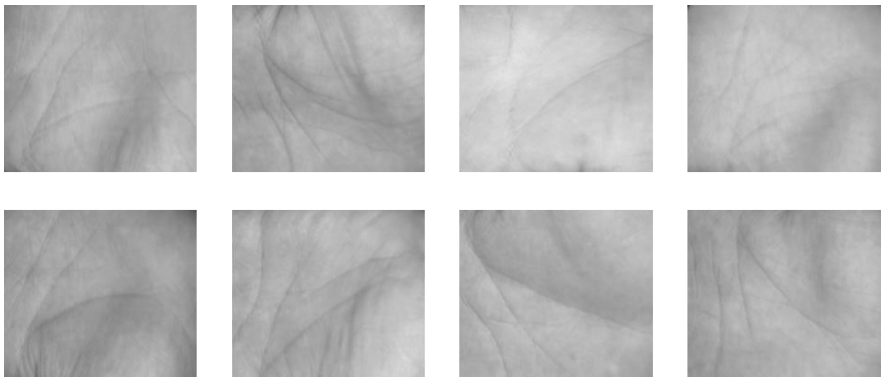

Figure 2.9: ROI images of CASIA palm-print database.

Figure 2.5 and Figure 2.6 shows the sample hand images of IIT-Delhi and CASIA palm-print databases respectively. The subsequent ROIs are cropped and resized to 128 × 128 pixels. Figure 2.7 shows the sample ROI images of PolyU database. Figure 2.8 and Figure 2.9 shows the sample ROI images of IIT-Delhi and CASIA databases respectively. The experiments are conducted on Dell Precision Tower 5810 by using MATLAB (R2018a), CPU as Intel Xeon Processor and two 2 GB Nvidia Quadro K620 GPUs, Windows 10 (operating system 64 bit).

The kernel function used in FDA along with their parameter values is listed in Table 2.1 for identification experiment. The parameters of the kernel function are selected empirically. The recognition performance when adopting kernel function as (a) polynomial kernel, (b) cosine kernel, and (c) RBF kernel is listed in Table 2.1. The recognition rate with the RBF kernel yields the best performance. The highest recognition rate is 98.34% on PolyU database. The RBF kernel yields best performance on all three palm-print datasets. The results with and without image enhancement and quality estimation are listed in Table 2.2, that shows the effect of pre-processing module on recognition results.

Table 2.1: Recognition results with different kernel functions.

Kernel		**Polynomial**	**RBF**	**Cosine**
Function		$km(a, a_i) = [q(a.a_i) + c]^v$	$km(a, a_i) = exp(-\gamma\|a - a_i\|^2)$	$km(a, b) = [q(a\,.\,b) + c]^v$
Parameters		$q = 1 \times 10^{-3}$,$c = 1$, $v = 2$	$\gamma = 1 \times 10^{-4}$	$q = 1 \times 10^{-3}$, $c = 1$, $v = 2$
Recognition Rate	**PolyU**	90%	98.34%	93.04%
	IIT-Delhi	80.11%	90.19%	85.43%
	CASIA	81.23%	96.43%	91.02%

Table 2.2: Comparative results with and without quality estimation.

Database	**Recognition Rate**	
	Without Quality estimation	**With Quality estimation**
PolyU	94.23%	98.34%
IIT-Delhi	87.56%	90.19%
CASIA	90.12%	96.43%

1) **Comparison with the existing DR methods:** The proposed method is compared with state-of-art methods such as PCA, 2DPCA, MFA, and FDA with their variants (KFDA, LFDA) on three palm-print databases. The proposed method achieves best performance with five training samples as listed in Table 2.3, 2.4, and 2.5.

Table 2.3: Comparisons of recognition rate (%) for different state-of-art methods on PolyU database.

Methods	Number of training samples per class			
	2-Train	3-Train	4-Train	5-Train
PCA [20]	83.34	89.87	93.98	95.12
2DPCA [22]	85.25	90.78	94.09	95.56
MFA [25]	79.77	82.89	88.80	92.34
FDA [28]	80.01	84.54	90.32	93.04
KFDA [30]	81.33	89.00	94.12	96.44
LFDA [29]	80.10	84.13	90.00	94.08
Proposed	89.34	93.45	96.11	98.34

Table 2.4: Comparisons of recognition rate (%) for different state-of-art methods on IIT-Delhi database.

Methods	Number of training samples per class			
	2-Train	3-Train	4-Train	5-Train
PCA [20]	78.01	80.73	87.08	89.07
2DPCA[22]	80.28	84.11	88.58	89.17
MFA [25]	75.89	78.90	84.01	86.31
FDA [28]	77.32	79.50	86.00	87.33
KFDA [30]	79.31	81.03	88.24	89.74
LFDA [29]	77.00	78.93	85.21	87.85
Proposed	80.34	86.31	88.98	90.19

The proposed method gives percentage recognition rate of 98.34%, 90.19% and 96.43% on PolyU, IIT-Delhi and CASIA databases respectively. KFDA method also gives comparable performance in terms of recognition rate of 96.44%, 89.74% and 94.21% on PolyU, IIT-Delhi and CASIA databases respectively. The comparative analysis of ROC curve of the proposed method with other FDA variants, for example, FDA and KFDA on PolyU and IIT-Delhi databases are shown in Figure 2.10.

2) **Comparison with the existing methods:** The proposed method is compared with some existing methods as shown in Table 2.6. The least EER esteem is 0.051% for PolyU database. The EERs of 0.312% and 0.264% for IIT-Delhi

and CASIA palm-print information base separately, which are far better than all other existing methodologies.

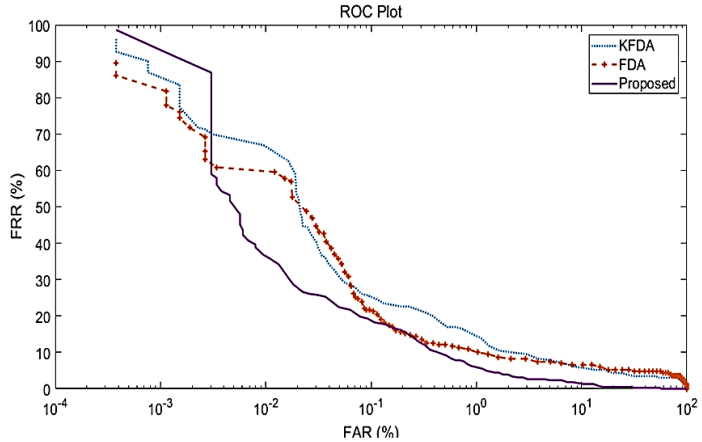

(a)

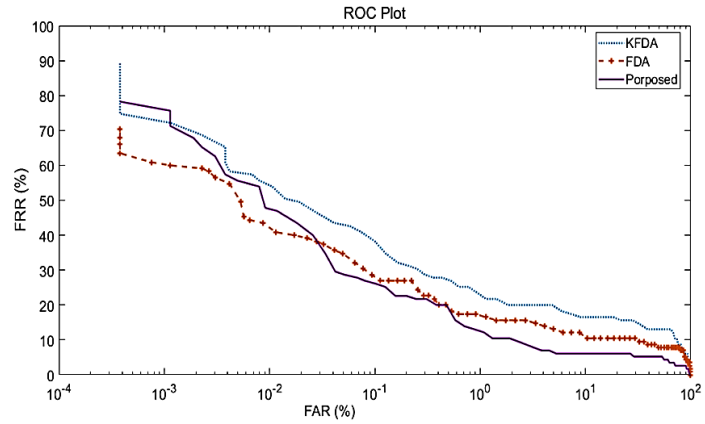

(b)

Figure 2.10: ROC curve comparison performance of proposed one with FDA variants on various databases (a) PolyU database (b) IIT-Delhi database.

3) **Comparison with the texture-based methods:** The proposed method is compared with the state-of-the-art methods (LBP, LDP, ELDP, LDN, and LLDP) on different palm-print databases as listed in Table 2.7. The least EER value is 0.051% for PolyU palm-print database. The EERs of 0.312%

and 0.264 %for IIT-Delhi and CASIA palm-print database respectively, which are far superior to all other existing strategies.

Table 2.5: Comparisons of recognition rate (%) for different state-of-art methods on CASIA database.

Methods	Number of training samples per class			
	2-Train	3-Train	4-Train	5-Train
PCA [20]	80.01	84.19	92.10	94.21
2DPCA [22]	82.45	90.23	93.25	94.82
MFA [25]	76.00	80.90	89.18	90.13
FDA [28]	79.41	81.31	91.11	91.31
KFDA [30]	81.89	82.45	93.21	94.21
LFDA [29]	80.00	80.17	92.67	91.67
Proposed	85.22	91.12	93.98	96.43

Table 2.6: Comparative results.

Method	Criteria (%)	Database		
		PolyU	IIT-Delhi	CASIA
LBP [53]	EER	6.36	10.94	11.78
LDP [55]	EER	5.43	10.01	8.34
ELDP [60]	EER	4.78	9.82	5.34
LDN [59]	EER	1.701	6.24	5.02
LLDP [56]	EER	0.163	4.13	5.78
Proposed	EER	0.051	0.312	0.264

Table 2.7: Comparative performance of different methods.

Method	Criteria	Database		
		PolyU	IIT-Delhi	CASIA
Block-wise Scale Invariant Feature Transform BSIFT-2D^{2}PCA [150]	EER CRR	2.09% 97.27%	3.012% 96.29%	2.423% 98.88%
TCCM-2D^{2}PCA [150]	EER CRR	2.70% 96.09%	3.24% 95.74%	2.14% 96.09%
Discrete Orthogonal S-Transform (DOST) [151]	EER	0.12%	0.93%	0.97%
Vese–Osher (VO) decomposition model [58]	EER	0.1071%	0.921%	-
Comp Code [44]	EER	-	1.5235%	0.385%
Orthogonal line ordinal features (OLOF) [45]	EER	-	1.5407%	0.4652%
Proposed	EER	0.051%	0.312%	0.264%

4) **Computational efficiency:** The total execution time is roughly 1s, which is speedy enough for real time application. The total time includes the feature extraction time and matching time. The time comparison of the proposed method with certain existing strategies on PolyU database is given in Figure 2.11. The less time (ms) consumed by proposed method is due to smaller dimension of Gabor feature vector.

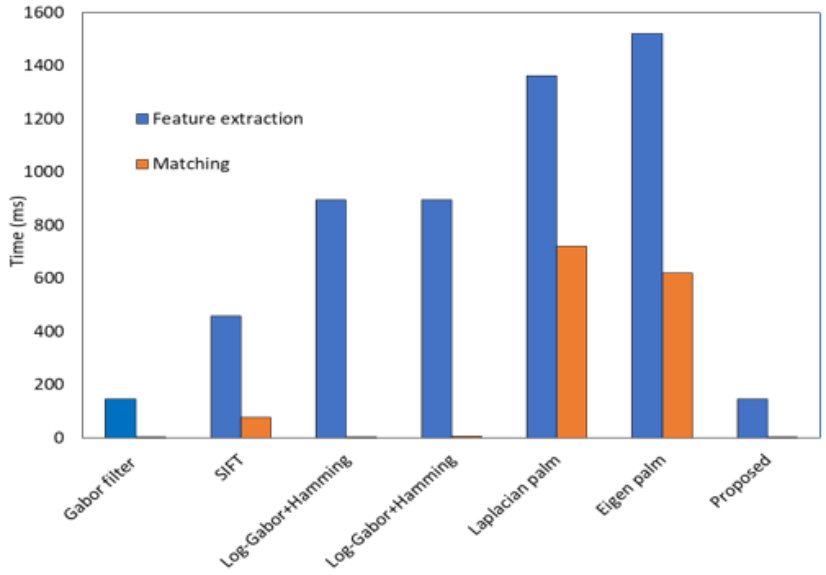

Figure 2.11: Comparison of Computational complexity.

2.6 Palm-print recognition, designed using Gabor filter with neural network

Artificial neural network (ANNs) are statistical information models that are inspired by the construction and effective parts of natural neural networks. ANNs are progressively

alluring, effective, and productive in accomplishing pattern recognition in numerous issues because of its great simulation capacity [152, 153]. There are various applications of ANNs, for example, biometrics (finger impression, iris, gait, voice, face recognition), speech recognition, handwritten (computerized and word acknowledgment) [154], deciphering DNA successions, crime detection, clinical finding, and so on. The basic ANN structure comprises of data sources (inputs), hidden and output layers that are made out of neuron components and their inter links [155] as shown in Figure 2.12. The training of the model is performed with sufficient number of input and output information utilizing an optimization algorithm. ANNs can be utilized to show complex high dimensional issues easily when appropriate design and activation function is used. The output of the model is determined by a weighted normal of the contributions through a sigmoid function [156].

$$f(x) = \mathrm{w}_o + \sum_{i=1}^{n} w_i x_i \tag{2.22}$$

$$A(x) = \frac{1}{1 + e^{-x}} \tag{2.23}$$

The weights between the neuron links that depend on the distinction among forecasted and real outputs are changed during the training procedure. The calculations in ANN can be parallelized with the incorporation of hidden layers and all the while keeping up with the capacity to appreciate complex constructions [157, 158].

It is seen that the deep-learning methods can achieve comparable performance than the conventional palm-print recognition methods, which give us guidance for examining the deep learning-based palm-print recognition frameworks. Afterward, the best way to combine the traditional methods with the deep learning seems to be a fascinating and significant direction of contactless palm-print recognition. The contactless palm-print

recognition is effectively adequate in real-world applications because of its high ease of use. In this way, it is significant to additionally develop the contactless palm-print recognition to boost the performance.

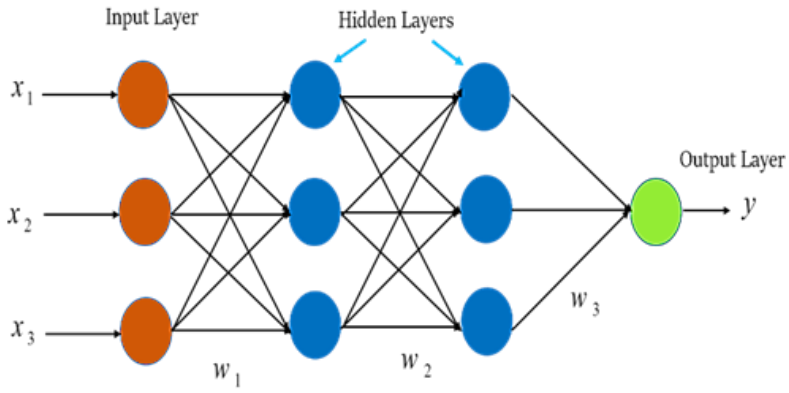

Figure 2.12: Representation of ANN [155].

2.6.1 Feature extraction

In this work, Gabor energy is calculated that involves the response of symmetric Gabor response $R^2_{\sigma,\,\mu,\,\varphi,\pi}(x,y)$ and anti-symmetric Gabor response $R^2_{\sigma,\,\mu,\,\varphi,\pi/2}(x,y)$.

The Gabor energy is computed as given in Eq. (2.24)

$$G^E_{\sigma,\,\mu,\,\varphi}(x,\mathrm{y}) = \sqrt{R^2_{\sigma,\,\mu,\,\varphi,\pi/2}(x,y) + R^2_{\sigma,\,\mu,\,\varphi,\pi}(x,y)} \tag{2.24}$$

Figure 2.13(c) shows the symmetric Gabor response $R^2_{\sigma,\,\mu,\,\varphi,\pi}(x,y)$ having 5 scales and 8 orientations to a sample ROI image in Figure 2.13(a). The anti-symmetric Gabor response $R^2_{\sigma,\,\mu,\,\varphi,\pi/2}(x,y)$ with the same scale and orientation for the same input ROI

image (Figure 2.13(a)) is shown in Figure 2.14(c). The Gabor energy representation calculated (in Eq. (2.24)) is shown in Figure 2.15.

Wang et al. [159] suggested different methods of utilizing PSO with other search algorithms. Every particle possesses a velocity and it can be categorized as a swarm component, an inertial component and a cognitive component. The updated velocity is computed as given in Eq. (2.25),

$$u(t+1) = w(t) * u(t) + a_1 * rand1 * \left(p_b(t) - x(t)\right) + a_2 * rand2 * \left(g_b(t) - x(t)\right) \tag{2.25}$$

The particle position is given as

$$x(t+1) = x(t) + u(t+1) \tag{2.26}$$

Where, a_1 and a_2 are accelerating coefficients. The cognitive component and global components are enhanced by augmenting the estimation of a_1 and a_2 respectively.

Further these accelerating coefficients boost the investigation of the search space that lead the particle towards the convergence. The cognitive element is ensuring exploitation of the positions of the particle's best configuration ($p_b(t)$). The global elements are determined using the global best ($g_b(t)$) position among the population. $rand1$ and $rand2$ are two random numbers in [0, 1].

The particles are moved around their own best position when we select large a_1 and small a_2 [160]. Over the iterations, the best solutions were obtained when a_1 and a_2 are linearly decreased and linearly increased respectively [161, 162].

$$a_1 = a_{1i} + a_{1f} * \left(\frac{t}{t_m}\right) - a_{1i} * \left(\frac{t}{t_m}\right) \tag{2.27}$$

$$a_2 = a_{2i} + a_{2f} * \left(\frac{t}{t_m}\right) - a_{2i} * \left(\frac{t}{t_m}\right) \tag{2.28}$$

a_{1i} and a_{1f} are the initial and final values of the accelerating coefficient (a_1). a_{2i} and a_{2f} are the initial and final values of the accelerating coefficient (a_2). t_m is maximum number of iterations.

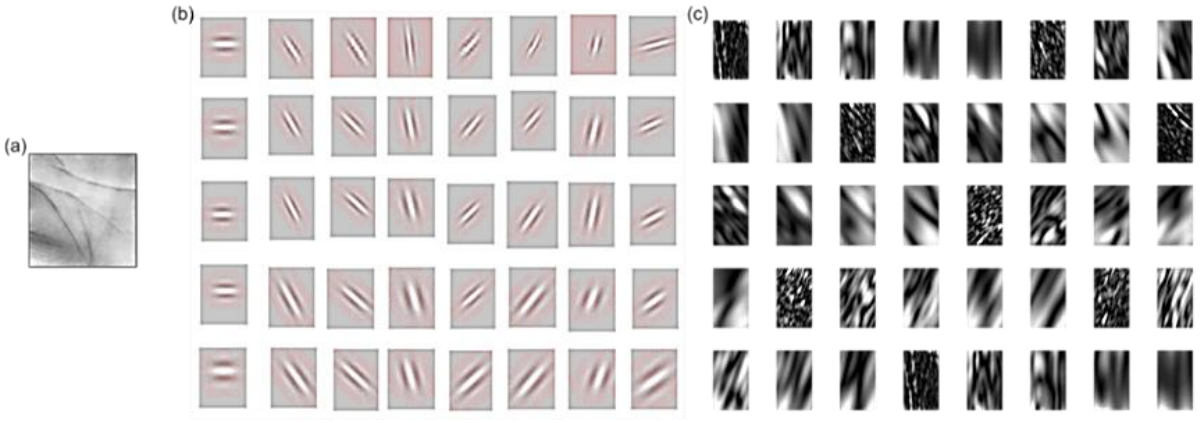

Figure 2.13: Response of Gabor filter (a) sample ROI image, (b) symmetric Gabor filter with 5 scale and 8 orientations, (c) response of the symmetric Gabor filter bank to ROI image in (a).

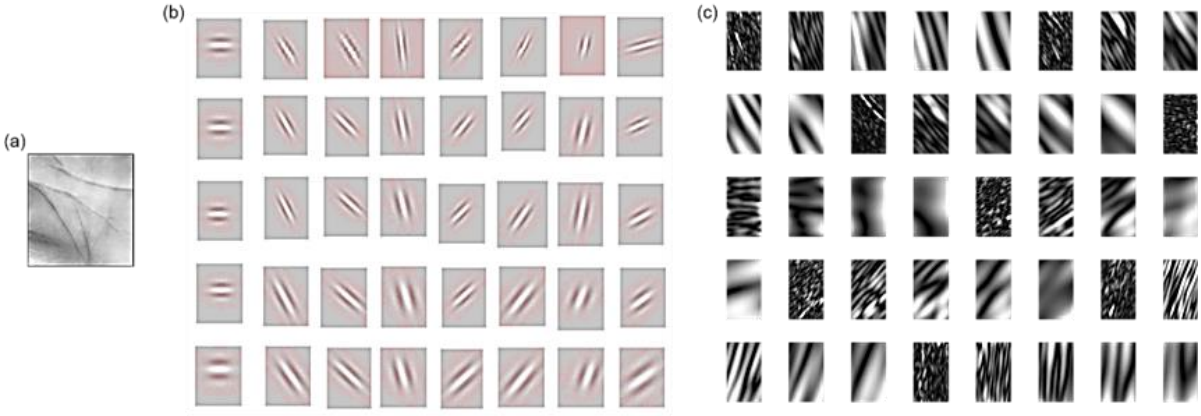

Figure 2.14: Response of Gabor filter (a) sample ROI image, (b) anti-symmetric Gabor filter with 5 scale and 8 orientations, (c) response of the anti-symmetric Gabor filter bank to ROI image in (a).

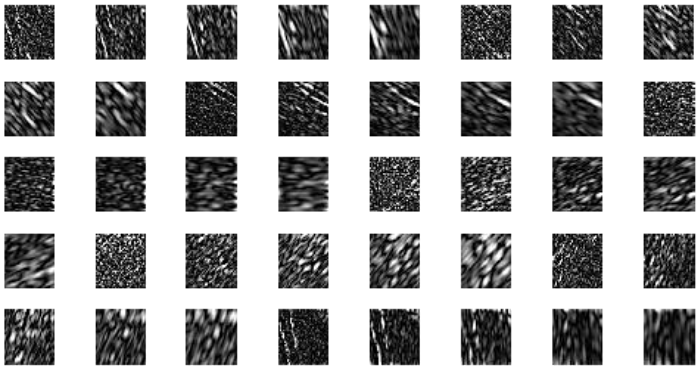

Figure 2.15: Gabor energy feature representation of a sample ROI image.

The acceleration rate is bounded as given in Eq. (2.29),

$$|a_k(g_b + 1) - a_k(g_b)| \leq \alpha \tag{2.29}$$

Where, α is the acceleration rate taken in [0.05, 0.1]. In order to bound the sum of the two boundaries we take the interval of [3, 4]. Assuming the total is bigger than 4, both a_1 and a_2 are standardized as given in Eq. (2.30),

$$a_k = \frac{a_k}{(a_1 + a_2)} * 4 \qquad k = 1, 2 \tag{2.30}$$

The inertia weight $w(t)$ deals with the involvement of the previous velocity [163]. By changing $w(t)$ dynamically, the global and local search abilities are progressively changed.

The inertia weight is characterized as given in Eq. (2.31)

$$W(f) = \frac{1}{1 + 1.5^{-2.6f}} \in [0.4, 0.9] \quad \forall f \in [0, 1] \tag{2.31}$$

$$s_k = \frac{1}{P_s - 1} \sum_{j=1,\, j \neq i}^{P_s} \sqrt{\sum_{l=1}^{d} \left(x_i^l - x_j^l\right)^2} \tag{2.32}$$

Here, s_k is the mean distance measured using Euclidian metric. d and P_s are the number of dimensions and population size respectively. f is evolutionary factor as given in Eq. (2.33)

$$f = \frac{s_{gb} - s_{min}}{s_{max} - s_{min}} \in [0, 1] \tag{2.33}$$

The value of evolutionary factor is larger in exploration state and turns out to be smaller in the convergence state. The maximal and minimal distances ($s_{max}\, and\, s_{min}$) are determined by comparing all s_k values. s_k of the globally best particle is represented as s_{gb}. The global best position (g_b) is the best particle position among all particles. Figure 2.16 shows the flowchart of the proposed hybrid PSO. As the probability condition is satisfied then the two arbitrary particles are chosen and updated as given,

$$P^1(t+1) = P^2(t) + \varpi * \left(P^1(t) - P^2(t)\right) \tag{2.34}$$

$$P^2(t+1) = P^1(t) + \varpi * \left(P^2(t) - P^1(t)\right) \tag{2.35}$$

Here, ϖ is the crossover operator in $[0, 1]^d$.

Further, the condition of mutation probability is explored, if it is satisfied then, at that point, mutation operator changes every particle according to the Eq. (2.36),

$$x(t+1) = x(t) + rand * \zeta \tag{2.36}$$

Here, ζ is a constant and defined as ζ =0.1 $*$ ($maximum\, domain - minimum\, domain$).

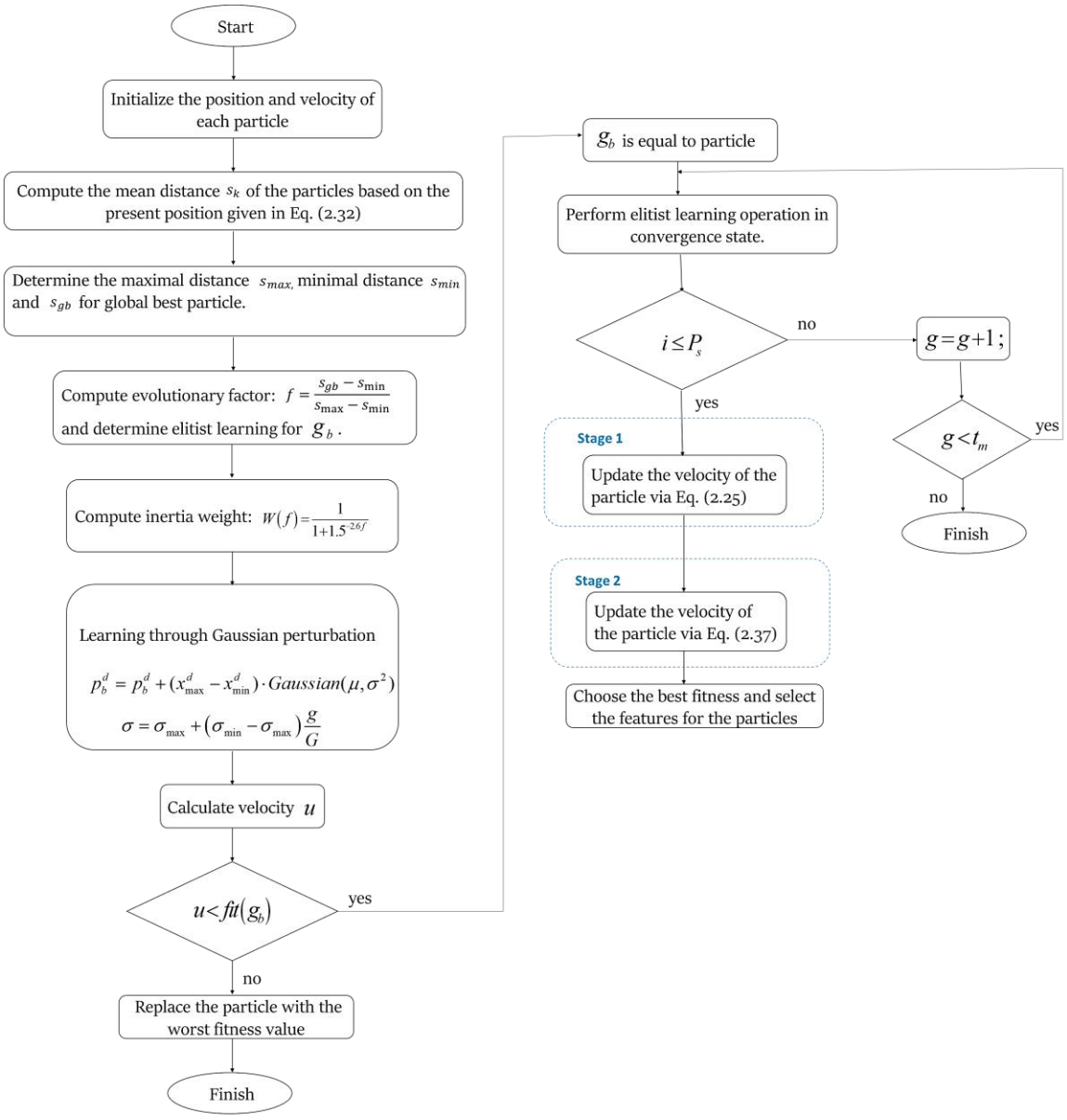

Figure 2.16: Flowchart of the proposed hybrid PSO.

It ought to be noticed that the mutation and crossover operators are changed in comparison of [164, 74] to acquire better outcomes over the traditional algorithms.

The PSO suffers from trapping in local minima and premature convergence. The convergence property of PSO can be utilized to achieve faster convergence in ANN models [165].

The proposed work integrated PSO and back propagation to achieve faster convergence towards optimum. In this model the derivative term obtained through back propagation is relate to the velocity of each particle. The proposed approach proficiently works on the balance among exploration and exploitation.

The updated velocity and position of the HPSO-ANN approach is given as

$$u(t+1) = w(t) * u(t) + a_1 * rand1 * \left(p_b(t) - x(t)\right) + a_2 * rand2 * (g_b(t) - x(t)) - \alpha \Delta \mathrm{w} \quad (2.37)$$

$$x(t+1) = x(t) + u(t+1) \quad (2.38)$$

Here, Δw is Back propagation component. The idea of moving averages of the slopes that upgrades the viability of the BP term as given in Eq. (2.37). Figure 2.17 shows the change in velocity for the PSO and the proposed HPSO-ANN.

The update rule is defined as

$$y_t = \beta_1 * m_{t-1} + (1 - \beta_1) * g_t \quad (2.39)$$

$$e_t = \beta_2 * e_{t-1} + (1 - \beta_2) * g_t^2 \quad (2.40)$$

Eq. (2.40) can be written as a function of the gradients at all previous time steps as

$$e_t = (1 - \beta_2) \sum_{j=1}^{t} \beta_2^{t-j} * g_j^2 \quad (2.41)$$

$$y_{tc} = \frac{e_t}{(1 - \eta_{t1})} \quad (2.42)$$

$$e_{tc} = \frac{s_t}{(1-\eta_{t2})} \tag{2.43}$$

$$\Delta w = \Delta w_{t-1} - \delta \frac{y_{tc}}{\sqrt{e_{tc}} + \varepsilon} \tag{2.44}$$

Where, y and e are moving averages, g is gradient on current batch, β_1 and β_2 are hyper-parameters of the algorithm, δ determine the learning rate and ε is a constant having value 10^{-8}.

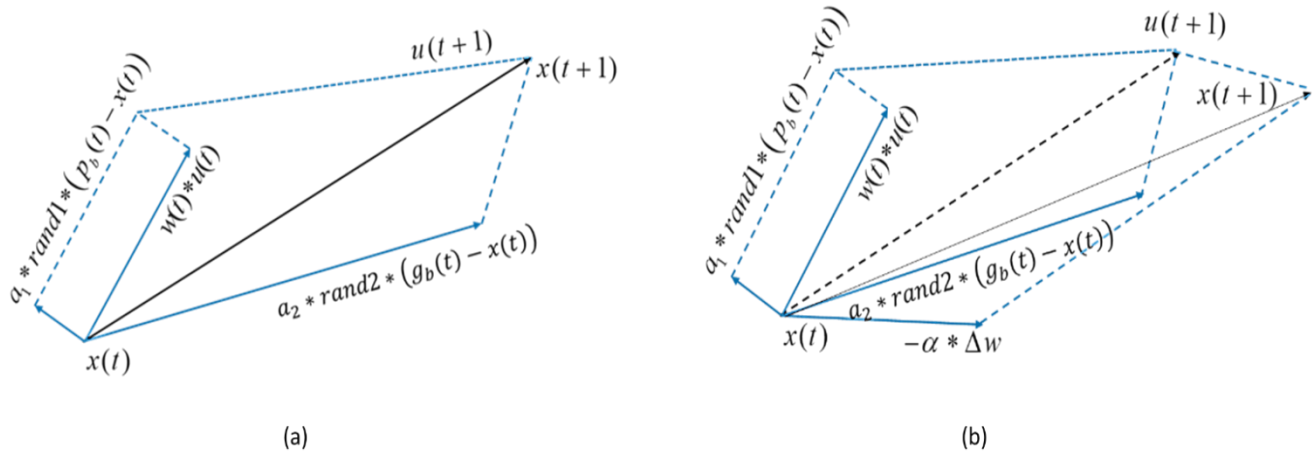

Figure 2.17: Formation of velocity vector (a) PSO [74] (b) Proposed HPSO with artificial neural network.

2.6.2 Experimental results and discussion

The recognition performance of the proposed method is evaluated by considering four contactless palm-print databases such as CASIA, IIT-Delhi, REST, and Tongji. Figure 2.18 and Figure 2.19 shows the sample hand images of REST and Tongji databases. The subsequent ROIs are cropped and resized to 128×128 pixels. The training and testing

subsets are selected randomly and each contained around half of the subjects in the database. The subjects in training and testing subsets are disjoint.

Algorithm

Require: $\beta_1, \beta_2 \in [0,1),\ \lambda \in [0,1]$: Exponential decay rates for the moment estimates

Δw_0 : Initial parameter vector

δ : Step size

1) Initialize the population

   $y_0 = 0$: Initialize initial 1st moment vector

   $e_0 = 0$: Initialize initial 2nd moment vector

   $t = 0$: Initialize time step

2) Repeat till Δw_t not converged or allowed number of generations are exhausted

   $t \to t+1$

   $\beta_{1,t} \to \beta_1 \lambda^{t-1}$

   $y_t = \beta_1 * y_{t-1} + (1-\beta_1) * g_t$ (Update biased first moment estimate)

   $e_t = \beta_2 * e_{t-1} + (1-\beta_2) * g_t^2$ (Update biased second raw moment estimate)

   $y_{tc} = \dfrac{e_t}{(1-\eta_{t1})}$ (Compute bias-corrected first moment estimate)

   $e_{tc} = \dfrac{s_t}{(1-\eta_{t2})}$ (Compute bias-corrected second raw moment estimate)

   $\Delta \mathrm{w}_t = \Delta \mathrm{w}_{t-1} - \delta \dfrac{y_{tc}}{\sqrt{e_{tc}} + \varepsilon}$ (Update parameters)

3) Update velocity of each particle

   $u(t+1) = w(t) * u(t) + a_1 * rand1 * (p_b(t) - x(t)) + a_2 * rand2 * (g_b(t) - x(t)) - \alpha \Delta \mathrm{w}_t$

4) Update position of each particle

   $x(t+1) = x(t) + u(t+1)$

---

1) **Test functions:** The population distribution characteristics in a PSO process is explored on standard benchmark functions [136] as listed in Table 2.8.

Function is unimodal that have one global optimum without any local optimum. The search algorithm converges fast and refines the response for high accuracy in unimodal space.

Table 2.8: Benchmark test functions.

Function	Formula	Threshold	Search range
Sphere	$F_1(x) = \sum_{i=1}^{d} x_i^2,$ $\min(F_1) = F_1(0,...,0) = 0.$	0.01	$[-100,\ 100]^d$
Schwefel	$F_2(x) = \sum_{i=1}^{d} \lvert x_i \rvert + \Pi_{i=1}^{d} \lvert x_i \rvert,$ $\min(F_2) = F_2(0,...,0) = 0$	0.01	$[-10,\ 10]^d$
Quadric	$F_3(x) = \sum_{i=1}^{d} \left(\sum_{j=1}^{i} \lvert x_i \rvert \right)^2,$ $\min(F_3) = F_3(0,...,0) = 0$	100	$[-100,\ 100]^d$
Rosenbrock	$F_4(x) = \sum_{i=1}^{d} \left\lfloor 100\left(x_{i+1} - x_i^2\right)^2 + (x_i - 1)^2 \right\rfloor,$ $\min(F_4) = F_4(0,...,0) = 0.$	100	$[-10,\ 10]^d$
Step	$F_5(x) = \sum_{i=1}^{d} (\lfloor x_i + 0.5 \rfloor)^2,$ $\min(F_5) = F_5(0,...,0) = 0.$	0	$[-100,\ 100]^d$
Quadric noise	$F_6(x) = \sum_{i=1}^{d} i x_i^4 + random[0,1),$ $\min(F_6) = F_6(0,...,0) = 0.$	0.01	$[-1.28, 1.28]^d$
Rastrigin	$F_7(x) = \sum_{i=1}^{d} \left[x_i^2 - 10\cos(2\pi x_i) + 10 \right],$ $\min(F_7) = F_7(0,...,0) = 0.$	50	$[-5.12, 5.12]^d$
Ackley	$F_8(x) = -20\, exp\left(-0.2 \sqrt{\frac{1}{d}\sum_{i=1}^{d} x_i^2} \right) - exp\left(\frac{1}{d}\sum_{i=1}^{d} cos(2\pi x_i) \right) + 20 + e,$ $min(F_8) = F_8(0,\ldots,0) = 0.$	0.01	$[-32, 32]^d$
Griewank	$F_9(x) = 1/4000 \sum_{i=1}^{d} x_i^2 - \Pi_{i=1}^{d} \cos\left(x_i / \sqrt{i}\right) + 1,$ $\min(F_9) = F_9(0,...,0) = 0.$	0.01	$[-600,\ 600]^d$

Table 2.9: Shifted optimal test function.

Function	Formula	Optimum point	Search range
Shifted Sphere	$F_{10}(x) = \sum_{i=1}^{d} h_i^2 + f_b$	-450	$[-100,\ 100]^d$
Shifted Schwefel	$F_{11}(x) = \sum_{i=1}^{d} \left(\sum_{j=1}^{i} h_j \right)^2 + f_b$	-450	$[-100,\ 100]^d$
Shifted Rosenbrock	$F_{12}(x) = \sum_{i=1}^{d-1} \left(100 \left(h_i^2 - h_{i+1} \right)^2 + \left(h_i - 1 \right)^2 \right) + f_b$	390	$[-100,\ 100]^d$
Shifted Rastrigin	$F_{13}(x) = \sum_{i=1}^{d} \left(h_i^2 - 10\cos(2\pi h_i) + 10 \right) + f_b$	-330	$[-5,\ 5]^d$
Shifted Rotated Ackley	$F_{14}(x) = -20\exp\left(-0.2\sqrt{1/d \sum_{i=1}^{d} h_i^2} \right) - \exp\left(1/d \sum_{i=1}^{d} \cos(2\pi h_i) \right) + 20 + e + f_b$	-140	$[-32,\ 32]^d$
Shifted Rotated Griewank	$F_{15}(x) = \sum_{i=1}^{d} \frac{h_i^2}{4000} - \Pi_{i-1}^{d} \cos\left(\frac{h_i}{\sqrt{i}} \right) + 1 + f_b$	-180	$[0,\ 600]^d$

Figure 2.18: Sample hand images of REST Palm-print database.

Function is multimodal having one global minimum with several local minima. The number of local minima increases exponentially with the issue measurement [166]. The "threshold" esteem (in Table 2.8) to ensure whether a solution would be acceptable or

not. The search behaviour of the hybrid PSO has been tested on the sphere function (in Table 2.8). To evaluate the performance of the proposed method, unimodal and multimodal shifted optimal test functions are generated as listed in Table 2.9. The benchmark functions ought to be minimized which makes particles ready to move to the nearby position of the global optimum. The population distribution of PSO is observed using sphere function.

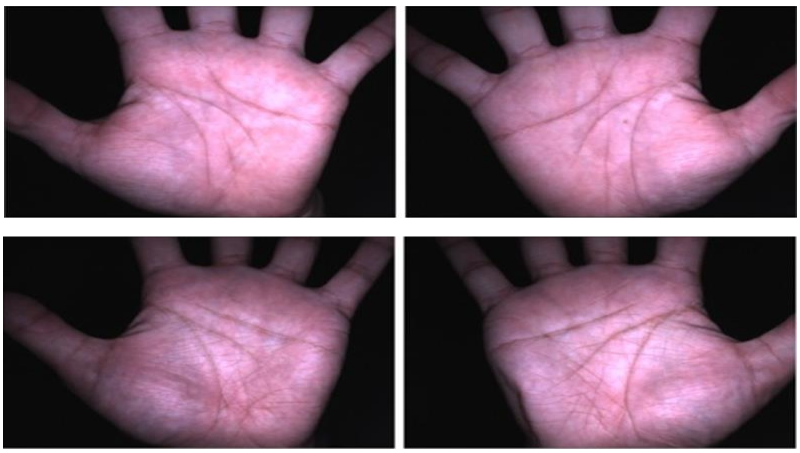

Figure 2.19: Sample hand images of Tongji Palm-print database.

1) **Population distribution:** Figure 2.20 shows the population distribution observed at various stages. The population in initial iteration is conveyed all through the search space without a control center as shown in Figure 2.20(a). The PSO learning behaviour where particles round to the position of the best particle is shown in Figure 2.20(b). The population converges to the best particle after 80 iterations. The elitist learning impacts the performance by aiding the multitude jump out of the neighborhood optima. Observational review shows that value of α is [0.1 1.0] result in good performance on most

of the test functions. During the experiments, δ (Eq. 2.44) taken in [0.05, 0.1].

2) **Evaluation procedure:** The accuracy of the proposed framework is assessed in both the verification and identification modes. For the verification mode, two biometric templates are compared to compute the Euclidean distance. The strategy was applied to the test subset and surveyed the recognition performance. The performance measures recognition rate, sensitivity, specificity and accuracy are considered for evaluating the accuracy of biometric frameworks [19]. CMC curves depicts the identification rate as a component of rank are also used.

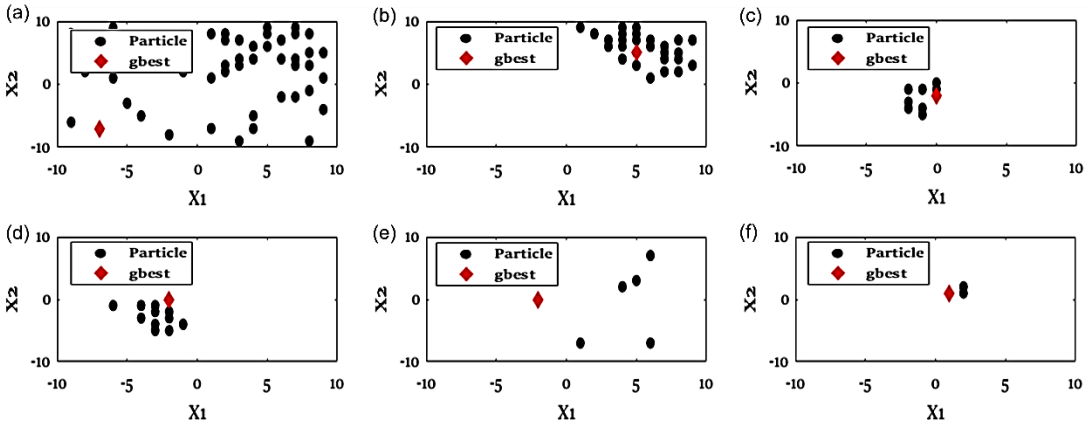

Figure 2.20: Population distribution observed at various stages in a hybrid PSO process for Sphere function.

The strategies in the writing that needn't bother with a training stage were assessed through a similar evaluation procedure. For this, we partition the database using a comparable cross validation procedure.

3) **Comparative analysis:** The recognition rate of the proposed method and state-of-art methods such as Gabor with different scale and orientations, point grouping Gabor and deep learning-based methods as listed in Table 2.10. The proposed method achieves highest recognition rate of 98.79% and 98.21% on Tongji and CASIA databases respectively. The performance measures sensitivity, specificity and accuracy of the present work is compared with state-of-art methods texture based and deep learning-based methods (AlexNet, VGG-16 and VGG-19) are listed in Tables 2.11 to 2.14. Tables 2.11 and 2.12 listed the performance of different methods on CASIA and IIT-Delhi databases respectively.

Table 2.10: Recognition rate (%) for different methods.

Database	**Method**						
	Gabor (3×5)	**Gabor (5×8)**	**PG-Gabor**	**AlexNet**	**VGG-16**	**VGG-19**	**Proposed**
CASIA	89.20	95.89	96.36	98.01	97.50	97.39	98.21
IIT-Delhi	86.78	92.89	93.02	95.29	93.24	94.45	97.01
Tongji	91.89	94.87	95.56	98.04	97.05	96.09	98.79
REST	59.45	61.78	69.23	79.05	70.50	78.45	94.25

Table 2.11: Performance of different methods on CASIA database.

Method	**Measures**		
	Sensitivity (%)	**Specificity (%)**	**Accuracy (%)**
Gabor (3×5)	82.37	84.36	89.23
Gabor (5×8)	89.13	92.14	91.89
PG-Gabor	89.50	91.50	93.52
AlexNet	90.48	95.67	96.23
VGG-16	91.34	94.52	94.74
VGG-19	90.50	92.50	94.20
Proposed	97.01	98.25	97.58

In the similar manner, the performance of different methods on Tongji and REST databases are listed in Tables 2.13 and 2.14 respectively.

Table 2.12: Performance of different methods on IIT-Delhi database.

Method	Measures		
	Sensitivity (%)	Specificity (%)	Accuracy (%)
Gabor (3×5)	79.34	81.36	81.78
Gabor (5×8)	81.13	84.11	85.03
PG-Gabor	85.09	88.54	90.21
AlexNet	88.81	91.64	94.39
VGG-16	90.34	92.03	92.64
VGG-19	89.50	90.58	92.24
Proposed	95.11	97.56	95.83

Table 2.13: Performance of different methods on Tongji database.

Method	Measures		
	Sensitivity (%)	Specificity (%)	Accuracy (%)
Gabor (3×5)	85.76	87.78	92.33
Gabor (5×8)	89.78	94.56	93.92
PG-Gabor	91.54	93.11	93.89
AlexNet	92.86	96.78	97.31
VGG-16	91.34	94.89	95.84
VGG-19	90.81	93.58	94.89
Proposed	98.11	98.91	98.18

Table 2.14: Performance of different methods on REST database.

Method	Measures		
	Sensitivity (%)	Specificity (%)	Accuracy (%)
Gabor (3×5)	68.17	70.11	71.13
Gabor (5×8)	69.31	72.41	73.91
PG-Gabor	81.07	83.51	85.51
AlexNet	86.41	88.64	92.13
VGG-16	89.31	89.12	89.74
VGG-19	88.51	89.56	91.14
Proposed	92.11	94.15	93.81

As shown, the proposed method accomplished the best results on completely thought to be contactless palm-print databases. Specifically, accomplished the highest classification accuracy among the reported methods. Figure 2.21 shows the convergence plot of various methods PSO, Genetic Search Algorithm (GSA)

and the hybrid PSO. The method converges with 100 iterations to find the global optimum. The proposed method exhibits uniform accuracy for all considered databases. Proposed technique achieved an accuracy of 98.18%, sensitivity of 98.11% and specificity of 98.91% because of its capacity to adjust the particular attributes of all databases.

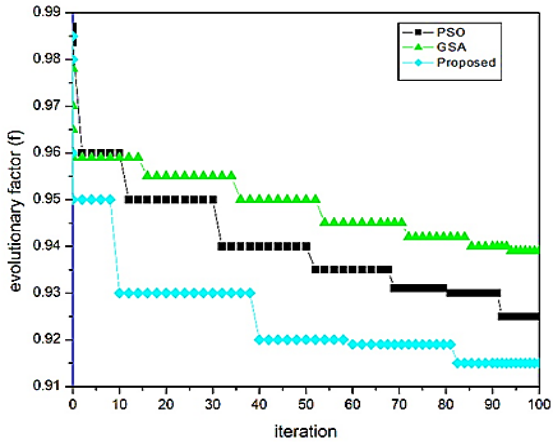

Figure 2.21: Convergence plot of the proposed Hybrid PSO.

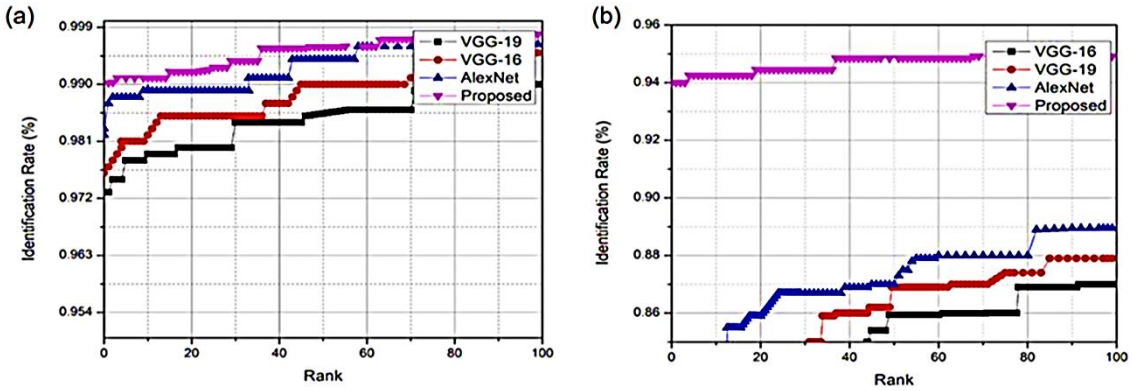

Figure 2.22: CMC curves for the considered databases: (a) CASIA, (b) REST.

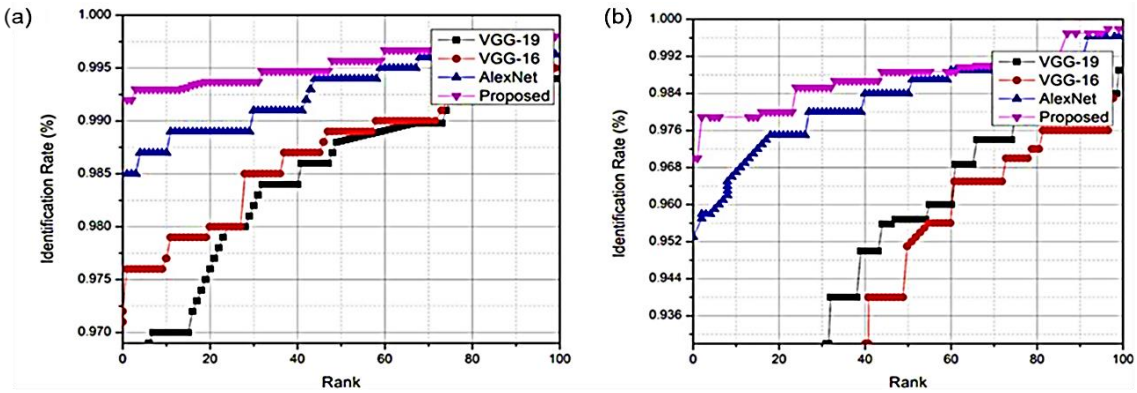

Figure 2.23: CMC curves for the considered databases: (a) Tongji, (b) IIT-Delhi.

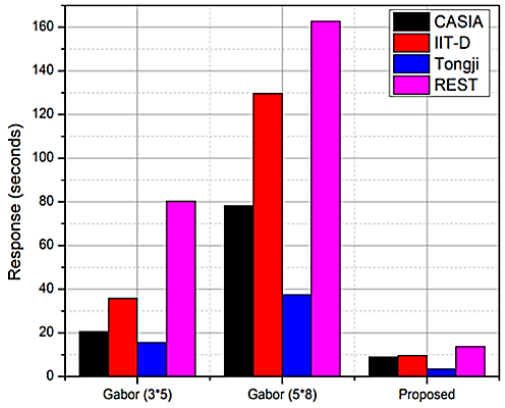

Figure 2.24: Response time (seconds).

Gabor with 3 scale and 8 orientations achieved an accuracy of 92.33% where the Gabor filter with 5 scales with the same orientations achieved an accuracy of 93.92%. The CMC curves shown in Figure 2.22 and Figure 2.23 affirm the better accuracy of the proposed method contrasted with the methods in the writing for all considered databases. The response time of the proposed method is compared

with Gabor filter-based method as shown in Figure 2.24. The figure clearly indicates that the proposed method takes less time for palm-print recognition.

2.7 Conclusion

In this Chapter, we developed palm-print recognition methods using two different Gabor filter-based methods namely Gabor filter with kernel-based full space FDA and Gabor filter with neural network to improve the performance of existing texture descriptors. Firstly, we implemented Gabor filter designed using the parameter estimation. Then, a kernel-based FDA is applied for dimension reduction of the high-dimensional Gabor features. It reduces the computational complexity and feature dimensions. The method yields a high RR of 98.34% and least EER of 0.051% on PolyU database.

Secondly, we design a contactless palm-print recognition method based on the integration of the texture descriptor and evolutionary algorithms. Gabor filter bank is replaced by a single optimal Gabor filter and energy features are extracted. A two-stage hybrid PSO with artificial neural network is applied to optimize the filter parameters. The method can attain better fitness results and prevent premature convergence. The remarkable results of 98.79% recognition rate were obtained. Experimental results shows that the proposed method, significantly outperforms the state-of-art methods.

Chapter 3

Structure based Palm-print recognition: Local binary pattern-based approach

3.1 Introduction

The use of palm-prints for user access and human authentication has increased in the last decade due to its unique and stable characteristics along with rich feature set (large area). In recent past, numbers of algorithms, to extract efficient and accurate features have been proposed. The palm-print features are extracted using coding-based methods including palm code [38], fusion code [43], ordinal code [45], and competitive code [44]. It has been found that using coding-based methods makes it difficult to fully exploit the scale attributes of palm-prints. The existing literature has demonstrated that the orientations of palm lines hold more steady and discriminative features contrasting with magnitude features. Jia et al. [167] proposed histogram of oriented lines (HOL), a variant of histogram of oriented gradients (HOG). Mokni et al. [168] proposed a feature extraction method that extracts the line and geometric features. Texture based approach extract texture features of given palm images. Texture features are not extracted uniformly, due to the variations in scale, orientation or other visual appearance. In the previous chapter Gabor filter-based methods gives satisfactory results but cannot be exploited the specific attributes of the palm-prints for example orientation and scale features, which restricts the palm-print recognition performance.

LBP is a powerful local image descriptor, which extract uniform patterns, is widely used in personal authentication [60].

Using a local distribution of uniform patterns, such as uniform LBP (ULBP), the palmprint recognition method in [61] was developed. Line and wrinkle-like characteristics, a type of homogeneous pattern, can be found in the texture of the palm. It describes a pattern with a consistent appearance and little discontinuities. The PolyU 2D, CASIA, and palmprint databases are used in experiments.

Liao et al. [169] suggest a novel feature extraction method for texture classification. The features are less susceptible to histogram equalization and robust to image rotation. It is characterized by two feature sets: (a) dominant local binary patterns (DLBP) in a texture image and (b) additional features retrieved from circularly symmetric Gabor filter outputs. The dominant local binary pattern technique captures relevant textural information by using the most typically occurring patterns. Gabor-based features strive to provide extra global texture data to the DLBP features. The experiments are conducted Outex, Meastex, CUReT and Brodatz texture image datasets. The suggested method offers the maximum classification accuracy under various image circumstances.

Guo et al. [64] proposed the hierarchical multiscale local binary pattern (HM-LBP), a novel collaborative representation model for palm-print recognition. Non-uniform patterns can be used to extract useful information. Principal component analysis is used to minimise the feature dimension. Then, to properly use the discriminating information, a collaborative classification with HM-LBP is given. To prove its practicality and performance, the suggested algorithm is tested on PolyU database. The results show that the algorithm outperforms existing approaches in terms of recognition accuracy. Gray scale, rotation, and illumination can all be reduced to use this technique.

A modified LBP and weighted SRC combination were suggested as a solution for coarse-to-fine palmprint recognition [65]. By using WACS-LBP, the invariant feature

vector of the local weighted histogram is extracted. The proposed method is therefore resistant to noise, variations in light, and rotation. On the PolyU and CASIA, the proposed method is evaluated and contrasted with the current methods. The choice of parameters imposes restrictions on the procedure. Due to the edge gradient's higher level of consistency compared to pixel intensity, it will perform better to recognize objects using a descriptor based on edge gradient. Therefore, for recognizing faces and expressions, edge gradient will perform better than unique LBP [66]. According to the literature, the approaches covered above were unable to simultaneously exploit discriminant scale characteristics and discriminant orientation features.

Considering the improvement presented by the LBP [60, 65, 69] in extracting palm-print features with good recognition performance, this chapter details the theory of LBP to explore the multiscale edge-oriented palm-print features. Here, we developed a new descriptor named multi-scale edge angles LBP (MSEALBP) for palm-print recognition. Sobel vertical and horizontal edges of the ROIs have been used to produce the edge angle images. Then, a local binary pattern having multiple scales (MSLBP) is employed to the Sobel edge angle images. The resulting characteristics are formed into non-overlapping blocks and statistical calculations are implemented to form a texture vector. The method uses an optimal technique that improves the accuracy of the classifier by tuning the network parameters. The extracted texture features are applied as an input to the artificial neural network (ANN). Levenberg–Marquardt is employed to develop an optimized network. The ANN structure is optimized to find out network parameters. The method has great generalization capacity and less training cost. In addition, new information can be added whenever without the need to re-train the whole network. PolyU [132], IIT-Delhi [134] and CASIA [133] palm-print databases are considered to validate the performance of our method. Comparative experiments were carried out to exhibit the accuracy of the proposed approach. Its high discrimination capacity and effortlessness in calculation have made it truly appropriate for online recognition framework.

3.2 Local binary pattern (LBP)

Ojala et al. [60] originally proposed the standard LBP as a texture descriptor that measures neighbourhood evaluation in texture analysis finds microtextons in a surrounding area. Figure 3.1 shows an example of LBP code. By comparing nearby pixels with the pixel in the center of them, a binary pattern is created [62].

The following is the definition of the LBP operator:

$$LBP_{R,P}(x_C) = \sum_{n=0}^{P-1} 2^n S(x_{R,P,n} - x_c) \tag{3.1}$$

$$S(x) = \begin{cases} 1, & x \geq 0 \\ 0, & x < 0 \end{cases} \tag{3.2}$$

Where, x_c is the gray value of the central pixel, $x_{R,P,n}$ is the value of its Pth neighbor, P is the number of associated neighbors, while R is the neighborhood's radius.

LBP is limited by some inherent problems such as gray-scale and rotation variant, non-directional patterns, and sensitive to certain texture patterns.

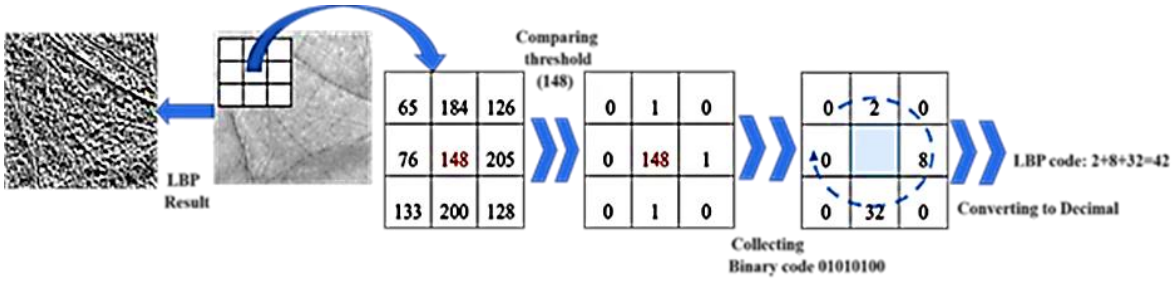

Figure 3.1: Example of LBP [62] computation for a 3×3 window.

A gray-scale and rotation invariant texture operator based on LBP i.e. Multi-scale LBP was proposed to enhance the LBP features [170]. It uses circular neighborhood pixels

having dissimilar spatial sampling P and different radius value R. Figure 3.2 shows LBP with different (P, R) sets.

The MSLBP is computed as given in Equation (3.3)

$$LBP_{P,R}^{MS} = \sum_{P=0}^{P-1} S(g_p - g_c) \times 2^p \tag{3.3}$$

The multi-scale LBP is sensitive to certain pattern of texture features and also produce non-directional patterns.

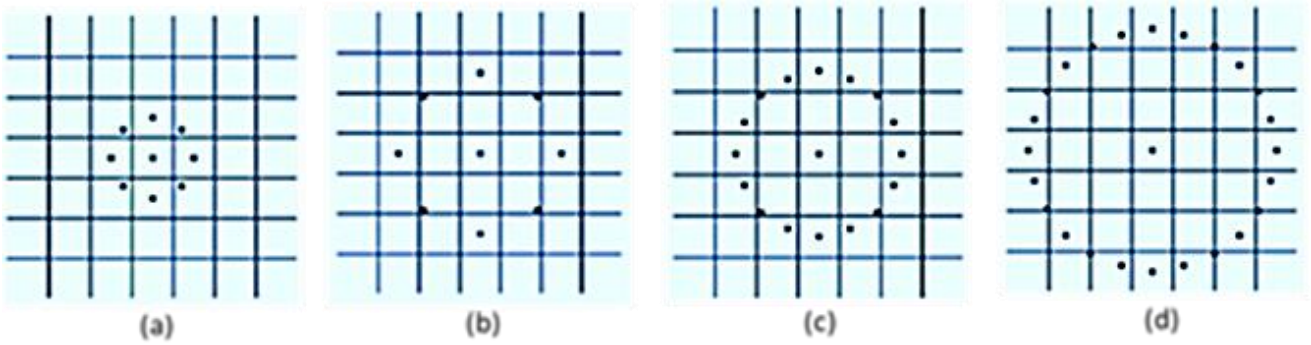

Figure 3.2: Representation of LBP with different (P, R) sets [170] (a) (P=8, R=1), (b) (P=8, R=2), (c) (P=16, R=2),(d)(P=24, R=3).

Certain LBP patterns were discovered to form the basic textural microstructures, and these patterns named as uniform patterns.

$$U(LBP_{R,P}) = \sum_{n=0}^{P-1} \left| S(x_{R,P,n} - x_c) - S(x_{R,P,mod(n+1,P)} - x_c) \right| \tag{3.4}$$

By organizing uniform patterns into $p + 1$ different categories, Ojala et al. [170] presented a rotation invariant uniform descriptor as follows:

$$LBP_{R,P}^{RIU2} = \begin{cases} \sum_{n=0}^{P-1} S(x_{R,P,n} - x_c), & if \quad U(LBP_{R,P}) \leq 2 \\ P+1, & else \end{cases} \tag{3.5}$$

To improve the discriminative power of LBP, Guo et al. [171] developed Completed LBP (CLBP). The central pixel has the following encoding:

$$d_P = x_{R,P} - x_c \tag{3.6}$$

$$\chi_p = s(x_{R,P} - x_c)$$

$$A_P = |d_P|$$

$$A_P = |x_{R,P} - x_c|$$

$$CLBP_{R,P} = \sum_{n=0}^{P-1} 2^n S(A_P - u) \tag{3.7}$$

$$CLBP\_C_{R,P} = S(x_c, C_F) \tag{3.8}$$

Where, d_P characterizes the image local structure at central point, A_P is the magnitude component. u is a threshold and here set as the mean value of A_P from the whole image.

3.3 Motivation

1. The texture descriptor discussed are unable to successfully exploit the advantages provided by discriminant orientation features and the discriminant scale features simultaneously.
2. The majority of texture descriptors are concerned with encoding local intensity variations between a center pixel and its sample points. They can't explain the intensity ordering between adjacent sample points. Also they can't detect long-

range pixel relationships outside of a compact region. The issue of learning robust and discriminative characteristics for palm-print recognition remains a fascinating and demanding topic.

3.4 Implementation of proposed approach using multi scale edge angles LBP (MSEALBP)

This section elaborates the proposed multi-scale palm-print recognition process. The block diagram of the proposed scheme is shown in Figure 3.3. The first step is preprocessing, which extracts aligned and stable ROI from input palm-print images. The resulting ROI images are filtered with Sobel gradient operator in both vertical and horizontal directions to produce directional angle images. The directional angle images are, then passed through multi-scale LBP to produce uniform patterns of palm-prints. The uniform images are divided into non-overlapping blocks of size 5×5 pixels. Then, coefficient of variation (CV) value of each block is computed. Further, the CV values of each block are concatenated to form a 1-D vector for a palm-print. Then, the resulting vector is feed as an input into the ANN [32]. PSO is utilized to find out network parameters.

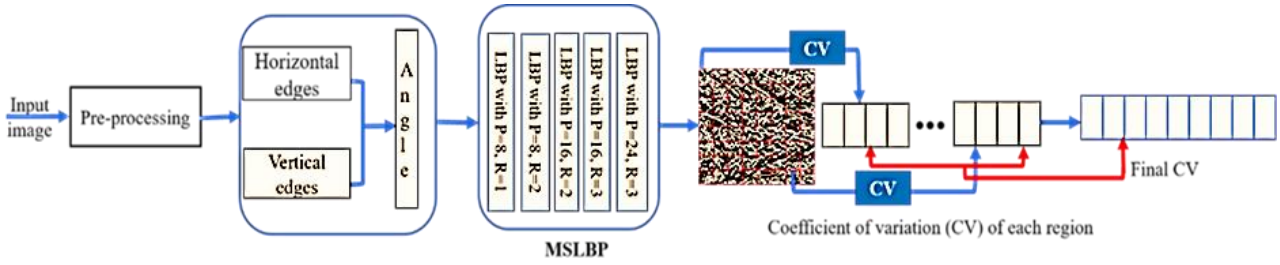

Figure 3.3: The block diagram of the proposed scheme.

3.4.1 Proposed Multi-scale edge angles LBP (MSEALBP)

Multi-scale edge angles LBP is proposed to extract effective features of palm-prints. It produces uniform patterns as well as gray-scale and rotation invariant texture information. Due to the utilization of phase information, it produces less sensitive directional patterns to the pixel level values. Firstly, the ROI image is filtered with gradient operator mask such as Robert, Prewitt and Sobel in both horizontal and vertical directions. The magnitude and phase information can be computed by fusing horizontal and vertical operators as given in equation (3.9) and (3.10).

$$|G| = \sqrt{G_x^2 + G_y^2} \tag{3.9}$$

$$\theta = a\,tan\,2\left(G_y, G_x\right) \tag{3.10}$$

where $|G|$ is the gradient magnitude, θ represents angle direction and $atan2$ represents the 4-quadrant inverse as discussed in [172].

The gradients of certain patterns are described more effectively with less sensitivity to the pixel values by angle features than magnitude features. The magnitude can be effected by noise, brightness and range problems [173]. Also, the directional information produced by the magnitude calculation is not robust as in angle calculation [174]. Hence, the angle direction of the Sobel operator can be designed to achieve consistent performance. Figure 3.4 shows Sobel horizontal operator and Sobel vertical operator. The experimental results proves that the angle direction gives better results as compared to the magnitude. Figure 3.5 shows the resulting sample images of the proposed MSEALBP.

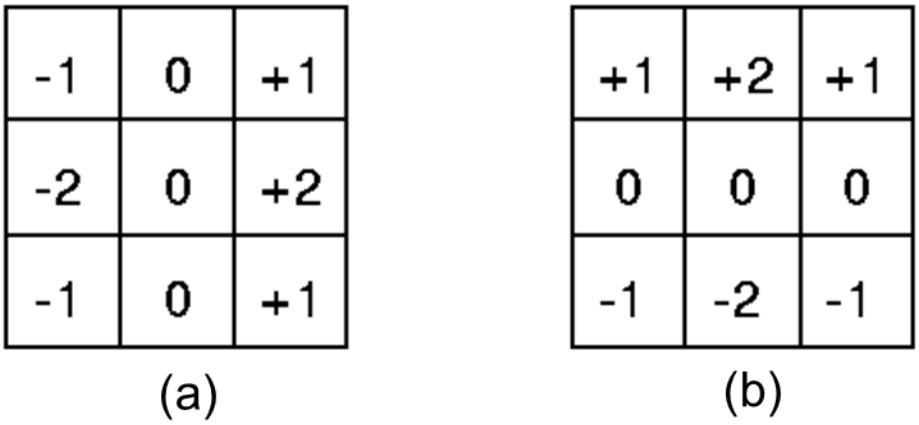

Figure 3.4: Sobel operator mask [174] (a) horizontal operator, (b) vertical operator.

Equation (3.3) has been modified to calculate proposed MSEALBP on the edge angle direction as follows:

$$LBP_{P,R}^{MSEA} = \sum_{P=0}^{P-1} S(gt_p - gt_c) \times 2^p,\ S(gt_p - gt_c) = \begin{cases} 1, & gt_p \geq gt_c \\ 0, & gt_p < gt_c \end{cases} \quad (3.11)$$

where, gt_p and gt_c are the p^{th} neighbor pixel value and the center pixel value of each sub-block after applying Sobel angle direction images respectively.

The proficiency of the proposed approach is evaluated by using different values of P and R of palm-print patterns. Before, the blocking operation, the pixels of the ROI image are allocated with the values of MSEALBP of each palm-print. The extracted images will be divided into non-overlapping blocks. Equation (3.12-3.14) are used to compute Coefficient of variation values of each block.

$$M_{bl} = \frac{1}{n}\sum_{i=1}^{n} bl_i \quad (3.12)$$

$$STD_{bl} = \sqrt{\frac{1}{n-1}\sum_{i=1}^{n}(bl_i - M_{bl})^2} \tag{3.13}$$

$$CV_{bl} = \frac{STD_{bl}}{M_{bl}} \tag{3.14}$$

Where n is the number of pixels in each block, bl is the block size here it is 5×5 pixels, M_{bl} refers to average of block pixels, i is the pointer of pixels in a block, STD_{bl} is standard deviation and CV_{bl} is the coefficient of variation. The CV values of palm-prints will be concatenated to form a 1-D vector for further classification stage. The 1-D feature vector is feed as an input to the classification algorithm.

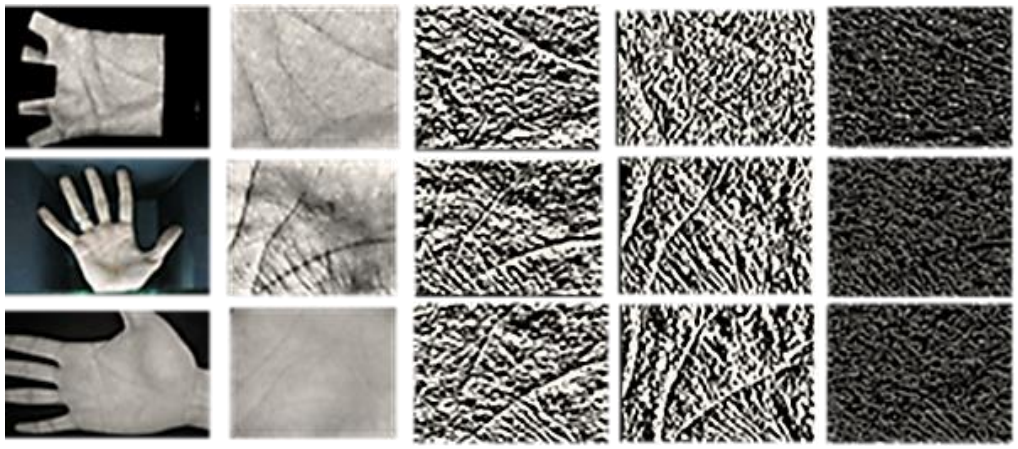

Figure 3.5: Multi-scale edge angle LBP operator results: Each row shows a palm-print; from the Top; PolyU palm-print, IIT-Delhi hand im-age, CASIA palm-print databases respectively. Each column depicts; from the left: original palm images, the ROI extracted images, horizontal edge images, vertical edge images, Multi-scale LBP of the angle images respectively

Within the customary classifiers, network structure is taken into account to be fixed and known to be as un-optimized network structure [175]. The accuracy of a fixed network structure depends on the network parameters: (a) number of hidden layers (HL_n), (b)

number of neurons in each hidden layer (NHL_n). These parameters are not defined properly, which results poor accuracy for some categories [176]. This work uses an optimization technique that improves the accuracy of the classifier by tuning the network parameters. Levenberg–Marquardt [177] is employed to develop an optimized network. The ANN structure is optimized to find out number of hidden layers and number of neurons in each hidden layer. The PSO optimization technique is used and then palm-print classification is carried.

In this work, PSO is effectively employed to get optimal values of (HL_n) and (NHL_n) of the neural structure to maximize the fitness function (accuracy). The updated velocity of the PSO is computed from Eq. (2.25) and the updated particle position is computed from Eq. (2.26).

The inertia weight $w(t)$ manages the contribution of the previous velocity. During the experiment, 60% samples are used to minimize the error function by adjusting weight vector and reaming samples are used for testing.

The steps of the ANN with PSO are given as follows:

Step 1. Initialize parameters

Maximum iteration (I_{max})= 500, population size (p_s) = 30, a_1=1.5, a_2=2 and w =1.

Initialize two parameters number of hidden layers (HL_n) and number of neurons in each hidden layer (NHL_n) as

$(HL_n)_{min}= 1, (HL_n)_{max}= 10, (NHL_n)_{min}= 1, (NHL_n)_{max}= 50;$

Step 2. Initialize population

HL_n value= randi$((HL_n)_{min}, (HL_n)_{max})$;

NHL_n value= randi$([(NHL_n)_{min}, (NHL_n)_{max}], [1, HL_n])$

Step 3. Fitness computation

Update particles best position as

$p_b\,(t) = p\,(t)$; bestfitness (t) = fitness; bestnet (t) = net;

Update global best: $if(bestfitness\,(t) > g_b(t)), g_b(t) = bestfitness\,(t)$;

Step 4. Update velocity as given in Eq. (2.25)
Update position as given in Eq. (2.26)
Update best position as $p_b(t)\ if\ (fitness < prefitness)$;

Update global best with maximum iteration as $p\,(t)$.

$fitness = max(Accuracy)$;

Step 5. Repeat step 4 until $iteration \leq maximum\ iteration$.

3.4.2 Experimental results and discussion

The proposed framework is validated on three different large-scale publicly accessible palm print databases viz. (a) PolyU palm-print, (b) CASIA palm-print and (c) IIT-Delhi palm-print.

The sample hand images of PolyU and CASIA databases are shown in Figure 3.6 and Figure 3.7 respectively. In Figure 3.8 sample hand images of IIT- Delhi database is depicted. In the experimental setup of proposed method, primarily 60% images are used for training and remaining images are used for testing for all the three databases. There is no overlap in training and testing samples.

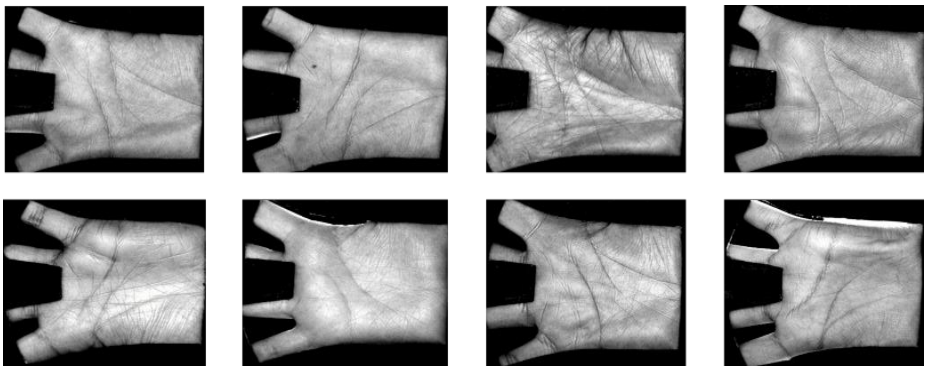

Figure 3.6: Hand images (PolyU database).

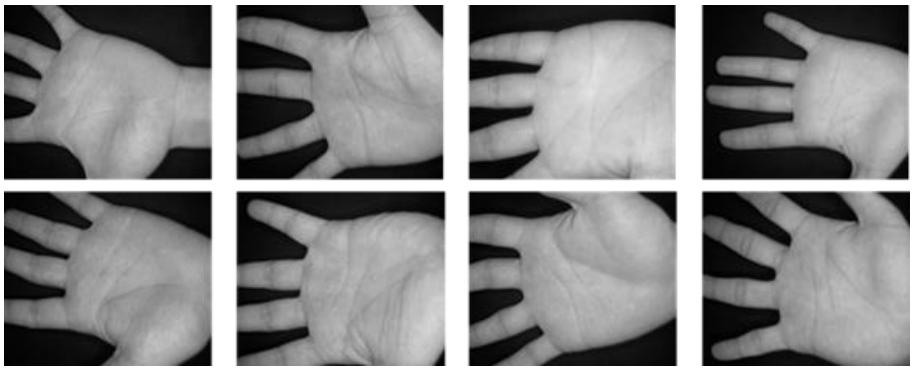

Figure 3.7: Hand images (CASIA database).

The ROI extracted images of PolyU and CASIA databases are shown in Figure 3.9 and Figure 3.10 respectively. Figure 3.11 shows the sample ROI images of IIT-Delhi database.

Various edge analysis techniques such as Roberts, Prewitt and Sobel have been examined on the three palm-print databases to decide the gradient operator for filtering the ROIs. The summary of parameters used in the proposed method is listed in Table 3.1.

Figure 3.8: Hand images (IIT-Delhi database).

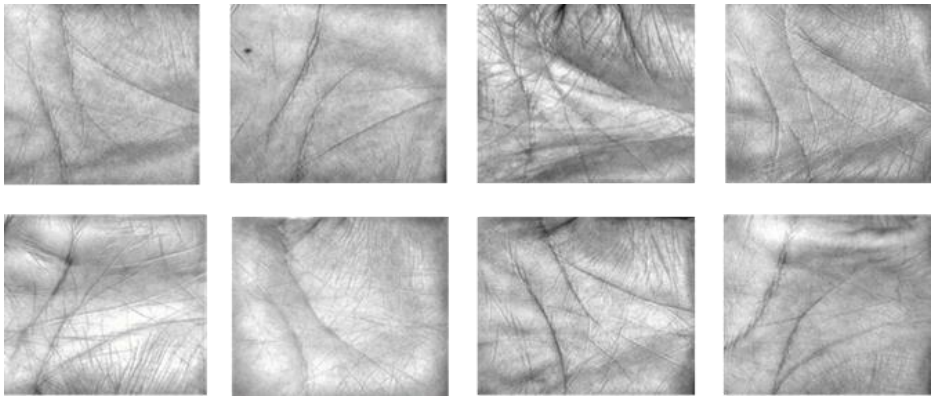

Figure 3.9: ROI images (PolyU database).

After extracting the ROI using preprocessing, Sobel horizontal and vertical edges operator are applied on the ROI images to compute the magnitude and angle.

As the mask weights of Sobel operator is higher than the Robert and Prewitt it discloses the key palm-print features in better fashion [62]. Table 3.2 shows the comparison of EER for magnitude and angle of different edge detection methods. The EER for the PolyU database was diminished from 2.79% using the magnitude to 0.26% with the angle and for IIT-Delhi database from 4.01% to 3.25%.

Also, EER was decreased from 5.11% using the magnitude to 2.76% with the angle for CASIA database. The performance of angle in terms of EER is better than magnitude as magnitude is easily effected by the illumination, imagining contrast and camera gain of an image. Furthermore, Sobel angular approach utilizes the ratio of the outputs of vertical and horizontal operators, resulting in producing effective information by angle patterns in comparisons to magnitude patterns. The results of Sobel are better than Prewitt, because Sobel is less effected by image contrast in comparisons to Prewitt. The EER for PolyU database was diminished from 1.31% using the magnitude to 1.05% with the angle for the Prewitt operator. Prewitt and Sobel operations utilize both horizontal and vertical edges, while Robert considered only diagonal edges.

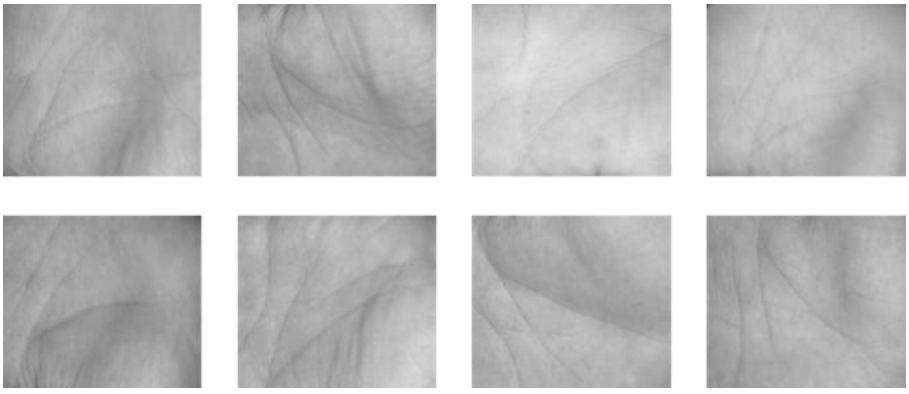

Figure 3.10: ROI images (CASIA database).

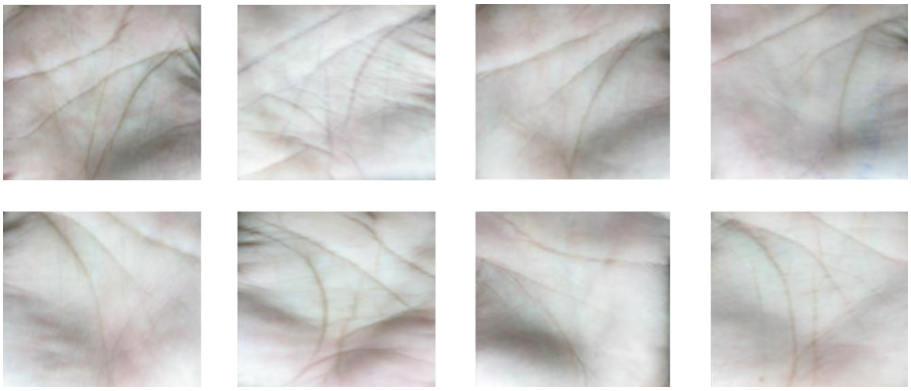

Figure 3.11: ROI images (IIT-Delhi database).

The EER for PolyU database was increased from 1.53% using magnitude to 2.19 % with the angle and from 8.19% to 9.28% for the IIT-Delhi database for Robert operator.

Table 3.1: Summary of the parameters of the optimized neural network.

Parameters	**Value**
Population Size, p_s	30
accelerating coefficients	$a_1 = 1.5, a_2 = 2$
inertia weight w	$w_{min} = 0.4, w_{max} = 0.9$
Number of maximum iterations (I_{max})	500
number of hidden layers (HL_n)	5
number of neurons in each hidden layer (NHL_n)	21, 7, 10, 3, 30
Range of (HL_n)	$(HL_n)_{min} = 1, (HL_n)_{max} = 10$
Range of (NHL_n)	$(NHL_n)_{min} = 1, (NHL_n)_{max} = 50$

Table 3.2: Comparison of EER for magnitude and angle of different edge detection methods.

Database	**EER**					
	Roberts		**Prewitt**		**Sobel**	
	Magnitude	Angle	Magnitude	Angle	Magnitude	Angle
PolyU database	1.53 %	2.19%	1.31%	1.05%	2.79%	0.26%
CASIA Database	8.45%	8.34%	3.98%	7.45%	5.11%	2.76%
IIT-Delhi database	8.19 %	9.28%	4.18%	4.17%	4.01%	3.25%

Multi-scale LBP (MSLBP) as discussed in section 3.4.1 is applied on the resulting Sobel edge angle images to obtain the uniform patterns of palm-prints. The MSLBP is tested for different values of neighbor Pixel (P) and Radius (R) on PolyU, CASIA and IIT-Delhi palm-print databases for Robert, Prewitt and Sobel operators as listed in Table 3.3, 3.4 and 3.5 respectively. The best recognition performance in terms of EER is achieved using the Sobel angles LBP with a multi-scale parameter of P=8 and R=2 for all three palm-print databases. The percentage EER achieved for P=8, R=2 is 0.26%, 2.76% and 3.25% on PolyU, CASIA and IIT-Delhi databases respectively. As the number of neighboring pixels (P) relates to the amount of processed information, increasing its value will increase the redundant information processed. Similarly, increasing the value of radius (R) greater than 2 will cause a loss of the micro texture information while decreasing the value of R less than 1 will incorporate the miniature surfaces and the implanted noise also.

Table 3.3: Comparison of EER for different values of neighbor pixels (P) and radius (R) of various edge detection methods on PolyU database.

Parameters		**EER**					
		Roberts		**Prewitt**		**Sobel**	
		Magnitude	Angle	Magnitude	Angle	Magnitude	Angle
P=8	R=1	1.98%	2.78%	2.01%	1.67%	3.02%	1.01%
	R=2	1.53 %	2.19%	1.31%	1.05%	2.79%	0.26%
P=16	R=2	1.88%	2.95%	2.56%	2.01%	2.99%	1.11%
	R=3	2.88%	3.67%	4.12%	3.09%	4.37%	2.59%
P=24	R=3	3.78%	4%	4.79%	3.74%	4.99%	3.58%

Table 3.4 Comparison of EER for different values of neighbor pixels (P) and radius (R) of various edge detection methods on CASIA database.

Parameters		**EER**					
		Roberts		**Prewitt**		**Sobel**	
		Magnitude	Angle	Magnitude	Angle	Magnitude	Angle
P=8	R=1	8.89%	9.88%	4.01%	8.63%	6.09%	4.78%
	R=2	8.45%	8.34%	3.98%	7.45%	5.11%	2.76%
P=16	R=2	8.81%	9.95%	4.68%	9.01%	5.45%	4.51%
	R=3	9.08%	10.67%	6.02%	9.78%	7.37%	5.09%
P=24	*R=3*	10.78%	10.87%	9.79%	9.94%	7.46%	7.76%

Table 3.5 Comparison of EER for different values of neighbor pixels (P) and radius (R) of various edge detection methods on IIT-Delhi database.

Parameters		EER					
		Roberts		Prewitt		Sobel	
		Magnitude	Angle	Magnitude	Angle	Magnitude	Angle
P=8	R=1	8.77%	9.08%	5.96%	5.06%	5.02%	4.01%
	R=2	8.19 %	9.28%	4.18%	4.17%	4.01%	3.25%
P=16	R=2	8.56%	9.95%	5.98%	5.69%	4.93%	4.89%
	R=3	9.11%	10.01%	7.78%	7.09%	6.30%	5.09%
P=24	R=3	10.14%	10.99%	9.23%	7.23%	6.99%	6.58%

To obtain CV, the resulting uniform images obtained from MS-LBP are divided into N×N non-overlapping blocks. The performance of the proposed framework is analyzed over the different block size of 3×3, 5×5, 7×7, 9×9, 11×11, 13×13and 15×15 on all three palm-print database as shown in Figure 3.12.

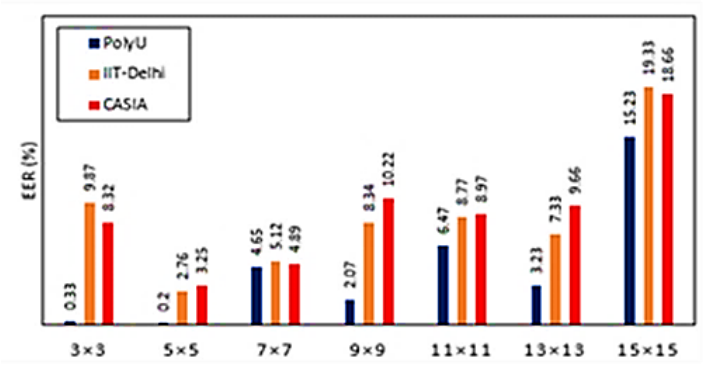

Figure 3.12: EER (%) of proposed method for different block sizes.

The best recognition performance is achieved for the block size of 5×5, as from the experiment it is observed that by changing impeding size to more than or not exactly the reasonable size, raises the error rate. The best EER value is obtained with a block size of 5×5 is 0.26 % and 2.76% and 3.25% for PolyU, CASIA and IIT-Delhi palm-print databases respectively.

Table 3.6 shows the performance of the suggested neural network structure in terms of accuracy, sensitivity and specificity. The method yields an accuracy of 98.52%, specificity of 98.60% and sensitivity of 92.50% for P=8, and R=2. In the similar manner, CASIA and IIT-Delhi databases generates an accuracy of 97.85% and 95.32% respectively.

The CMC curves are created by collecting the viable ANN yield esteems from the summation layer and remapping these qualities as per the ANN characterizations [178]. Comparison of CMC curve of the proposed method with other methods such as LBP, LDP, DGLBP, HOL, VGG-16 and VGG-19 on PolyU palm-print databases is shown in Figure 3.13. For CASIA and IIT-Delhi database, the comparative CMC curve are shown in Figure 3.14 and 3.15 respectively. The method is compared with the existing methods discussed in literature and yields better performance in terms of EER and accuracy. Table 3.7 listed the percentage EER comparison of the proposed method with existing method. Directional gradient LBP (DGLBP) proposed by Michael et al. [62] gives an EER of 1.52%, 6.45% and 8.34% on PolyU, CASIA and IIT-Delhi databases respectively. Neural network-based method VGG-16 and VGG-19 yields EER of 5.14% and 5.29% respectively.

Table 3.6: Performance of LBP with different (P, R) sets.

Database		**Parameter**				
		(P=8, R=1)	**(P=8, R=2)**	**(P=16, R=2)**	**(P=16, R=3)**	**(P=24, R=3)**
PolyU	Specificity (%)	94.52	98.60	91.50	91.89	92.14
	Accuracy (%)	94.74	98.52	93.32	90.34	91.89
	Sensitivity (%)	91.34	92.50	89.50	86.37	89.13
CASIA	Specificity (%)	96.00	98.73	95.71	93.45	87.15
	Accuracy (%)	93.68	97.85	92.31	89.56	83.76
	Sensitivity (%)	90.48	94.14	89.86	85.24	80.13
IIT-Delhi	Specificity (%)	95.62	96.88	95.34	89.02	89.29
	Accuracy (%)	93.62	95.32	92.12	86.29	88.12
	Sensitivity (%)	88.84	89.75	89.13	82.14	84.12

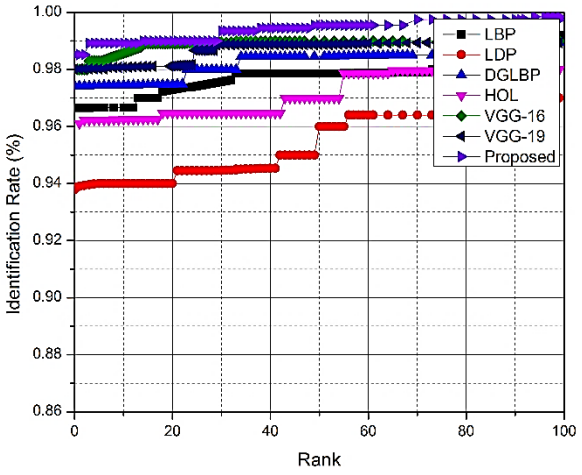

Figure 3.13: CMC curve comparison performance of different methods with proposed one on PolyU database.

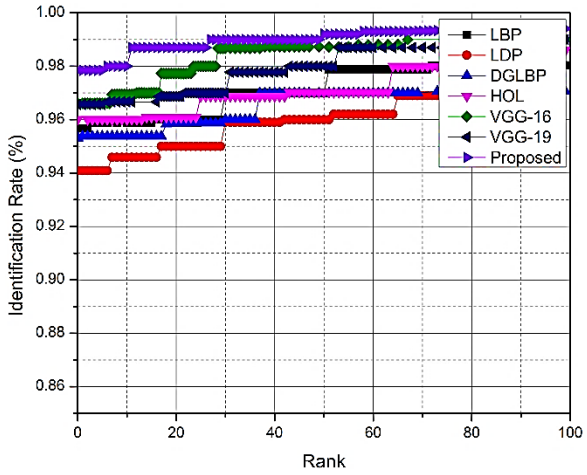

Figure 3.14: CMC curve comparison performance of different methods with proposed one on CASIA database.

The best recognition performance is observed for the proposed method with percentage EER as 0.26%, 2.76% and 3.25% on PolyU, CASIA and IIT-Delhi databases respectively. The proposed method drives better results as it produces uniform patterns and rotation invariant texture information, which enhances the performance.

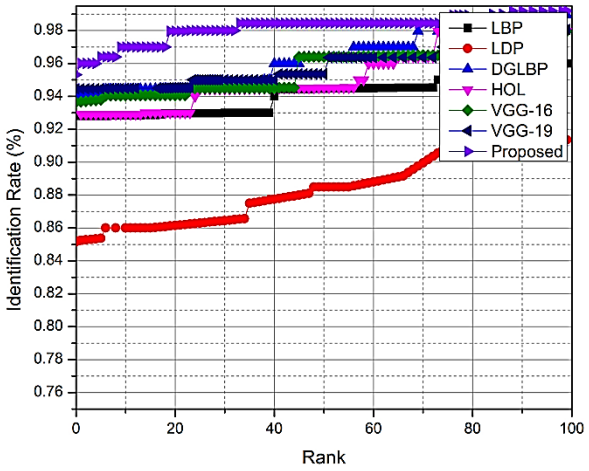

Figure 3.15: CMC curve comparison performance of different methods with proposed one on IIT-Delhi database.

Table 3.7: EER (%) of the proposed method compared with existing methods.

Reference	Method	EER (%)		
		PolyU	IIT-Delhi	CASIA
Wang et al. [189]	Local binary pattern (LBP)	2.12	10.79	4.37
Jabid et al. [190]	Local directional pattern (LDP)	3.45	11.87	4.84
Michael et al. [62]	Directional gradient LBP (DGLBP)	1.52	8.34	6.45
Jia et al. [167]	HOL	3.98	6.70	4.62
Tarawneh et al. [179]	VGG-16	5.14	7.44	7.86
	VGG-19	5.29	7.75	7.84
Proposed	Multi-scale Sobel Angles LBP with (P=8, R=1)	1.01	4.01	4.78
	Multi-scale Sobel Angles LBP with (P=8, R=2)	0.2	3.25	2.76
	Multi-scale Sobel Angles LBP with (P=16, R=2)	1.11	4.89	4.51
	Multi-scale Sobel Angles LBP with (P=16, R=3)	2.59	5.09	5.09
	Multi-scale Sobel Angles LBP with (P=24, R=3)	3.58	6.58	7.76

A comparative analysis of the proposed framework with the state-of-art methods is tabulated in terms of accuracy is listed in Table 3.8. Tarawneh et al. [179] proposed neural network-based methods that yields an accuracy of 98.12% for VGG-16 and 98.02% for VGG-19. The accuracy of the proposed classifier is 98.52% for PolyU database, 97.85% for CASIA database and 95.32% for IIT-Delhi database.

The descriptor based on edge gradient will give preferable recognition performance because the edge gradient is more consistent than the pixel intensity. The edge gradient will give better outcomes over unique LBP for face and expression acknowledgment [177]. Hence, the performance of the proposed method is better in terms of EER is 0.26% and accuracy of 98.52% on the PolyU database.

Table 3.8: Accuracy (%) of the proposed method compared with existing methods.

Reference	Method	Accuracy (%)		
		PolyU	IIT-Delhi	CASIA
Wang et al. [189]	Local binary pattern (LBP)	96.65	92.81	95.67
Jabid et al. [190]	Local directional pattern (LDP)	93.78	85.16	94.09
Michael et al. [62]	Directional gradient LBP (DGLBP)	97.41	94.04	95.29
Jia et al. [167]	HOL	96.11	92.90	96.01
Tarawneh et al. [179]	VGG-16	98.00	93.64	96.61
	VGG-19	98.02	94.45	96.57
Proposed	Multi-scale Sobel Angles LBP with (P=8, R=1)	94.74	93.62	93.68
	Multi-scale Sobel Angles LBP with (P=8, R=2)	98.52	95.32	97.85
	Multi-scale Sobel Angles LBP with (P=16, R=2)	93.32	92.12	92.31
	Multi-scale Sobel Angles LBP with (P=16, R=3)	90.34	86.29	89.56
	Multi-scale Sobel Angles LBP with (P=24, R=3)	91.89	88.12	83.76

3.5 Implementation of proposed approach using LBP and multi feature learning

The contactless database includes posture, translation, and scale variations, making palm-print detection more understandable and reliable [180]. Because of the COVID-19 outbreak, most contact-based biometric recognition systems have become inconvenient due to hygiene concerns. Contactless palm-print recognition frameworks enable persons to achieve high accuracy through less obligatory and extremely useable ways that do not require the palm to make touch with a surface. In existing literature, various methods have been proposed for palm-print recognition [59]. Texture is an essential characteristic of many kinds of images.

Retrieving discriminative yet stable texture features is difficult due to extensive texture patterns and uncertain imaging circumstances [10, 53, 54, 60]. The majority of texture descriptors are concerned with encoding local intensity variations between a center pixel and its sample points. They can't explain the intensity ordering between adjacent sample points. They can't detect long-range pixel relationships outside of a compact region. The issue of learning robust and discriminative characteristics for palm-print recognition remains a fascinating and demanding topic. The method has been evaluated on four contactless palm-print databases with images of varying quality and resolution.

3.5.1 Proposed multi feature learning

Here, we developed an encoding scheme of multi-view feature learning based on robust texture description. Two complementary robust operators, one with dominating directional pattern (DP) and the other with the texture patterns (TP), extract multi-view information simultaneously. The DP and TP are combined via central pixel encoding to construct data vectors. Further, we learn feature mapping to project the multi-view data into hash codes. The pipeline of the proposed framework is illustrated in Figure 3.16.

1) **Directional Patterns (DP):** Our operator is primarily concerned with ranking approaches that are insensitive to monotonic photometric modifications. For each central pixel, the proposed operator uses neighbourhood ordinal data to describe the intensity connections between nearby sample locations [181, 89]. Figure 3.17 shows the proposed descriptor.
    - **Dominant direction encoding:** Given an image F having a central pixel x, calculate the average grey values of local image

regions in the vicinity of the central pixel and nearby sample points:

$$\eta_{R,P} = \lambda\left(B_{P,R,m}\right) \tag{3.15}$$

Further, the nearby sample points are rotated in relation to their dominating direction. The location of the sample point well with highest grey difference nearer to the center pixel is regarded the dominant direction [182].

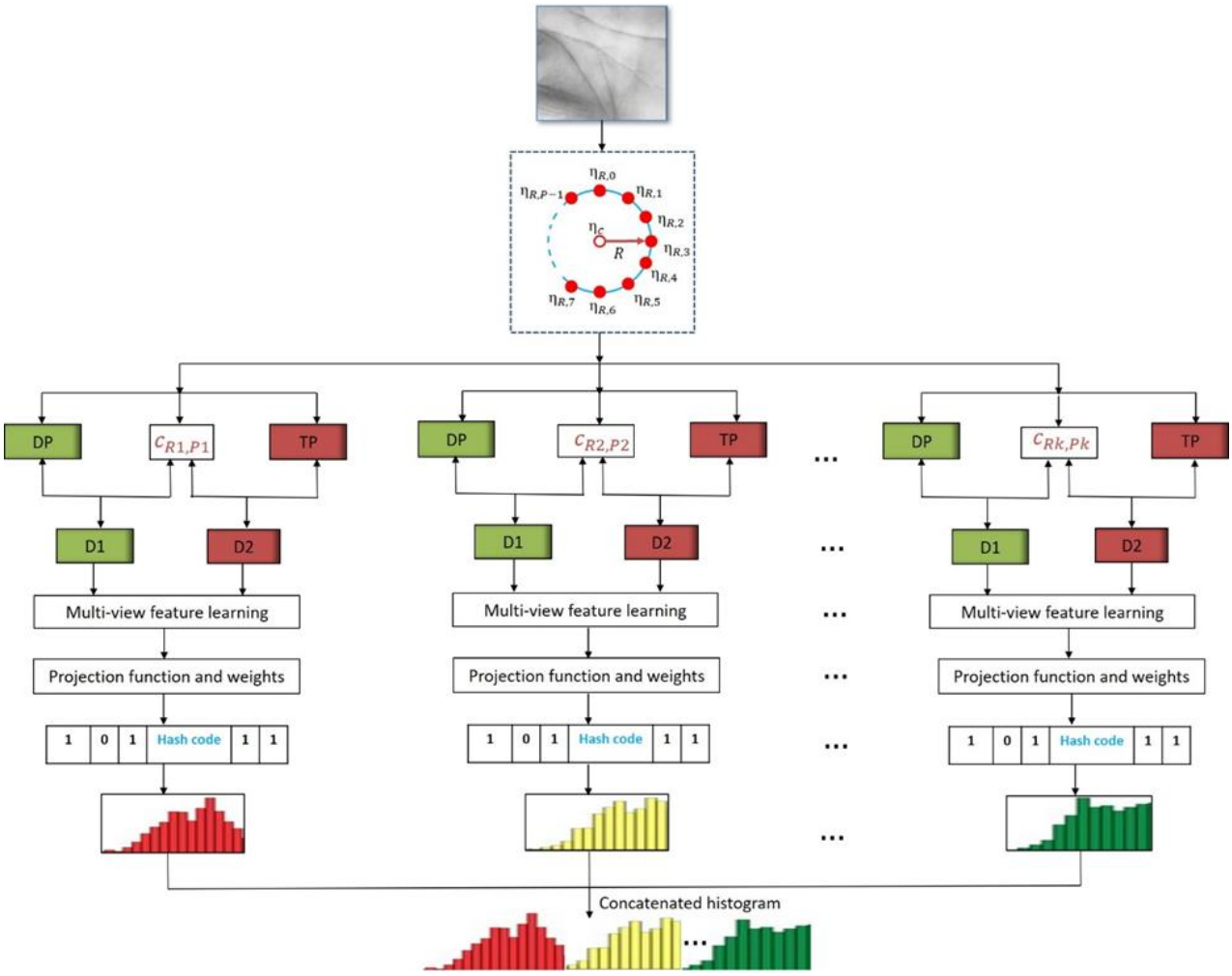

Figure 3.16: Representation of the proposed methodology.

$$\eta_c = \lambda(B_{c,m}) \tag{3.16}$$

$$(\eta'_{0,R}, \ldots, \eta'_{P-1,R}) := (\eta_{\varphi,R}, \ldots \eta_{P-1,R}, \eta_{0,R}, \ldots, \eta_{\varphi-1,R}) \tag{3.17}$$

- **Encoded features:** Upon establishing the dominant direction, the sampling sequence is rotated in a circle till the point labeled by φ is presented from the first position:

$$\varphi = \max_{0 \le P < P-1} |\eta_{P,R} - \eta_c| \tag{3.18}$$

The points in the rotational sample sequence are then evenly divided into numerous groups. Each group points are evenly spread around the circle. To achieve lower dimensions of coded characteristics, we reduce the number of points for each group to four, makes a total of $l = {}^{P}/_{4}$ categories for each sample sequence.

$$\eta'_i = \begin{cases} (\eta'_{0,R}, \eta'_{l,R}, \eta'_{2l,R}, \eta'_{3l,R}), & i = 1 \\ (\eta'_{1,R}, \eta'_{l+1,R}, \eta'_{2l+1,R}, \eta'_{3l+1,R}), & i = 2 \\ \vdots & \vdots \\ (\eta'_{l-1,R}, \eta'_{2l-1,R}, \eta'_{3l-1,R}, \eta'_{P-1,R}), & i = l \end{cases} \tag{3.19}$$

Furthermore, in each group, we preserve the intensity order connections between surrounding sampling points:

$$E_{P,R,i} = f(\beta(\eta'_i)) \tag{3.20}$$

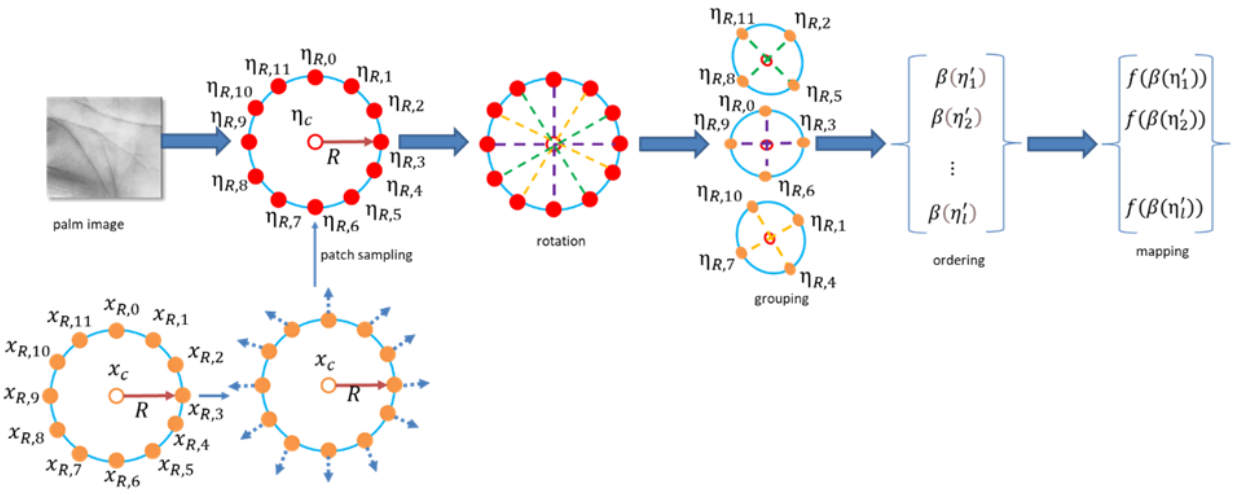

Figure 3.17: Representation of the proposed descriptor.

2) **Texture Patterns (TP):** To illustrate long-range interactions, the suggested operator is conceptually linked to non-local neural networks [183]. The global restrictions [184, 185] are used by the suggested operator. The difference is that in TP, non-local image redundancy is used to produce numerous new global image data [186]. Initially, for a given image we arrange the gray values from all central pixels (x) in increasing order and then divide the ordered pixels into (Q) regular intervals [187]. Then, for each interval, calculate an anchor:

$$(\eta'_{c1}, \dots, \eta'_{cK}) := sort(\eta_{c1}, \dots, \eta_{cK}) \tag{3.21}$$

$$g_{I_t} = \frac{1}{\left\lfloor \frac{K}{Q} \right\rfloor} \sum_{k=(t-1)\left\lfloor \frac{K}{Q} \right\rfloor + 1}^{t\left\lfloor \frac{K}{Q} \right\rfloor} \eta'_{ck} \tag{3.22}$$

Furthermore, we use an extended $riu2$ to represent the intensity variations between nearby data samples and each anchor:

$$U(TP_{P,R}) = \left|S\left(\eta_{P-1,R} - g_{I_t}\right) - S\left(\eta_{0,R} - g_{I_t}\right)\right| + \sum_{p=1}^{P-1}\left|S\left(\eta_{P,R} - g_{I_t}\right) - S\left(\eta_{P-1,R} - g_{I_t}\right)\right| \quad (3.23)$$

$$TP_{P,R,t}^{riu2} = \begin{cases} \sum_{p=0}^{P-1} s(\eta_{P,R} - g_{I_t}), & U(TP) \leq 2 \\ P+1, & U(TP) = 4 \\ P+2, & U(TP) = 6 \\ P+3, & U(TP) = 8 \\ P+4, & U(TP) = 10 \\ P+5, & otherwise \end{cases} \quad (3.24)$$

Now, we transform the grey values into binary values using center operator as discussed in [171]:

$$C_{P,R} = S(\eta_c, c_F) \quad (3.25)$$

Then, for each central pixel, we adopt joint feature encodes that construct two different types of texture data:

$$D_1 = DP_{P,R,i} + C_{P,R} \times P \quad (3.26)$$

$$D_2 = TP_{P,R,j} + C_{P,R} \times (P+6) \quad (3.27)$$

The D_1 is the dominant directional vector and D_2 is the texture vector. The multi feature vector includes both D_1 and D_2 vectors.

3) **Multi feature learning:** We aim to learn the most discriminative features from the D_1 and D_2. The respective steps are given as follows:

Step1: let $x_{p,i}^{y} \epsilon U^{d_y \times 1}$ is the yth feature vector of the pth pixel of the ith palm-print sample. $x_{p,i}^{D_1}$ is the directional vector and $x_{p,i}^{D_2}$ is texture vector. The proposed multi-view feature learning aims to learn S hash functions to map the feature vectors as given in equation (3.28)

$$a_{p,i}^{y} = \frac{sgn\left((M^{y})^{T} x_{p,i}^{y}\right) + 1^{S\times 1}}{2} \tag{3.28}$$

here, $M^{y} = [M_1^{y}, M_2^{y}, M_3^{y}, \dots, M_k^{y}]$ is the projection matrix. $sgn(x)$ is sign function. $1^{S\times 1}$ is a vector of element 1.

Step 2: Now, we define the objective function as

$$\min_{M^{y}} J(M^{y}) = \sum_{y=1}^{Y=2} (\mu^{y})^{\lambda} \left(\sum_{p=1}^{P} \sum_{i=1}^{N} \left\| b_{p,i} - \left(\frac{1}{2}\right)^{S\times 1} - (M^{y})^{T} a_{p,i}^{y} x_{p,i}^{y} \right\|^2 - \sigma_1 \sum_{p=1}^{P} \sum_{i=1}^{N} \left\| a_{p,i}^{y} - \frac{1}{N} \sum_{i=1}^{N} a_{p,i}^{y} \right\|^2 \right) - \sigma_2 \sum_{p=1}^{P} \sum_{i=1}^{N} \left\| a_{p,i}^{1} - a_{p,i}^{2} \right\|^2 \tag{3.29}$$

Here, $b_{p,i}$ is binary code vector, N is number of training images. μ^{y} is weight of the yth multi-view data, λ is the control parameter for weight. σ_1 and σ_2 are the control parameter to balance the conditions of objective function. $(M^{y})^{T} M^{y} = I$. I is an identity matrix.

Now, we can simplify the objective function as follows:

$$J(M^{y}) = \sum_{y=1}^{Y=2} (\mu^{y})^{\lambda} \sum_{p=1}^{P} \left\| b_p - \left(\frac{1}{2}\right) - (M^{y})^{T} X_p^{y} \right\|^2 - \sigma_1 \sum_{p=1}^{P} \left\| (M^{y})^{T} X_p^{y} - (M^{y})^{T} E_p^{y} \right\|^2 - \sigma_2 \sum_{p=1}^{P} \left\| (M^{1})^{T} X_p^{1} - (M^{2})^{T} X_p^{2} \right\|^2 \tag{3.30}$$

Here, $X_p^y = [x_{p,1}^y, x_{p,2}^y, x_{p,3}^y, \dots, x_{p,N}^y]$, $b_p = [b_{p,1}, b_{p,2}, b_{p,3}, \dots, b_{p,N}]$ and $E_p^y = [e_{p,1}^y, e_{p,2}^y, e_{p,3}^y, \dots, e_{p,N}^y]$.

To obtain the optimal solution of Equation (3.29), we update the variables b_p, M^y and μ^y.

a. Update b_p and fix M^y and μ^y. The objective function can be reduced as

$$J(b_p) = \sum_{p=1}^{P} \sum_{y=1}^{y=2} (\mu^y)^\lambda \left\| b_p - \left(\frac{1}{2}\right) - (M^y)^T X_p^y \right\|^2 \tag{3.31}$$

$$= \sum_{p=1}^{P} \sum_{y=1}^{Y} tr\left(b_p b_p^T - 2\left(\frac{1}{2} + (M^y)^T X_p^y\right) b_p^T + \left(\frac{1}{2} + (M^y)^T X_p^y\right)\left(\frac{1}{2} + (M^y)^T X_p^y\right)^T \right) \tag{3.32}$$

By taking $\frac{\partial J}{\partial b_p} = 0$, we calculate b_p as

$$b_p = \frac{1}{2} + \frac{1}{\sum_{y=1}^{Y} (\mu^y)^\lambda} \sum_{y=1}^{Y} (\mu^y)^\lambda \, (M^y)^T X_p^y$$

By using Equation (3.29), we can obtain b_p as

$$b_p = \frac{(sgn \sum_{y=1}^{Y} (\mu^y)^\lambda \left((M^y)^T X_p^y\right) + 1)}{2} \tag{3.33}$$

b. Update μ^y and fix M^y and b_p. The objective function can be reduced as

$$J(\mu^y) = \sum_{y=1}^{Y} (\mu^y)^\lambda \sum_{p=1}^{P} \left\| b_p - \left(\frac{1}{2}\right) - (M^y)^T X_p^y \right\|^2 - \sigma_1 \sum_{p=1}^{P} \left\| (M^y)^T X_p^y - (M^y)^T E_p^y \right\|^2 \tag{3.34}$$

Here, $\sum_{y=1}^{Y} \mu^y = 1$.

After simplifying, μ^y can be obtained as

$$\mu^{y} = \frac{\left(\sum_{p=1}^{P}\left\|b_p-\left(\frac{1}{2}\right)-(M^{y})^{T}X_p^{y}\right\|^{2}-\sigma_1\sum_{p=1}^{P}\left\|(M^{y})^{T}X_p^{y}-(M^{y})^{T}E_p^{y}\right\|^{2}\right)^{1/1-r}}{\sum_{y=1}^{N_y}\left(\sum_{p=1}^{P}\left\|b_p-\left(\frac{1}{2}\right)-(M^{y})^{T}X_p^{y}\right\|^{2}-\sigma_1\sum_{p=1}^{P}\left\|(M^{y})^{T}X_p^{y}-(M^{y})^{T}E_p^{y}\right\|^{2}\right)^{1/1-r}} \quad (3.35)$$

c. Update M^{y} and fix μ^{y} and b_p. The objective function can be reduced as

$$J(M^{y}) = \sum_{y=1}^{Y}(\mu^{y})^{\lambda}(G^{y}) - (\sigma_1)(\xi) - (\sigma_1)(\varpi) \quad (3.36)$$

Here, $G^{y} = \sum_{p=1}^{P} tr\left(b_p - \left(\frac{1}{2}\right)\left(b_p - \left(\frac{1}{2}\right)\right)^{T} - 2\left(b_p - \left(\frac{1}{2}\right)\right)\left(X_p^{y}\right)^{T} M^{y} + (M^{y})^{T}X_p^{y}\left(X_p^{y}\right)^{T} M^{y}\right)$,

$\xi = \sum_{p=1}^{P} tr\left((M^{y})^{T}X_p^{y}\left(X_p^{y}\right)^{T} M^{y} + (M^{y})^{T}\left(E_p^{y}\right)^{T}E_p^{y}\, M^{y} - 2\,(M^{y})^{T}X_p^{y}\left(E_p^{y}\right)^{T} M^{y}\right)$

and $\varpi = \sum_{p=1}^{P} tr\left((M^{1})^{T}X_p^{1}\left(X_p^{1}\right)^{T} M^{1} + (M^{2})^{T}X_p^{2}\left(X_p^{2}\right)^{T} M^{2} - 2(M^{1})^{T}X_p^{1}\left(X_p^{2}\right)^{T} M^{2}\right)$

Finally, a nearest-neighborhood classifier is used to classify the data using the chi-square distance measure, as described in [188].

3.5.2 Experimental results and discussion

The experiments are conducted on four contactless palm-print databases, namely CASIA database, IIT-Delhi database, REST database, and Tongji database.

1) **Parameter selection:** There are various factors and critical components in the proposed method that will influence recognition performance. To acquire the robust characteristics, we evaluate the following sets of (P, R): (8, 1), (16, 2), and (24, 3). The effect of sample radius on recognition performance is shown in Figure 3.18, we see those higher values of sampling radius such as $(R = 3, 4, 5)$ gives higher accuracy results. When R is too large, however,

classification performance degrades (by comparing $R = 7$ and $R = 8$). We analyzed different values of number of anchors as $Q_1 = 1; Q_2 = 2; Q_3 = 3; Q_4 = 4; Q_5 = 5$. For texture pattern, number of anchors is selected in the range of [3, 5], which achieves higher recognition performance as depicted in Figure 3.19. The size of the image patch is 3×3 during the experiment. The multi feature learning contains the two important parameters σ_1 and σ_2. The multi feature learning with different values of σ_1 and σ_2 from a set of [0, 0.001, 0.01, 0.1, 1, 10, 100] is taken for the experiment

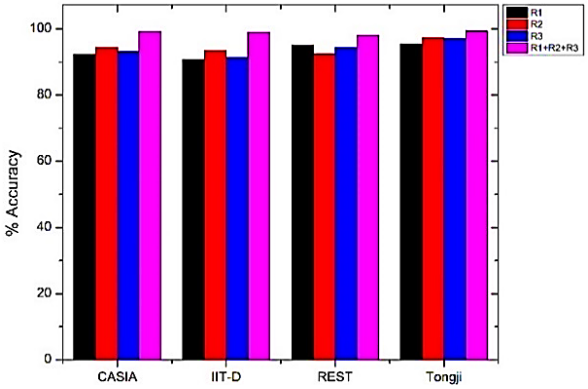

Figure 3.18: Performance comparison of sampling radius.

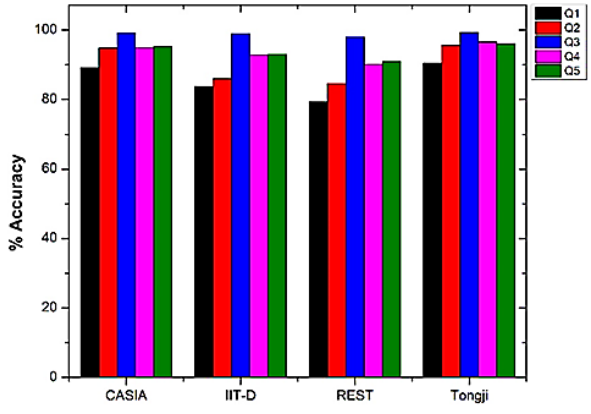

Figure 3.19: Performance comparison with number of anchors.

It is observed that σ_1 close to 1 achieves better performance. Whereas larger value of σ_2 achieves better performance. In the proposed work, we empirically tuned $\sigma_1 = 1$ and $\sigma_2 = 100$ respectively. The train and test sets were picked at random and each contained around half of the persons in the database. During training and testing, subsets of subjects are disconnected.

2) **Comparative results:** We compare and contrast the proposed multi feature learning with existing methods LBP, CLBP, FRLD, and HM-LBP in terms of several evaluation measures.

- **Results on CASIA database:** In terms of accuracy, precision, recall, F-measure, specificity, and FPR, Table 3.9 compares the proposed and existing methods: LBP, CLBP, FRLD, and HM-LBP. The precision of the proposed method is 16.46%, 21.19%, 5%, and 0.89% higher than the LBP, CLBP, FRLD and HM-LBP, respectively. The recall of the proposed method is 10.77%, 18.11%, 3.8%, and 1.11% higher than the LBP, CLBP, FRLD and HM-LBP, respectively. The F- measure of the proposed method is 6.23%, 17.01%, 8.49%, and 6.62% higher than the LBP, CLBP, FRLD and HM-LBP, respectively.

Table 3.9: Results of proposed and existing methods on CASIA database.

Method	**Measures (%)**					
	Accuracy	**Precision**	**Recall**	**F-measure**	**Specificity**	**FPR**
LBP	68.91	80.54	87.34	90	90.89	9.6
CLBP	82.74	75.81	80	79.22	93.26	8.45
FRLD	90.73	92	94.31	87.74	91.55	7.75
HM-LBP	97.62	96.41	97	89.61	91.38	6.64
Proposed	99.16	97	98.11	96.23	95.34	4.02

The specificity of the proposed method is 4.45%, 2.08%, 3.79%, and 3.96% higher than the LBP, CLBP, FRLD and HM-LBP, respectively. The FPR of the proposed method is 4.02% which is lower than the LBP, CLBP, FRLD and HM-LBP, respectively.

- **Results on IIT-D database:** Table 3.10 compares the performance of the proposed method to that of existing methods for the IIT-D database. The accuracy of the proposed method is 30.86%, 24.72%, 7.62%, and 3.22% higher than the LBP, CLBP, FRLD and HM-LBP, respectively. The precision of the proposed method is 25.5%, 29.8%, 3.34%, and 5.11% higher than the LBP, CLBP, FRLD and HM-LBP, respectively. The recall of the proposed method is 24.36%, 28%, 3.22%, and 5% higher than the LBP, CLBP, FRLD and HM-LBP, respectively. The F-measure of the proposed method is 13.26%, 10.93%, 5.79%, and 0.64% higher than the LBP, CLBP, FRLD and HM-LBP, respectively. The specificity of the proposed method is 6.73%, 5.06%, 1.22%, and 3.14% higher than the LBP, CLBP, FRLD and HM-LBP, respectively. The FPR of the proposed method is 5.07% which is lower than the LBP, CLBP, FRLD and HM-LBP, respectively.

Table 3.10: Results of proposed and existing methods on IIT-D database.

Method	**Measures (%)**					
	Accuracy	**Precision**	**Recall**	**F-measure**	**Specificity**	**FPR**
LBP	68.11	69.84	72.64	83	89.14	9.64
CLBP	74.25	65.54	69	85.33	90.81	8.79
FRLD	91.35	92	93.78	90.47	94.65	8.56
HM-LBP	95.75	90.23	92	95.62	92.73	6.79
Proposed	98.97	95.34	97	96.26	95.87	5.07

- **Results on Tongji database:** Table 3.11 describes the performance of the proposed method on the Tongji palm-print

database. The accuracy of the proposed method is 16.39%, 8.54%, 3.01%, and 0.91% higher than the LBP, CLBP, FRLD and HM-LBP, respectively. The precision of the proposed method is 16.39%, 8.54%, 3.01%, and 0.91% higher than the LBP, CLBP, FRLD and HM-LBP, respectively. The recall of the proposed method is 23.09%, 6.37%, 1.58%, and 3.09% higher than the LBP, CLBP, FRLD and HM-LBP, respectively. The F-measure of the proposed method is 16.89%, 3.48%, 1.44%, and 0.53% higher than the LBP, CLBP, FRLD and HM-LBP, respectively. The specificity of the proposed method is 2.14%, 4.29%, 3.56%, and 1.85% higher than the LBP, CLBP, FRLD and HM-LBP, respectively. The FPR of the proposed method is 4.18% which is lower than the LBP, CLBP, FRLD and HM-LBP, respectively.

- **Results on REST database:** Table 3.12 compares the performance of the proposed method to that of existing methods for the REST database. The accuracy of the proposed method is 30.22%, 25.55%, 7.56%, and 4.61% higher than the LBP, CLBP, FRLD and HM-LBP, respectively. The precision of the proposed method is 27.11%, 33.22%, 3.5%, and 6.11% higher than the LBP, CLBP, FRLD and HM-LBP, respectively. The recall of the proposed method is 25.66%, 28.77%, 3%, and 4.84% higher than the LBP, CLBP, FRLD and HM-LBP, respectively. The F-measure of the proposed method is 8.25%, 7.52%, 4.89%, and 0.62% higher than the LBP, CLBP, FRLD and HM-LBP, respectively. The specificity of the proposed method is 1%, 1.83%, 1.1%, and 3% higher than the LBP, CLBP, FRLD and HM-LBP, respectively. The FPR of the proposed method is 5.87% which is lower than the LBP, CLBP, FRLD and HM-LBP, respectively. The accuracy of

the proposed method is 99.16%, 98.97%, 99.29%, and 98% for CASIA, IIT-D, Tongji and REST, respectively. It demonstrates that the suggested method achieves higher average accuracy than current methods. The precision of the proposed method is 97%, 95.34%, 99.09%, and 95.11% for CASIA, IIT-D, Tongji and REST, respectively. The recall of the proposed method is 98.11%, 97%, 98.11%, and 96% for CASIA, IIT-D, Tongji and REST, respectively. F-measure and specificity of the proposed method is 96.23% and 95.34%, 96.26 and 95.87%, 96% and 95.45, and 94.52% and 94% for CASIA, IIT-D, Tongji and REST, respectively.

Table 3.11: Results of proposed and existing methods on Tongji database.

Method	**Measures (%)**					
	Accuracy	**Precision**	**Recall**	**F-measure**	**Specificity**	**FPR**
LBP	82.90	76	81.22	79	93.31	8.98
CLBP	90.75	92.72	94.63	87.67	91.16	7.62
FRLD	96.28	97.51	96.67	89.17	91.89	6.81
HM-LBP	98.38	96	97.58	95	93.60	5.82
Proposed	99.29	99.09	98.11	96	95.45	4.18

Table 3.12: Results of proposed and existing methods on REST database.

Method	**Measures (%)**					
	Accuracy	**Precision**	**Recall**	**F-measure**	**Specificity**	**FPR**
LBP	67.78	68	70.34	86.27	93	9.8
CLBP	72.45	61.89	67.23	87	92.17	8.94
FRLD	90.44	91.56	93	89.63	92.90	8.01
HM-LBP	93.39	89	91.16	93.90	91	7.34
Proposed	98	95.11	96	94.52	94	5.87

It demonstrates that the suggested method achieves higher average F-measure and specificity than current methods. The FPR of the proposed method is 4.02%, 5.07%, 4.18%, and 5.87% for CASIA, IIT-D, Tongji and REST, respectively. The suggested method's FPR is lower than those of the existing methods LBP, CLBP, FRLD, and HM-LBP.

3.6 Conclusion

In this Chapter, we developed palm-print recognition methods using two different LBP based methods namely multi scale edge angles LBP (MSEALBP) and LBP with multi feature learning to improve the performance of existing texture descriptors. While implementing MSEALBP we combine edge operator and multi-scale uniform patterns, which extracts texture patterns at different angular space and spatial resolution. Thus, making the extracted uniform patterns less sensitive to the pixel level values. Further, an optimal artificial neural network structure is developed for classification, which helps in maintaining the higher classification accuracy by significantly reducing the computational complexity. The method yields an EER of 0.2% and classification accuracy of 98.52% on PolyU database.

In the second method, we designed two robust operators for multi feature representation. The descriptors represent the palm-images in a rotation and illumination invariant way. The proposed method employs two criterions to make the learned multi-view feature discriminative and complementary in an unsupervised manner. We evaluated the performance using CASIA, IIT-Delhi, Tongji and REST contactless palm-print databases. The comparison is performed against LBP, CLBP, FRLD and HM-LBP methods.

Chapter 4

Information security and protection of Palm-print templates

4.1 Introduction

The progress in information society, extended the need of secure identity systems. In modern information society, biometric recognition has been acquired a lot of public consideration as it is secure and convenient [1]. The ISO/IEC 24745 standard proposed primary security necessities of Biometric Template Protection (BTP) techniques in 2011 [191]. The BTP techniques stores some kind of transformed information as opposed to the original biometric template to offer the essential security level. Palm-print recognition is increasingly being used, and like other biometric modalities, this has greatly increased privacy concerns [90].

To preserve the confidentiality of the biometric data, random projection has recently been widely employed to create revocable biometric templates [115]. These methods safeguard the biometric templates using many-to-one mapping. The original feature vector is projected into a subsequent feature vector with less dimensions. A user-specific key is used to direct the projection and maintain security.

An effective approach for creating a cancelable biometric based on sectored random projections was presented [117]. If an existing pattern is copied, then system can create a new one, keep the original recognition performance, and avoid the extraction of relevant information from changed patterns. The technology is resistant to degradations brought on by eyelids and eyelashes and also addresses some of the shortcomings of current

techniques. The wide variety of abnormalities that can occur during acquisition can be resolved by random projections and sparse representations. In order to increase security and privacy, it provides techniques to generate cancellable iris templates [118]. It was suggested to secure a minutiae-based fingerprint template using a two-dimensional random projected MVD [119]. A set of fingerprint minutiae is first created, and this minutiae vicinity is then utilized to build MVD features. The template that has been stored is protected by cancellable biometric methods based on non-invertible transformation. Using these methods, unauthorized access to the system is prevented and the original fingerprint data cannot be recreated from the corrupted template [120].

Uhl proposed block remapping and image warping strategies to produce cancelable iris templates [121]. Secure iris images are processed using the non-reversible image domain transformation prior to feature extraction.

Jenisch and Uhl [122] uses block permutation and remapping of the iris texture as a strategy for template protection. The effects of two alternative situations on the system's security are examined. Multiple templates with the same biometric feature are presumably available to an attacker. When both the permutation key and the original template are available, the method can recover 60% of the original template. Based on randomized cuckoo hashing and minHash, a cancellable palm-print template was used [123].

In the above literature, the transformation techniques are vulnerable to token-stolen scenario if the token is compromised. Most of the transformation techniques are confirmed for a specific modality and not defined their performance for other modalities.

This chapter addresses the requirement for a secure and cancelable biometric template generation as an illustration to palm-print biometry. Here, we developed a secure and revocable biometric recognition framework. A cancelable and tunable security is planned by victimization random base-n codes to shield the authentication system from brute force attacks. PolyU, IIT-Delhi and CASIA palm-print databases are considered to

validate the performance of our method. Comparative experiments were carried out to exhibit the accuracy of the proposed approach.

4.2 Implementation of proposed approach

A palm-print recognition methodology is proposed which achieves high level of security and accuracy, using no pre-assumptions in terms of variations in illumination, pose and the type of security attack. Aiming to exploit the benefits of CNN and transformation scheme in a single mechanism is proposed as illustrated in Figure 4.1. Initially pre-processing is done in order to get stable and aligned ROIs. After that, CNN is used as a feature extraction module which takes ROIs as input image. The extracted features are classified into classes by the fully connected layers. The last layer can be used as features (bottle neck features (BNFs) with any generic classifier [192]. CNN having penultimate layer which, generates generic descriptor. Researchers have shown that these descriptors are very efficient for classification [193]. Further, the generated feature vector is transformed into a new feature vector.

Standard biometric systems store original biometric information that may be susceptible to data theft and data extortion and can becoming an issue of security. So, random base-n codes are used to ensure security. The codes are not correlated with the original biometric sample and used as output labels (for classification). Further, secure hash algorithm (SHA-3) is applied to hash (random codes) and kept as a template. Hashing is non-invertible transformation. It is used as classification labels which, ensures secure storage of codes. Initially an input (test sample) is fed to the trained model which further computes a hash code. To authenticate the user, the hash code compared with the stored database codes. The noninvertible property of Hash codes eliminates the probability of extracting the original biometric sample. Random codes with different set are used as labels which introduces cancellability in the proposed approach.

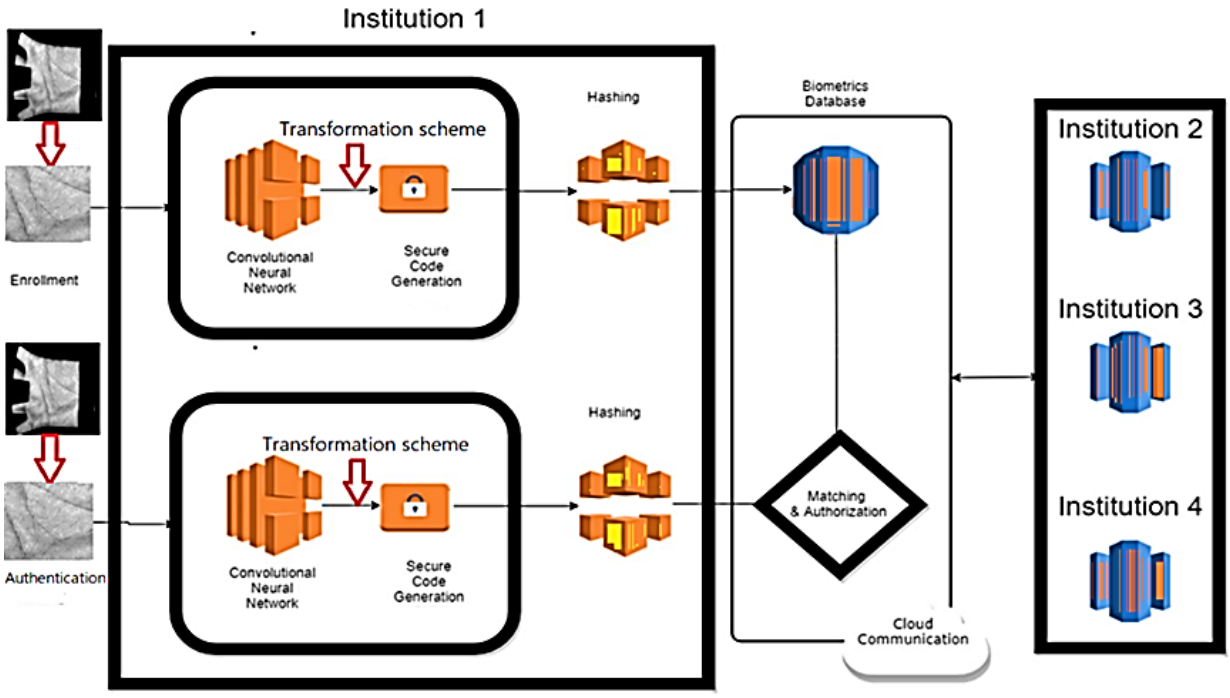

Figure 4.1: The representation of the proposed authentication system.

4.2.1 Convolutional Neural Networks (CNN)

CNNs are multi-layer neural networks. Like customary neural systems, they are made out of a few loads and inclinations that are learned according to the ideal planning of sources of info and yields [194]. A CNN is a start to finish non-direct framework that can be prepared to gain significant level portrayals straightforwardly from raw images [195, 196]. The principle segments of the CNN design are convolution, pooling furthermore, completely associated layers.

The input could be a ROI extracted grayscale image I. A weight matrix $W \in R^{m \times m \times c \times k}$ is convolved with input I. The weight matrix spans across a tiny low patch of size $(m \times m)$

with a stride s, wherever $m \leq min(b, h)$. The weight sharing is used to model correlations within the input I. Further, k feature maps are generated by weight matrix.

The convolution operation is given as follows:

$$Output = \sigma\left(\sum_{c} W \times I + B\right) \tag{4.1}$$

Where image with a matrix $I \in R^{b \times h \times c}$, b is input breadth, h is height and c is number of channels. The output matrix is calculated as $Output \in R^{((b-m)/s) \times ((h-m)/s) \times k}$, B refers bias and σ is a non-linearity operation.

Further, a pooling operation is performed to retain necessary info whereas reducing spatial resolution. The max-pooling operation preserved the utmost price of spatial neighbourhood (like 2×2 window). So, pooling operation helps in removing variability that exists because of illumination, noise, rotation and pose. It additionally helps to scale back the computation for later layers by reducing the matrix dimensions. The proposed CNN consists of 4 stacks of convolution and pooling layers followed by a completely connected layer. The proposed CNN design is summarized in Table 4.1. Throughout training, the last layer is related to a multiclass cross-entropy loss perform as conferred within the given Eq. (4.2):

$$loss = -\sum_{n=1}^{N} x_{pr,t}\, log\left(p_{pr,t}\right) \tag{4.2}$$

Where N is number of training samples, pr is predicted user id, p is predicted probability, t is actual target user id and x is binary indicator (0 or 1), determining whether prediction is the same as target.

The CNN parameters are trained victimization Adam optimiser [197] that takes into consideration advantages of Adagrad [198] by computing adaptive learning rates and RMSpropoptimiser [199] by shrewd decaying average of past square gradients

$$\theta_{p+1} = \theta p - \Delta \frac{m_p}{\sqrt{v_p + \epsilon}} \tag{4.3}$$

where $\theta_{p+1}$is parameter value (updated), θ_p is previous parameter value, m_p is mean, Δ is step size, v_p is variance, and ϵ is small number (say 10^{-9} to prevent division-by-zero).

Table 4.1 Summary of CNN architecture.

Layers	**Parameters**
Convolution	Patch size: 7×7 depth: 16
Batch normalization >ReLU activation	momentum: 0.9 epsilon: 0.001
maxpooling	patch size: 2 × 2 depth: 16
regularisation	dropout: 0.2 L2 beta: 0.5
convolution	patch size: 5 × 5 depth: 32
batch normalisation > ReLU activation	momentum: 0.9 epsilon: 0.001
max pooling	patch size: 2 × 2 depth: 32
regularisation	Dropout L2 beta: 0.5
convolution	patch size: 3 × 3 depth: 64
batch normalisation > ReLU activation	momentum: 0.9 epsilon: 0.001
max Pooling	patch size: 2 × 2 depth: 64
regularisation	dropout: 0.2 L2 beta: 0.5
convolution	patch size: 1 × 1 depth: 128
batch normalisation > ReLU activation	momentum: 0.9 epsilon: 0.001
max pooling	patch size: 2 × 2 depth: 256
regularisation	dropout: 0.2 L2 beta: 0.5
fully connected layer	number of neurons: 512
fully connected layer	number of neurons: 80
regularisation	dropout: 0.2 L2 beta: 0.5
fully connected layer	number of neurons: 100

The algorithm has a preference of flat minima in error hyper plane that avoid native minima and therefore achieving higher generalization [200]. So, it is economical across deep learning tasks. To avoid dropout, overfitting and $L2$ regularization square measure applied to each convolutional and absolutely connected layers [201]. Thus, nodes co-adaptation and over-dependence on massive weights is prevented. Additionally, using batch social control [202] ensures that variance shift is least, rising consistency and reproducibility of the proposed work.

4.2.2 Feature transform scheme

Suppose the extracted feature vector b is derived from the feature extraction process conducted on an input ROI image. Now the extracted features are transformed by using random slope method.

Initially b feature vector is generated using random grid (q) and basic OR operation as given in Eq. (4.4)

$$s = b + q \tag{4.4}$$

The user-specific random key is generated with a dimension similar to the original feature vector b. The q contains the random integral value in the range of [-255 to 255].

The feature vector s is divided in two equal parts as given below

$a = s(1{:}\, f/2)$ and $b = s(f/2 + 1{:}\, f)$

Now these values are used to define the feature points (p)

$$(x_i = a(i), y_i = b(i)\,)$$

Now, we generate a user specific key ξ having randomly distributed non-integral values. The dimension of ξ is $1 \times f$ and further divide in ξ_0 and ξ_1 in order to define mapping for the random point rp_i. Where $(x_i = (i), and\ y_i = b(i)\,)$.

The basic line equation is given as $y = gx + r$, where g stands for slope or gradient and r is the intercept made by the line. The slope and intercept [203] of all the lines passing

through the feature points (p) and random point rp_i are calculated and normalized as given in Eq. (4.5) and (4.6)

$$NG_i = \frac{G_i - min(G)}{max(G) - min(G)} \tag{4.5}$$

$$NR_i = \frac{R_i - min(R)}{max(R) - min(R)} \tag{4.6}$$

Where $G = \{g_i\}$ and $R = \{r_i\}$. g_i is the slope of the line and G is the slope vector. r_i is the intercept of the lines and R is the intercept vector.

The transformed template is computed as given in Eq. (4.7),

$$Tb_i = NG_i + NR_i \tag{4.7}$$

Hence, the transformed feature Tb is used for storing and matching process. The user can utilize vector q and ξ in token form. At every authentication, users' biometric is transformed using the same vectors. If compromised, new transformed template can be generated by changing the keys. Also, the dimension of transformed features reduces by 50%.

4.2.3 Random code generation

The base-n codes (length of m) that are randomly generated and used as labels for various users. As an example, binary (base-2) uses solely 2 symbols (0 and 1), ternary (base-3) uses 3 symbols (0, 1 and 2) and a couple of then on. Random generation of codes ensures no alikeness to the original biometric sample. Therefore, associate degree persona non grata would need to brute-force all attainable codes i.e., m^n attacks that is computationally not possible provided ($m > t$), a manually chosen threshold.

For an n-ary code entropy is defined as given in Eq. (4.8),

$$H = -\sum_{i}^{n} p_i \, log_{n\,\mathrm{p}_i} \tag{4.8}$$

where H denotes entropy, p_i is occurrence probability of symbol i, here $p_i > 0$.
According to Eq. (4.8), the utmost entropy of associate degree n-ary code, every image i have occurrence probability of $1/n$. Completely different base-n codes are used as classification labels so as to evaluate the performance of the proposed scheme. The work is additionally evaluated for various code lengths. The range of experimentations was chosen as $n \in (2,9)$ and $m \in 2^{(7,\,10)}$ to evaluate the impact of code length on recognition accuracy.

4.2.4 Cryptographic Hash

The random codes are hashed using secure hash algorithm to protect the palm-print template [204]. In the proposed work, SHA-3 [205] is employed as a result of it's the new customary for sturdy security. A user is verified by matching hash digest of his take a look at biometric sample with the hash digest guide. The proposed methodology uses SHA3-256 with the permutation perform of the sponge construction [206, 207]. The parameters bit rate, output size and capacity are 1088, 256 and 512 respectively.

4.2.5 Matching

The transformed feature vector $Tb^T$and Tb^Q obtained from the template and query images respectively. The similarity score [208] is calculated as given in Eq. (4.9)

$$S(Tb^T, \mathrm{Tb}^Q) = 1 - \frac{\|Tb^T - Tb^Q\|_{2^2}}{\|Tb^T\|_{2^2} + \|Tb^Q\|_{2^2}} \tag{4.9}$$

Where $\|.\|_2$ denotes the 2-norm. The similarity score is either 0 or 1. ‘0’ indicates the completely different feature vectors, while ‘1’ indicates similar feature vectors.

4.3 Experimental results and discussion

Three palm-print databases PolyU, CASIA and IIT-Delhi were utilized to evaluate the performance of the proposed framework. Figure 4.2 shows the sample hand images of PolyU database. Figure 4.3 and Figure 4.4 shows the sample hand images of IIT-Delhi and CASIA palm-print databases respectively. The subsequent ROIs are cropped and resized to 128 × 128 pixels.

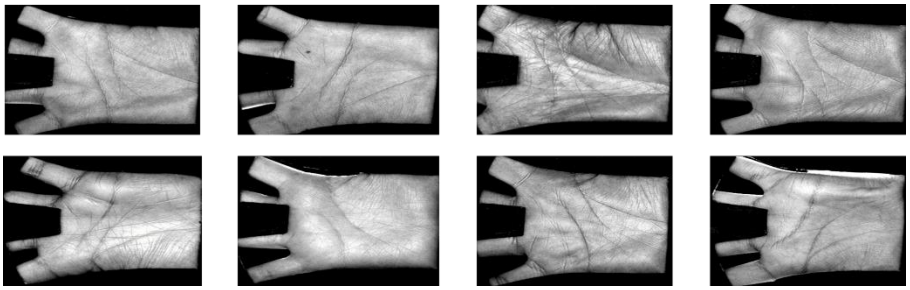

Figure 4.2: Sample hand images from PolyU database.

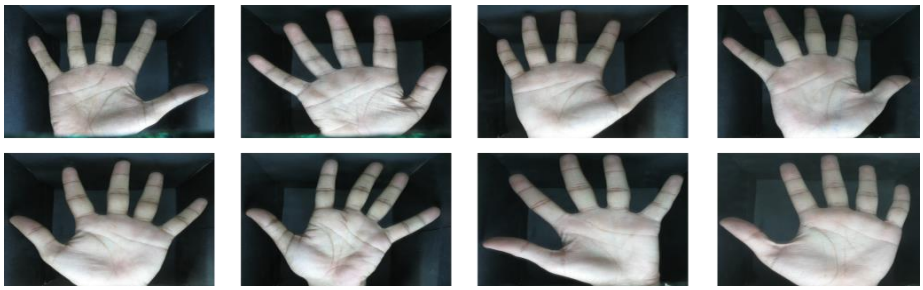

Figure 4.3: Sample hand images from IIT-Delhi database.

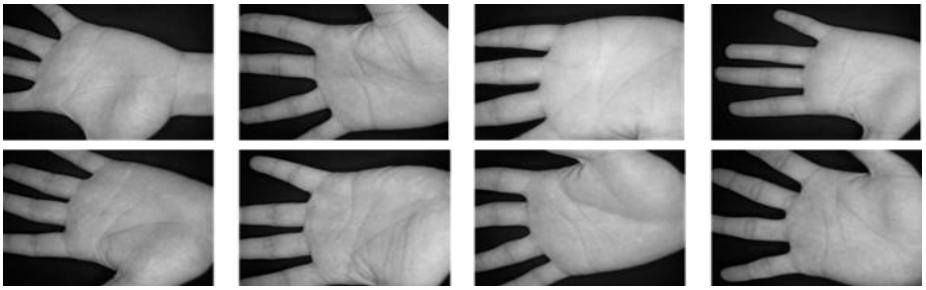

Figure 4.4: Sample hand images from CASIA database.

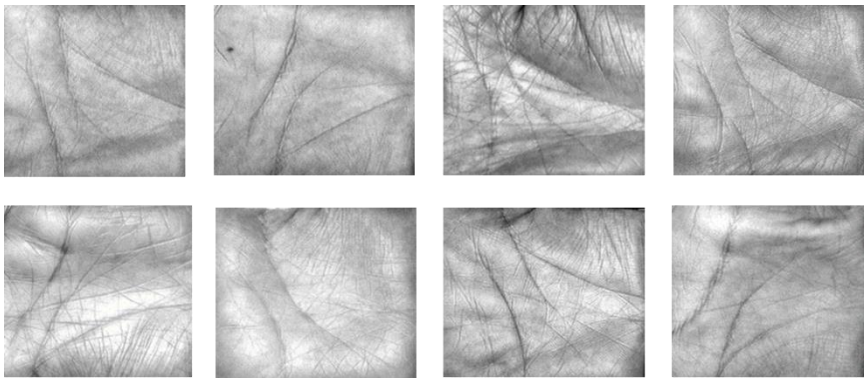

Figure 4.5: Sample ROIs from PolyU database.

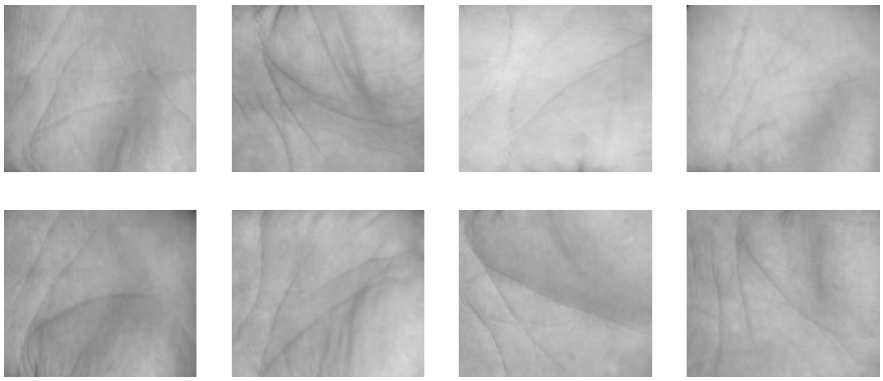

Figure 4.6: Sample ROIs from CASIA database.

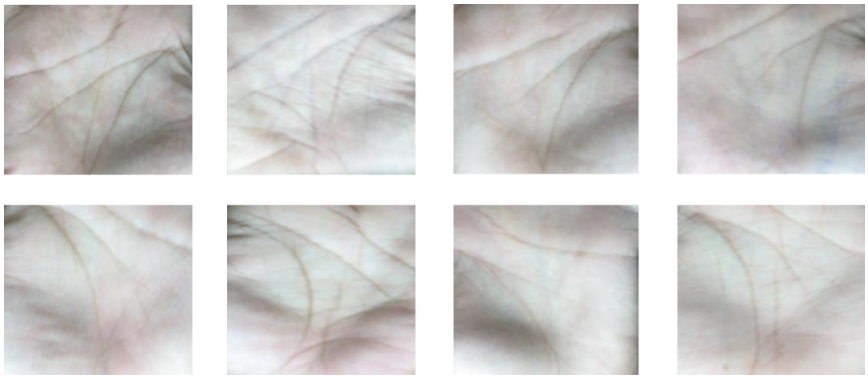

Figure 4.7: Sample ROIs from IIT-Delhi database.

Figure 4.5 and Figure 4.6 shows the sample ROI images of PolyU and IIT-Delhi databases respectively. Figure 4.7 shows the sample ROI images of CASIA database. The performance of the proposed method is evaluated using GAR, EER and Decidability Index (d). False Non-Match Rate (FNMR) and False Match Rate (FMR) are defined as given in Eq. (4.10) and (4.11),

$$FNMR = \frac{FN}{FN + TP} \tag{4.10}$$

$$FMR = \frac{FP}{FP + TN} \tag{4.11}$$

Where, FP and FN are number of false positives and number of false negatives respectively. TN and TP are number of true negatives and number of true positives. EER is defined as the point at which FMR equals FNMR.

The decidability index (d) is a measure of the degree of separation between genuine and imposter populations [80]. It is defined as

$$d = \frac{\left|\mu_g + \mu_i\right|}{\sqrt{\frac{\sigma_g^2 + \sigma_i^2}{2}}} \tag{4.12}$$

Where, μ_g and μ_i are mean of genuine and imposter respectively. σ_g and σ_i are variance of genuine and imposter respectively.

4.3.1 Comparative results

The recognition preformation in terms of the EER (%) and GAR (%) with different code lengths (256 and 1024) is listed in Table 4.2 on three palm-print databases. The proposed strategy accomplishes up to 0.62% average EER and 99.05% GAR on PolyU database with a code length of 1024.

Table 4.2 Recognition preformation in terms of the EER (%) and GAR (%) with different code lengths.

Database	Length (m)	GAR (%)	EER (%)
PolyU	256	98.12	0.71
	1024	99.05	0.62
CASIA	256	97.11	0.78
	1024	98.99	0.70
IIT-Delhi	256	95.21	1.21
	1024	97.11	1.01

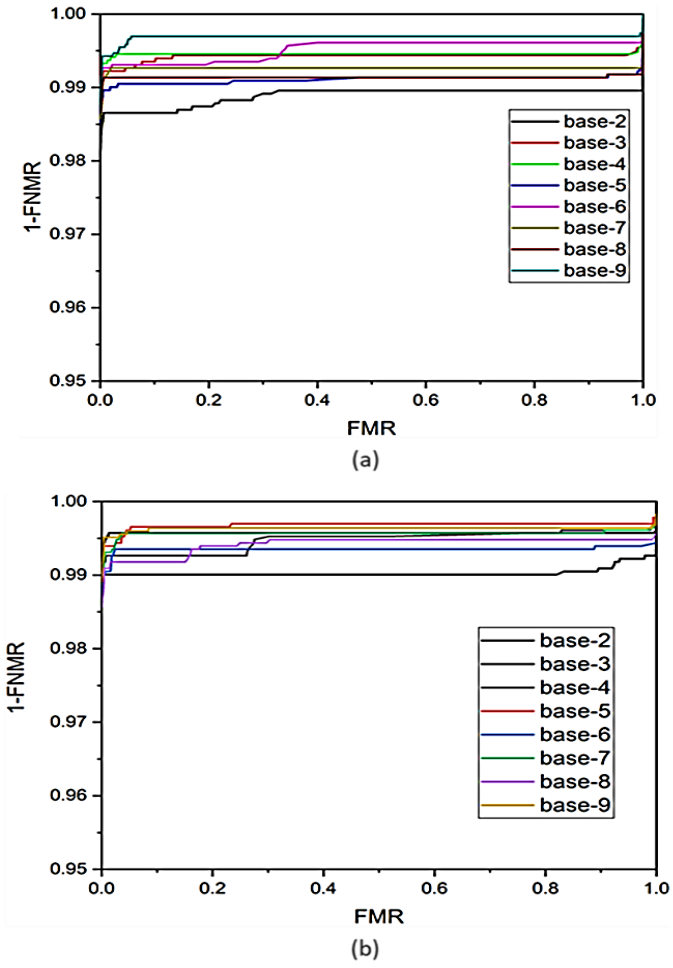

Figure 4.8 ROC curve on PolyU database (a) for code length 256 and (b) for code length 1024.

The CASIA database gives an EER of 0.70% whereas IIT-Delhi database yields EER of 1.01%. The GAR is 98.99% and 97.11% for CASIA and IIT-Delhi databases respectively. The ROC curves are appeared in Figure 4.8, 4.9 and 4.10 displaying execution of methodology relating to the different lengths of random codes (256 and 1024). Each curve in a sub-figure compares to a ROC curve for an alternate length of the arbitrary code. Table 4.3 listed genuine and imposter distribution along with EER and decidability index values on three palm-print databases.

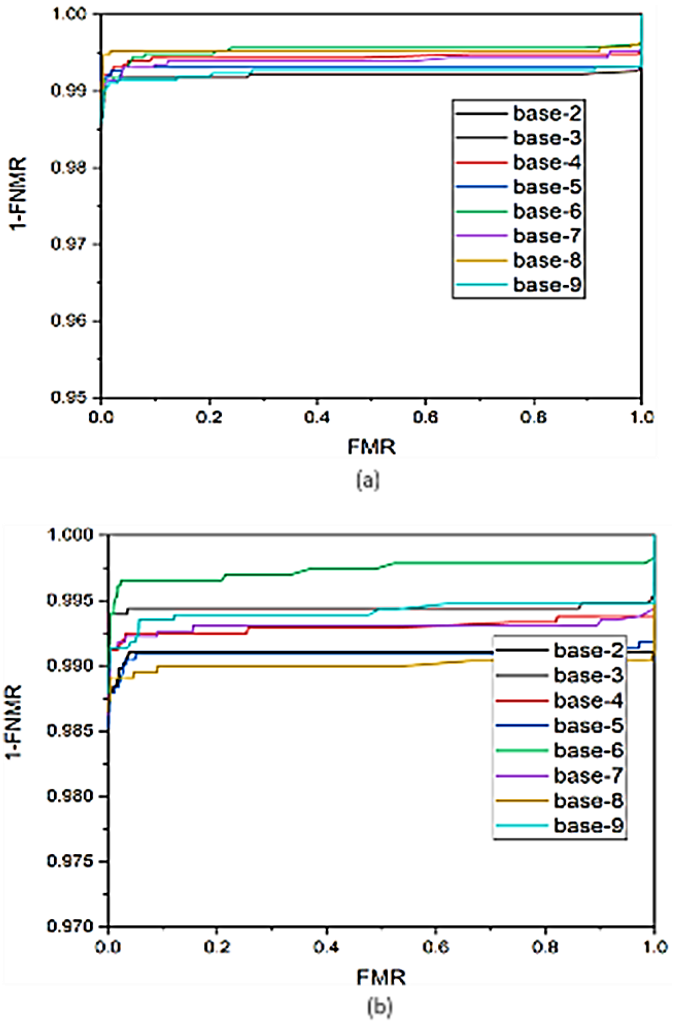

Figure 4.9: ROC Curve on CASIA database (a) for code length 256 and (b) for code length 1024.

Table 4.3 Genuine and imposter distribution along with EER and decidability index.

Database	Genuine		Imposter		EER (%)	decidability index (d)
	mean	variance	mean	variance		
PolyU	0.901	0.315	0.264	0.061	0.62	29.32
CASIA	0.801	0.082	0.398	0.070	0.70	26.98
IIT-Delhi	0.613	0.019	0.401	0.080	1.01	25.25

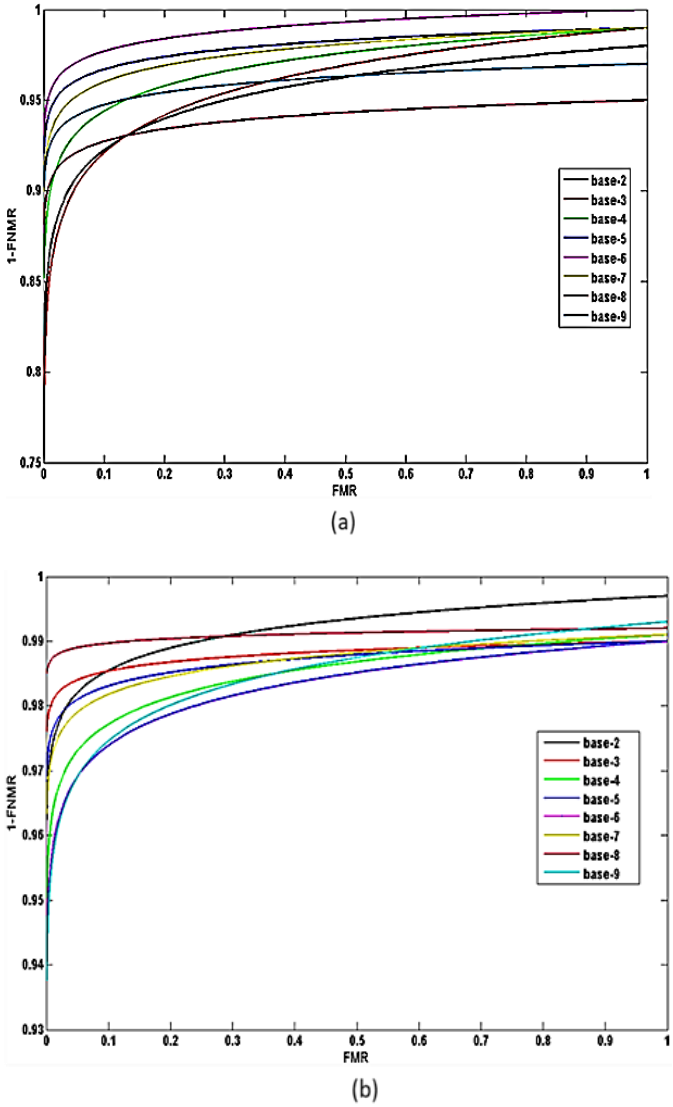

Figure 4.10 ROC Curve on IIT-Delhi database (a) for code length 256 and (b) for code length 1024.

The mean and variances for genuine and impostor are reported and further observed that the separability between genuine and impostor is good. The higher value of decidability index (d>25) indicates high separability and supports low error rates as a result. The proposed approach gives decidability index of 29.32% and 26.98% on PolyU and CASIA databases respectively.

A comparative investigation of the proposed system with some of the state-of-art methods have been explored. Some feature transformation schemes base on random projection such as Gray Salting [5], Palmhash [104], BioConvolving [210], RPM (Random permutation maxout transform) [209] are listed in Table 4.4. The proposed scheme outperforms than gray salting and BioPhasor. The strategy additionally gives preferred outcomes over BioConvolving and permutation-based RPM methods. The proposed scheme achieves an EER of 0.62%. Figure 4.11 represent the appropriation of EER values as box plots (utilizing least, lower quartile, middle, upper quartile and greatest). The comparative inter quartile areas over all code lengths shows that EER esteems are steady concerning code length and base. This permits the verification framework to deftly pick a security level.

4.3.2 Security analysis

Revocability is the basic requirement for cancelable biometrics [115]. The first image of each palm-print in PolyU database is used to create 60 transformed templates and assigning different random grids (q) and different user-specific key (ξ). The first template is matched with the rest of the templates. Mean and variance of the genuine and imposter are listed in Table 4.3. It is demonstrated that the separability between genuine and impostor is good and generates uncorrelated transformed templates.

Hill climbing attacks comprise of an application that sends artificially created particulars layouts to the matcher and, as indicated by the match score, arbitrarily adjusts the formats until the decision threshold is exceeded. This weakness of the standard biometric system is self-addressed in this work by mistreatment indiscriminately generated base-n codes

(length of m) as labels for various users. Further, SHA-3 is used to hash the codes for secured storage. The stored hash digests are non–invertible and bear no alikeness to input biometric information, an intruder would have to be compelled to brute-force all potential codes, i.e., m^n attacks, that is computationally not possible provided ($m > t$), a manually chosen threshold.

Table 4.4: Comparison of EER (%) with state-of-art methods.

Reference	Method	EER (%)
Zuo et al. [5]	Gray Salting	1.02
Leng and Zhang [104]	Biophasor	1.30
Maiorana et al. [210]	BioConvolving	5.95
Leng and Zhang [104]	Palmhash	2.70
Cho and Teoh [209]	RPM (Random permutation maxout transform)	2.91
Proposed	Transformation scheme and secure hash algorithm	0.62

For instance, if a code of length 256 is employed for authentication associate aggressor would have to be compelled to brute force 2^{256} codes that is unworkable.

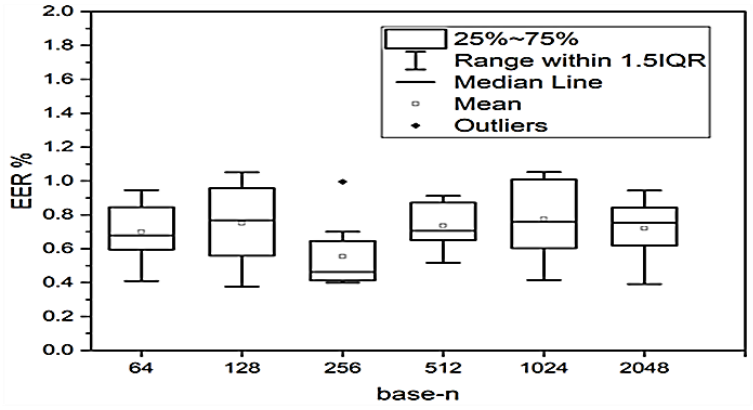

Figure 4.11: EER values across different base-n codes.

4.4 Conclusion

In this Chapter, we developed a secure and cancellable palm-print biometric recognition system. The combined CNN and feature transform structure is employed for mapping palm-prints to random base-n codes. We design CNN to extract features from ROIs. Random slope takes feature vectors extracted by CNN as information samples. The transformation scheme can be considered as reliable and competitive template transformation techniques. SHA-3 is used for storage of templates that's non-invertible, and hence, there's no scope for an intrusion. The good separability between genuine and impostor generates uncorrelated transformed templates. The proficiency of the proposed approach has been tested on PolyU, CASIA and IIT-Delhi palm-print datasets. The evaluations and experiments show high GAR of 99.05% with an EER of 0.62% irrespective of the base and length of labels. Hence, any enterprise can choose the specified bit length for a tunable level of security.

Chapter 5

Conclusion, Future scope and Comparison of Proposed methods

5.1 Introduction

Palm prints are widely accepted as a biometric, hence researchers have invested a lot of time and energy into researching palm print recognition techniques in the scope of image processing, computer vision, and pattern recognition. Unrestricted conditions make palm-print identification a very difficult problem to solve.

This thesis presents five novel feature extraction techniques for palm print recognition that address issues with scale, rotation, and illumination. This work uses a number of databases, including PolyU, CASIA, IIT-Delhi, REST, and Tongji palm-print databases, to test the effectiveness of the proposed and developed methods.

5.2 Comprehensive Study of Different Proposed Methods

In this chapter, we present a comparative analysis of many proposed approaches, including the Gabor filter with kernel-based full space FDA method (Gabor+KFSFDA), the Gabor filter with neural network (Gabor+NN), the MSEALBP, the LBP and multi feature learning (LBP+Feature Learning), and the deep learning-based method (CNN+Feature Transform). In this regard, experiments are conducted on five palm-print databases. The subsequent ROIs are cropped and resized to 128×128 pixels. The training

and testing subsets are selected randomly and each contained around half of the subjects in the database. The subjects in training and testing subsets are disjoint. Table 5.1 depicts the comparative results of these methods on IIT-Delhi database. The highest recognition rate of 98.24% is achieved using MSEALBP. The least EER is achieved 0.0312% using Gabor+ KFSFDA method. Figure 5.1 depicts the CMC curves of proposed methods on IIT-Delhi database. Table 5.2 depicts the comparative results of proposed methods on CASIA database. The least EER esteem is 0.264% using Gabor+KFSFDA method.

Table 5.1: Performance comparison of different proposed methods for IIT-Delhi database.

Methods	Recognition Rate (%)	EER (%)
Gabor+KFSFDA	98.34	0.312
MSEALBP	98.24	1.25
CNN+Feature Transform	97.87	2.89

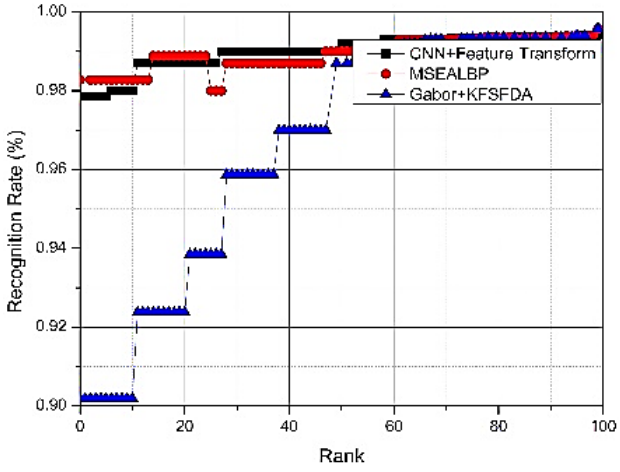

Figure 5.1: CMC curve for IIT-Delhi database.

Table 5.2: Performance comparison of different proposed methods for CASIA database.

Methods	EER (%)
Gabor+KFSFDA method	0.264
MSEALBP	2.76
CNN+Feature Transform	0.70

The performance measures sensitivity, specificity and accuracy of the proposed methods on CASIA database is listed in Table 5.3. The accuracy of 99.16% is obtained using LBP+Feature Learning. The remarkable sensitivity of 97.01% using Gabor+NN. The highest specificity of 98.73% is obtained using MSEALBP. Figure 5.2 depicts the CMC curves of proposed methods on CASIA database.

Table 5.3: Performance measures of different proposed methods for CASIA database.

Methods	**Measures**		
	Accuracy (%)	**Sensitivity (%)**	**Specificity (%)**
Gabor+NN	97.58	97.01	98.25
MSEALBP	97.85	94.14	98.73
LBP+Feature Learning	99.16	97	95.34

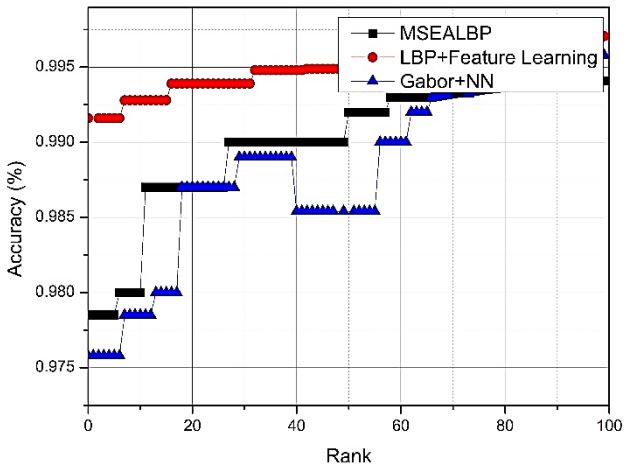

Figure 5.2: CMC curve for CASIA database.

The comparative results on PolyU database are listed in Table 5.4. The least EER esteem is 0.051% using Gabor+KFSFDA method.

The performance measures sensitivity, specificity and accuracy of the proposed methods on Tongji database is listed in Table 5.5.

Table 5.4: Performance comparison of Different proposed methods for PolyU database.

Methods	**EER (%)**
Gabor+KFSFDA method	0.051
MSEALBP	0.2
CNN+Feature Transform	0.62

The highest accuracy and sensitivity of 99.29% and 99.09% is obtained using LBP+Feature Learning. The specificity of 98.91% is achieved using Gabor+NN. Figure 5.3 depicts the CMC curves of proposed methods on Tongji database.

Table 5.5: Performance comparison of Different proposed methods for Tongji database.

Methods	**Measures**		
	Accuracy (%)	**Sensitivity (%)**	**Specificity (%)**
Gabor filter with neural network	98.18	98.11	98.91
LBP and multi-view feature learning	99.29	99.09	95.45

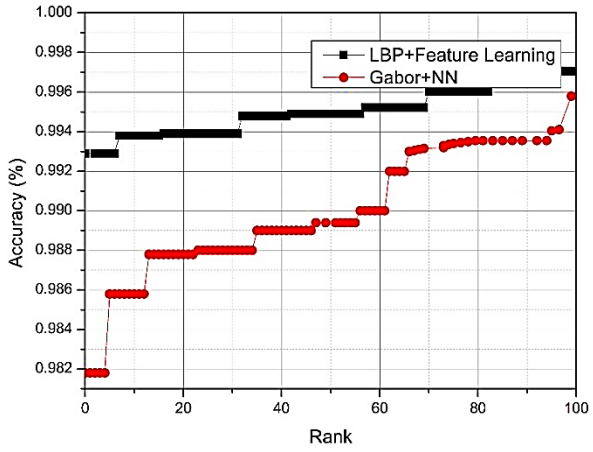

Figure 5.3: CMC curve for Tongji database.

5.3 Conclusion

Initially, palm-print recognition methods using two different Gabor filter designs namely Gabor+KFSFDA and Gabor+NN are proposed to enhance the performance of existing structural based methods. In the first method, the construction of the Gabor filter for palm-print recognition using a kernel-based full space FDA is proposed. To further illustrate the effectiveness of the Gabor filter with kernel-based full space FDA technique, the experiment is conducted on PolyU, CASIA, and IIT-Delhi palm-print datasets. The recognition rates, demonstrated that the Gabor+KFSFDA outperformed the conventional KFDA and FDA methods.

In the second method, we proposed to utilize the NN for palm-print recognition process. The experiments conducted on IIT-Delhi, CASIA, Tongji, and REST contactless palm-print databases. Experimental results show that the proposed method, significantly outperforms the state-of-art methods.

In the third method, a palm-print recognition method using two different LBP designs namely MSEALBP and LBP+Feature Learning are proposed to enhance the performance of existing structural based methods. In the first method, multi scale edge angles LBP (MSEALBP) using edge operators is proposed. Initially, Sobel gradient operator in both vertical and horizontal directions produce directional angle images and then passed through multi-scale LBP to produce uniform patterns of palm-prints. Further, uniform images are divided into non-overlapping blocks of size 5×5 pixels. Finally, the feature vector is feed as an input into the ANN. The experiments conducted on PolyU, IIT-Delhi, and CASIA palm-print databases. The recognition results, demonstrated that the MSEALBP outperformed the conventional LBP, LDP and DGLBP methods.

The fourth method addresses the requirement for a secure and cancelable biometric template generation as an illustration to palm-print biometry. We developed a secure and revocable biometric recognition framework. The combined CNN and feature transform structure is employed for mapping palm-prints to random base-n codes. We design CNN

to extract features from ROIs. Random slope takes feature vectors extracted by CNN as information samples. The transformation scheme can be considered as reliable and competitive template transformation techniques. SHA-3 is used for storage of templates that's non-invertible, and hence, there's no scope for an intrusion. The good separability between genuine and impostor generates uncorrelated transformed templates. The proficiency of the proposed approach has been tested on PolyU, CASIA and IIT-Delhi palm-print datasets. The proposed methodology is analyzed to be competent against attacks. Experimental results show that the proposed method, significantly outperforms the state-of-art methods.

5.4 Future work

Based on the work presented in thesis the directions for the future work could be

- Development of a multi-feature biometric system to form a feature vector by fusing more than one biometric feature of the same subject. Its real time implementation can be explored.
- Real-time implementation of a biometric system using palm-print features by processor.
- Design and development of model for next generation devices.
- Mobile devices have hardware limitation due to weight, storage capacity, and power consumption constraints. Multimodal biometric authentication for mobile devices with limited database would be a challenging task. This can be explored and implemented in future.

Publications from the Thesis

1. Poonia P., and Ajmera P. K., "Upgrading Information Security and Protection for Palm-Print Templates," Wireless Personal Communications, pp. 1-17, 2022.

2. Poonia P., and Ajmera P. K., "Palm-print recognition based on quality estimation and feature dimension," International Journal of Computational Science and Engineering, vol. 25, no. 2, pp. 116-127, 2022.

3. Poonia P., and Ajmera P. K., "Adaptive Linear Gabor Response Pattern for Palm-print Recognition," Trends in Opto-Electro & Optical Communication (TOEOC), vol. 12, no. 2 2022.

4. Poonia P., Ajmera P. K., and Bhalerao A., "Palm-print recognition based on scale invariant features," 2019 IEEE 16th India Council International Conference (INDICON), IEEE, 2019.

5. Poonia P., Ajmera P. K., and Shende V., "Palmprint recognition using robust template matching," Procedia Computer Science, vol. 167, pp. 727-736, 2020.

6. Poonia P., and Ajmera P. K., "Palm-print identification based on deep residual networks," 2021 Fourth International Conference on Computational Intelligence and Communication Technologies (CCICT), IEEE, 2021.

7. Poonia P., Deshmukh O. G., and Ajmera P. K., "Adaptive Quality Enhancement Fingerprint Analysis," 3rd International Conference on Emerging Technologies in Computer Engineering: Machine Learning and Internet of Things (ICETCE), IEEE, 2020.

8. Poonia P., and Ajmera P. K., "Palm-print recognition based on image quality and texture features with neural network," 2021 Sixth International Conference on Image Information Processing (ICIIP), IEEE, vol. 6, 2021.

9. Poonia P., and Ajmera P. K., "Robust palm-print recognition using multi-resolution texture patterns with artificial neural network," Wireless Personal Communications, (Under Review).

10. Poonia P., and Ajmera P. K., Secured human authentication based on multi-stage hybrid PSO with artificial neural network," The Imaging Science Journal, (Reviews completed).

11. Poonia P., and Ajmera P. K., "Multi-view feature learning based on texture description for palm-print recognition," Wireless Personal Communications, (Major Revision).

12. Poonia P., and Ajmera P. K., "Robust Multi-spectral Palm-print Recognition," International Conference on Next Generation Systems and Networks, BITS EEE CON 2022, (Accepted and Presented).

References

[1] Jain A.K., Ross A., Prabhakar S., "An introduction to biometric recognition," IEEE Trans. Circuits Syst. Video Technol., vol. 14, no. 1, pp. 4-20, 2004.

[2] Jain A.K., Ross A., Nandakuma K., "Introduction to Biometric," Springer USA, 2011.

[3] Shaveta Dargan, Munish K., "A comprehensive survey on the biometric recognition systems based on physiological and behavioral modalities," Expert Systems with Applications, vol. 143, 113114, 2020.

[4] Unar J. A., Woo C. S., Almas A., "A review of biometric technology along with trends and prospects," Pattern Recognition, vol. 47, no. 8, pp. 2673-2688, 2014.

[5] Zuo J., Ratha N.K., Connell J.H., "Cancelable iris biometric," IEEE conf. on Pattern Recognition, pp. 1– 4, 2008.

[6] Dantcheva A., Elia P., Ross A., "What else does your biometrics data reveal? A survey on soft biometrics," IEEE Transactions on Information Forensics and Security (TIFS), vol. 11, no. 3, pp. 441-467, 2016.

[7] Zhu Y., Dass S.C., "Statistical models for assessing the individuality of fingerprints," IEEE Trans. Inform. Forensics Secur., vol. 2, no. 3, pp. 391-401, 2007.

[8] Yinghui Zhu and Yuzhen Jiang, "Optimization of face recognition algorithm based on deep learning multi feature fusion driven by big data," Image and Vision Computing, vol. 104, 104023 2020.

[9] Qingqiao H., Siyang Y. and Huiyang N. et al., "An End-to-End Deep Neural Network for Iris Recognition," Procedia Computer Science, vol. 174, pp. 505-517, 2020.

[10] Yang C., Yang, Hong L., and Zengmei L., "Simultaneous texture image enhancement and directional field estimation based on local quality metrics," Optik, vol. 158, pp.1203-1219, 2018.

[11] Adams Kong, David Zhang, Mohamed Kame, "A survey of palmprint recognition," Pattern Recognition, vol. 42, pp. 1408 – 1418, 2009.

[12] Kong A., Zhang D., Lu G., "A study of identical twins palmprint for personal verification," Pattern Recognition, vol. 39, no. 11, pp. 2149–2156, 2006.

[13] Zhang L., Li L., Yang A., and Shen Y. et al., "Towards contactless palm print recognition: a novel device, a new benchmark, and a collaborative representation-based identification approach," Pattern Recognition, vol. 69, pp. 199-212, 2017.

[14] Feng J. F., Liu C.J., Wang H., "High-resolution palmprint minutiae extraction based on Gabor feature," Sci. China-Inf. Sci., vol. 57, pp. 1-15, 2014.

[15] Wang R. F., Ramos D., Veldhuis R., "Regional fusion for high resolution palmprint recognition using spectral minutiae representation," IET Biometrics, vol. 2014, 3, (2), pp. 94-100.

[16] Kong W.K., and Zhang D., "Palmprint texture analysis based on low-resolution images for personal authentication," IEEE Int. Conf. on Object recognition supported by user interaction for service robots, pp. 1-4, 2002.

[17] Priyanka S., and Milind R., "Survey of Palmprint Recognition," International Journal of Scientific & Engineering Research, Vol. 3, no. 2, 2012.

[18] Imad R., Romain H., Gian L. M., and Gilles G., "Palmprint recognition with an efficient data driven ensemble classifier," Pattern Recognition Letters, vol. 126, pp. 21–30, 2019.

[19] Fei L., Guangming L., Wei J., and Shaohua T. et al., "Feature Extraction Methods for Palmprint Recognition: A Survey and Evaluation," IEEE Transactions on Systems, Man, and Cybernetics: System, vol. 49, no. 2, 2019.

[20] Lu G. M., Zhang D., and Wang K. Q., "Palmprint recognition using eigenpalms features," Pattern Recognition Letters, vol. 24, no. 9, pp. 1463-1467, 2003.

[21] Sang H., Yuan W., Zhang Z., "Research of Palmprint Recognition Based on 2DPCA," International Symposium on Neural Networks (ISNN 2009), pp. 831–838, 2009.

[22] Pan X., and Ruan Q. Q., "Palmprint recognition using Gabor feature-based (2D)2PCA," Neurocomputing, vol. 71, no. 13, pp. 3032-3036, 2008.

[23] Wang L., Jin W., Liu Z., and He Y., "A Method of Palmprint Recognition Integrated by 2D-PCA and Sparse Representation," Opto-Electronic Engineering, vol. 39, no. 10, pp. 59-64, 2012.

[24] Wu X., Zhang D., and Wang K., "Fisherpalms based palmprint recognition," Pattern recognition letters, vol. 24, no. 15, pp. 2829-2838, 2003.

[25] Du F., Yu P., Li H. et al., "Palmprint recognition using Gabor feature based bidirectional 2DLDA," Computer Science for Environmental Engineering and Eco Informatics, pp. 230-235, 2011.

[26] Lu G. M., Wang K. Q., and Zhang D., “Wavelet based independent component analysis for palmprint identification,” International Conference on Machine Learning and Cybernetics, pp. 3547-3550, 2004.

[27] Hu D. G., Feng Z., Zhou Z., “Two-dimensional locality preserving projections (2DLPP) with its application to palmprint recognition,” Pattern Recognition, vol. 40, no. 1, pp. 339–342, 2007.

[28] Fukunaga K., “Introduction to Statistical Pattern Recognition,” 2nd ed., Academic Press, San Diego, 1990.

[29] Sugiyama M., “Dimensionality reduction of multimodal labeled data by local Fisher discriminant analysis,” Journal of Machine Learning Research, vol. 8, no. 37, pp.1027–1061, 2007.

[30] Wang Y. X., and Ruan Q., “Kernel Fisher discriminant analysis for palmprint recognition,” International Conference on Pattern Recognition, USA, pp. 457-460, 2006.

[31] Cui J., Wen J., and Fan Z., “Appearance-based bidirectional representation for palmprint recognition,” Multimedia Tools Application, vol. 74, no. 24, 10989–11001, 2015.

[32] Raghavendra R., and Busch C., “Novel image fusion scheme based on dependency measure for robust multispectral palmprint recognition,” Pattern Recognition, vol. 47, no. 6, pp. 2205–2221, 2014.

[33] Li S., “Palmprint recognition method based on a new kernel sparse representation method,” International conference on intelligent computing theories and technology, pp. 515–523, 2013.

[34] Shu W., and Zhang D., “Palmprint verification: an implementation of biometric technology,” International Conference on Pattern Recognition, Australia, pp. 219-221, 1998.

[35] Zhang D., and Shu W., “Two novel characteristics in palmprint verification: datum point invariance and line feature matching,” Pattern Recognition, vol. 32, no. 4, pp. 691-702, 1999.

[36] Wu X., Wang K., and Zhang D., “Line feature extraction and matching in palmprint,” Int. Conf. on Image and Graphics, pp. 583–590, 2002.

[37] Wu X., Wang K., Zhang D., “Fuzzy direction element energy feature (FDEEF) based palmprint identification,” Int. Conf. on Pattern Recognition, vol. 1, pp. 95–98, 2002.

[38] Diaz M.R., Travieso C.M., and Alonso J. B. et al., “Biometric system based in the feature of hand palm,” Int. Carnahan Conf. on Security Technology, pp. 136–139, 2004.

[39] Wang Y., and Ruan Q., “Palm-line extraction using steerable filters,” IEEE International Conference on Signal Processing, vol. 3, 2006.

[40] Huang D. S., Jia W., and Zhang D., “Palmprint verification based on principal lines,” Pattern Recognition, vol. 41, no. 4, pp. 1316-1328, 2008.

[41] Zia U., Zahoor J., Jamil A., and Almas A., “A Novel Technique for Principal Lines Extraction in Palmprint Using Morphological TOP-HAT Filtering,” World Applied Sciences Journal, vol. 31, no. 12, pp. 2010-2014, 2014.

[42] Zhang D., Kong W.K., and You J. et al., “On-line palmprint identification,” IEEE Transactions on Pattern Analysis and Machine Intelligence,” vol. 25, no. 9, pp. 1041-1050, 2003.

[43] Kong A., Zhang D., and Kamel M., “Palmprint identification using feature-level fusion,” Pattern Recognition, vol. 39, no. 3, pp. 478–487, 2006.

[44] Kong A.-K., and Zhang D., “Competitive coding scheme for palmprint verification,” Int. Conf. on Pattern Recognition, vol. 1, pp. 520– 523, 2004.

[45] Sun Z., Tan T., and Wang Y. et al., “Ordinal palmprint representation for personal identification,” IEEE Conf. on Computer Vision and Pattern Recognition (CVPR), vol. 1, pp. 279–284, 2005.

[46] Jia W., Huang D.-S., Zhang D., “Palmprint verification based on robust line orientation code,” Pattern Recognition, 2008, 41, (5), pp. 1504–1513, 2008.

[47] Guo Z., Zhang D., and Zhang L. et al., “Palmprint verification using binary orientation co-occurrence vector,” Pattern Recognition Letters, vol. 30, no. 13, pp. 1219–1227, 2009.

[48] Zhang L., Li H., and Niu J., “Fragile bits in palmprint recognition,” IEEE Signal Processing Letters, vol. 19, no. 10, pp. 663–666, 2012.

[49] Fei L., Xu Y., and Zhang D., “Half-orientation Extraction of palmprint features,” Pattern Recognition Letters, vol. 69, pp. 35–41, 2016.

[50] Fei L., Xu Y., and Tang W. et al., “Double orientation code and nonlinear matching scheme for palmprint recognition,” Pattern Recognition, vol. 49, pp. 89–101, 2016.

[51] Xu Y., Fei L., and Wen J. et al., “Discriminative and Robust Competitive Code for Palmprint Recognition,” IEEE Trans. Syst. Man Cybern. Syst., vol. 48, pp. 232-241, 2018.

[52] Fei L., Zhang B., and Zhang W. et al., “Local apparent and latent direction extraction for palmprint recognition,” Information Sciences, vol. 473, pp. 59–72, 2019.

[53] Xiao B., Wang K., Bi X., and Li W. et al., "2DLBP: An enhanced local binary feature for texture image classification," IEEE Trans. Circuits Syst. Video Technol., vol. 29, no. 9, pp. 2796–2808 2019.

[54] Song T., Li H., Meng F., and Wu Q. et al., "LETRIST: Locally encoded transform feature histogram for rotation-invariant texture classification," IEEE Trans. Circuits Syst. Video Technol., vol. 28, no. 7, pp. 1565–1579, 2018.

[55] Jabid T., Kabir M.H., and Chae O., "Robust facial expression recognition based on local directional pattern," ETRI Journal, vol. 32, no. 5, pp. 784–794, 2010.

[56] Luo Y., Zhao L., and Zhang B. et al., "Local line directional pattern for palmprint recognition," Pattern Recognition, vol. 50, no. 2, pp. 26–44, 2016.

[57] Hong D., Liu W., and Su J. et al., "A novel hierarchical approach for multispectral palmprint recognition," Neurocomputing, vol. 151, pp. 511– 521, 2015.

[58] Hong D., Liu W., and Wu X. et al., "Robust palmprint recognition based on the fast variation vese–osher model," Neurocomputing, vol. 174, pp. 999–1012, 2016.

[59] Li G., and Kim J., "Palmprint recognition with local micro-structure tetra pattern," Pattern Recognition, vol. 61, pp. 29–46, 2017.

[60] Ojala T., Pietikäinen M., and Harwood D., "A comparative study of texture measures with classification based on featured distributions," Pattern Recognition, vol. 29, no. 1, pp. 51–59, 1996.

[61] Tamrakar D., and Khanna P., "Occlusion invariant palmprint recognition with ULBP histograms," Int. conf. on Image and Signal processing, pp. 491-500, 2015.

[62] Michael G.K.O., Connie T., and Jin A.T.B., "Touch-less palm print biometrics: novel design and implementation," Image Vision Comput., vol. 26, no. 12, pp. 1551-1560, 2008.

[63] Mu M., Ruan Q., Guo S., "Shift and gray scale invariant features for palmprint identification using complex directional wavelet and local binary pattern," Neurocomputing, vol. 74, pp. 3351– 3360, 2011.

[64] Guo X., Zhou W., and Zhang Y., "Collaborative representation with HM-LBP features for palmprint recognition," Machine Vision and Applications, vol. 28, pp. 283–291, 2017.

[65] Zhang S., Wang H., and Wenzhun H. et al., "Combining Modified LBP and Weighted SRC for Palmprint Recognition," Signal, Image and Video Processing, vol. 12, pp. 1035–1042, 2018.

[66] Karanwal S., and Diwakar M., "Neighborhood and center difference-based-LBP for face recognition," Pattern Anal. Applic., vol. 24, pp. 741–761, 2021.

[67] Tarhouni W., Boubchir L., and Elbendak M. et al., “Multispectral palmprint recognition using Pascal coefficients-based LBP and PHOG descriptors with random sampling,” Neural Comput. Appl., vol. 4, pp. 1–11, 2017.

[68] Wang W., Jin W., and Xie Y. et al., “Palmprint recognition using uniform local binary patterns and sparse representation,” Opto Electron Eng., vol. 41, no. 12, pp. 60–65, 2014.

[69] Zhang S., Harry W., and Wenzhun H., “Palmprint identification combining hierarchical multi-scale complete LBP and weighted SR,” Soft Computing, vol. 24, pp. 4041–4053, 2020.

[70] Kumar A., and Zhang D., “Personal authentication using multiple palmprint representation,” Pattern Recognition, vol. 38, no. 10, pp. 1695–1704, 2005.

[71] Morles A., Ferrer M.A., and Kumar A., “Towards contactless palmprint authentication,” IET Comput. Vis., vol. 5, no. 6, pp. 407–416, 2011.

[72] Kumar A., and Shekhar S., “Personal identification using multi-biometrics Rank-level Fusion,” IEEE Trans. Syst. Man Cybern. Part C – Appl. Rev., vol. 41, no. 5, pp. 743–752, 2011.

[73] Yao H., Chuyi L., Dan H., and Weiyu Y., “Gabor Feature Based Convolutional Neural Network for Object Recognition in Natural Scene,” International Conference on Information Science and Control Engineering (ICISCE), pp. 386-390, 2016.

[74] Toghyani S., Ahmadi M.H., and Kasaeian A. et al., “Artificial neural network, ANN-PSO and ANN-ICA for modelling the Stirling engine,” Int. J. Ambient Energy, vol. 37, no. 5, pp. 456–468, 2016.

[75] Xie C., and Kumar A., “Finger vein identification using Convolutional Neural Network and supervised discrete hashing,” Pattern Recognition Letters, vol. 119, pp. 148-156, 2019.

[76] Svoboda J., Masci J., and Bronstein M. M., “Palmprint recognition via discriminative index learning,” Proc. ICPR, pp. 4232–4237, 2016.

[77] Ramachandra R., Raja K. B., Venkatesh S., and Hegde S. et al., “Verifying the newborns without infection risks using contactless palmprints,” Proc. ICB, pp. 209–216, 2018.

[78] Genovese A., Piuri V., Scotti F., and Plataniotis K. N., “PalmNet: Gabor- PCA convolutional networks for touchless palmprint recognition,” IEEE Trans. Inf. Forensics Security, vol. 14, no. 12, pp. 3160–3174, 2019.

[79] Minaee S., and Wang Y., “Palmprint recognition using deep scattering network,” Proc. Int. Symp. Circuits Syst., pp. 1–4, 2017.

[80] Meraoumia A., Kadri F., Bendjenna H., Chitroub S., and Bouridane A., “Improving biometric identification performance using PCANet deep learning and multispectral palmprint,” Biometric Security and Privacy (Signal Processing for Security Technologies), Cham, Springer, pp. 51–69, 2017.

[81] Dian L., and Dongmei S., “Contactless palmprint recognition based on convolutional neural network,” Int. Conf. Signal Process. (ICSP), pp. 1363–1367, 2016.

[82] Jalali A., Mallipeddi R., and Lee M., “Deformation invariant and contactless palmprint recognition using convolutional neural network,” Int. Conf. Hum.-Agent Interact., pp. 209–212, 2015.

[83] Izadpanahkakhk M., Razavi S. M., Taghipour-Gorjikolaie M., and Zahiri S. H. et al., “Deep region of interest and feature extraction models for palmprint verification using convolutional neural networks transfer learning,” Appl. Sci., vol. 8, no. 7, pp. 1210, 2018.

[84] European council, regulation of the european parliament and of the council on the protection of individuals with regard to the processing of personal data and on the free movement of such data (general data protection regulation), 04, 2016.

[85] Uludag U., Pankanti S., Prabhakar S., and Jain A.K., “Biometric cryptosystems: Issues and challenges,” Proc. IEEE, vol. 92, no. 6, pp. 948-960, 2004.

[86] Ross A. A., Shah J., and Jain A.K., “Toward reconstructing fingerprints from minutiae points, Defence and Security,” International Society for Optics and Photonics, pp. 68-80, 2005.

[87] Uludag U., and Jain A.K., “Attacks on biometric systems: a case study in fingerprints,” Proceedings of SPIE, pp. 622-633, 2004.

[88] Lai Y.L., Jin A., and Teoh A.B.J., “Cancellable iris template generation based on indexing-first-one hashing,” Pattern Recognition, vol. 64, pp. 105-117, 2017.

[89] Chan C. H., Yan F., Kittler J., and Mikolajczyk K., “Full ranking as local descriptor for visual recognition: A comparison of distance metrics on sn,” Pattern Recognition, vol. 48, no. 4, pp. 1328–1336, 2015.

[90] Gomez-Barrero M., Galbally J., Rathgeb C., and Busch C., “General framework to evaluate unlinkability in biometric template protection systems,” IEEE Trans. Inf. Forensics Security, vol. 13, no. 6, pp. 1406-1420, 2018.

[91] Juels A. and Sudan M., “A fuzzy vault scheme,” Des., Codes Cryptogr., vol. 38, pp. 237-257, 2006.

[92] Juels A., and Wattenberg M., “A fuzzy commitment scheme,” Proc. ACM Conf. Comput. Commun. Secur., pp. 28-36, 1999.

[93] Blanton M., and Aliasgari M., "Analysis of reusability of secure sketches and fuzzy extractors," IEEE Trans. Inf. Forensics Security, vol. 8, no. 9, pp. 1433-1445, 2013.

[94] Dodis Y., Rafail O., Reyzin L., and Adam S., "Fuzzy Extractors: How to Generate Strong Keys from Biometrics and Other Noisy Data," SIAM Journal on Computing, vol. 38, no. 1, pp 97-139, 2008.

[95] Tams B., Mihilescu P., and Munk A., "Security considerations in minutiae-based fuzzy vaults," IEEE Trans. Inf. Forensics Security, vol. 10, no. 5, pp. 985-998, 2015.

[96] Kim J. and Teoh A. B. J., "One-factor cancellable biometrics based on indexing-first-order hashing for fingerprint authentication," Proc. Conf. Pattern Recognit. (ICPR), China, pp. 3108-3113, 2018.

[97] Ratha N.K., Connell J., and Bolle R., "A biometrics-based secure authentication system," Proc. IEEE Workshop Automatic Identification Advanced Technologies, pp. 70-73, 1999.

[98] Connie T., Teoh J., Goh M., and Ngo D., "PalmHashing: a novel approach for cancelable biometrics," Inf Process Lett., vol. 93, no. 1, pp. 1-5, 2005.

[99] Khan M., Zhang J., and Tian L., "Chaotic secure content-based hidden transmission of biometric templates," Chaos Solitons Fractals, vol. 32, no. 5, pp. 1749-1759, 2007.

[100] Umer S., Dhara B.C., and Chanda B., "A novel cancelable iris recognition system based on feature learning techniques," Inf. Sci., vol. 406, pp. 102-118, 2017.

[101] Jin Z., Hwang J. Y., Lai Y., and Kim S. et al., "Ranking-Based Locality Sensitive Hashing-Enabled Cancelable Biometrics: Index-of-Max Hashing," IEEE Transactions on Information Forensics and Security, vol. 13, no. 2, pp. 393-407, 2018.

[102] Leng L., and Zhang J., "Dual-key-binding cancelable palmprint cryptosystem for palmprint protection and information security," J Network Comput. Appl., vol. 34, no. 6, pp. 1979-1989, 2011.

[103] Liu S., Mou X., and Cai Y., "Pseudo-random bit generator based on couple chaotic systems and its applications in stream-cipher cryptography," Progress in cryptology-IndoCrypt., vol. 2247, pp. 316-329, 2001.

[104] Leng L., and Zhang J. S., "PalmHash code vs palmphasor code," Neurocomputing, vol. 108, pp.1–12, 2013.

[105] Teoh A. B. J., Goh A., and Ngo D. C. L., "Random multispace quantization as an analytic mechanism for biohashing of biometric and random identity inputs," IEEE Trans Pattern Anal Mach Intell., vol. 28, no. 12, pp. 1892–1901, 2006.

[106] Sadhya D., and Raman B., “Generation of cancelable Iris templates via randomized bit sampling,” IEEE Trans Inf Forensic Secur., vol. 14, no. 11, pp. 2972–2986, 2019.

[107] Bringer J., Morel C., and Rathgeb C., “Security analysis of bloom filter-based iris biometric template protection,” International conference on biometrics, pp 527–534, 2015.

[108] Bringer J., Morel C., and Rathgeb C., “Security analysis and improvement of some biometric protected templates based on Bloom filters,” Image Vis. Comput., vol. 58, pp. 239–253, 2017.

[109] Marta G., Christian R., and Javier G. et al., “Unlinkable and irreversible biometric template protection based on bloom filters,” Inf. Sci., vol. 370, pp. 18–32, 2016.

[110] Debanjan S., and Sanjay K. S., “Providing robust security measures to Bloom filter based biometric template, protection schemes,” Comput. Secur., 67, pp. 59–72, 2017.

[111] Drozdowski P., Garg S., and Rathgeb C. et al., “Privacy-preserving indexing of Iris-codes with cancellable Bloom filter-based search structures,” Procd. of European Signal Processing Conference (EUSIPCO), 2018.

[112] Rathgeb C., Breitinger F., and Busch C., “Alignment-free cancelable iris biometric templates based on adaptive bloom filters,” Proceedings of ICB, pp. 1-8, 2013.

[113] Ahmad T., Hu J., and Wang S., “Pair-polar coordinate-based cancelable fingerprint templates,” Pattern Recognit., vol. 44, no. 25, pp. 55–64, 2011.

[114] Patel V. M., Ratha N. K., and Chellappa R., “Cancelable biometrics: a review,” IEEE Signal Process Mag., vol. 32, pp. 54–65, 2015.

[115] Teoh A. B. J., Kuan Y. W., and Lee S., “Cancellable biometrics and annotations on bio hash,” Pattern Recognit., vol. 41, no. 20, pp. 34–44, 2008.

[116] Jin A.T.B., “Cancellable biometrics and multispace random projections,” IEEE Conf. on computer vision and pattern recognition workshop (CVPRW’06), pp. 164-164, 2006.

[117] Pillai J. K., Patel V. M., Chellappa R., and Ratha N. K., “Sectored random projections for cancelable iris biometrics,” IEEE international conference on acoustics speech and signal processing (ICASSP), pp. 1838–41, 2010.

[118] Pillai J. K., Patel V. M., Chellappa R., and Ratha N. K., “Secure and robust iris recognition using random projections and sparse representations,” IEEE Trans Pattern Anal. Mach. Intell., vol. 33, no. 18, pp. 77–93, 2011.

[119] Jin Z., Goi B. M., Teoh A., and Tay Y. H., "A two-dimensional random projected minutiae vicinity decomposition based cancellable fingerprint template," Security and Communication Networks, pp. 1691-1701, 2013.

[120] Trivedi A. K., Thounaojam D. M., and Pal S., "Non-Invertible cancellable fingerprint template for fingerprint biometric," Comput. Sec., vol. 90, 101690, 2020.

[121] Uhl H. J., Pschernig E., and Uhl A., "Cancelable iris biometrics using block remapping and image warping," Information Security, Springer, pp. 135–142, 2009.

[122] Jenisch S., and Uhl A., "Security analysis of a cancelable iris recognition system based on block remapping," IEEE Int. Conference on Image Processing (ICIP), pp. 3213–3216, 2011.

[123] Li H., Qiu J., and Teoh A. B. J., "Palmprint template protection scheme based on randomized cuckoo hashing and MinHash," Multimed Tools Appl., pp. 1–25, 2020.

[124] Kong W.K., Zhang D., and Li, W., "Palmprint feature extraction using 2-D Gabor filters," Pattern Recogn., vol. 36, no. 10, pp. 2339-2347, 2003.

[125] Li W., Zhang B., Zhang L., and Yan J., "Principal line-based alignment refinement for palmprint recognition," IEEE Transactions on Systems, Man, and Cybernetics, Part C (Applications and Reviews), vol. 42, no. 6, pp.1491–1499, 2012.

[126] Zhang C., Zhong W., Zhang C., and Qin X., "Double Half-Orientation Code and Nonlinear Matching Scheme for Palmprint Recognition," International Conference on Mechatronics and Intelligent Robotics, pp. 36–42, 2018.

[127] Danlami M., Jamel S., Ramli S. N., and Azahari S. R. M., "Comparing the Legendre Wavelet filter and the Gabor Wavelet filter For Feature Extraction based on Iris Recognition System," IEEE 6th International Conference on Optimization and Applications (ICOA), pp. 1-6, 2020.

[128] Low C., Teoh A. B., and Ng C., "Multi-Fold Gabor, PCA, and ICA Filter Convolution Descriptor for Face Recognition," IEEE Transactions on Circuits and Systems for Video Technology, vol. 29, no. 1, pp. 115-129, 2019.

[129] Garg A., Chaudhary K., and Kumar V., "Fingerprint recognition using Gabor Filter," Int. Conf. on Computing for Sustainable Global Development, pp. 953-958, 2014.

[130] Bourkache N., Laghrouch M., and Sidhom S., "Gabor Filter Algorithm for medical image processing: evolution in Big Data context, International Multi-Conference on Organization of Knowledge and Advanced Technologies OCTA, pp. 1-4, 2020.

[131] Hinton G. E., and Salakhutdinov R. R., Reducing the dimensionality of data with neural networks," Science, vol. 313, pp. 504–507, 2006.

[132] PolyUpalmprint Database: http://www.comp.polyu.edu.hk/~biometrics/:

[133] CASIA palm print database: http://biometrics.idealtest.org/.

[134] IIT Delhi palmprint database: Available at http://www4.comp.polyu.edu.hk/~csajaykr/IITD/Database_Palm.htm.

[135] PolyU Multispectral Palmprint Database. Available at http://www4.comp.polyu.edu.hk/ biometrics/MultispectralPalmprint/MSP.htm.

[136] Charfi N., Trichili H., Alimi A. M., and Solaiman B., "Local invariant representation for multi-instance touchless palmprint identification," IEEE Int. Conf. Syst., Man, Cybern. (SMC), pp. 3522–3527, 2016.

[137] Tongji University. (2017). Tongji Contactless Palmprint Dataset. [Online]. https://cslinzhang.github.io/Contactless Palm/.

[138] Lee D.D., and Seung H.S., "Learning the parts of objects by non-negative matrix factorization," Nature, vol. 401, pp. 788–791, 1999.

[139] Guan N., Tao D., Luo Z., and Yuan B., "NeNMF: an optimal gradient method for non-negative matrix factorization," IEEE Trans. Signal Process., vol. 60, pp. 2882–2898, 2012.

[140] Turk M., and Pentland A., "Eigenfaces for recognition," J. Cogn. Neuroscience, vol. 3, pp. 71–86, 1991.

[141] Belhumeur P.N., Hespanha J.P., and Kriegman D.J. "Eigenfaces vs. fisherfaces: recognition using class specific linear projection," IEEE Trans. Pattern Anal. Mach. Intell., vol. 19, pp. 711–720, 1997.

[142] Mika S., Rätsch G., Weston J., and Schölkopf B. et al., "Fisher discriminant analysis with kernels," Proceedings of the IEEE Signal Processing Society Workshop on Neural Network for Signal Processing, pp. 41-48, 1999.

[143] Kwang I. K., Keechul J., and Hang J. K., "Face recognition using kernel principal component analyses," IEEE Signal Processing Letters, vol. 9, pp. 40-42, 2002.

[144] Zafeiriou S., Tzimiropoulos G., Petrou M., and Stathaki T., "Regularized kernel discriminant analysis with a robust kernel for face recognition and verification," IEEE Trans. Neural Netw. Learn. Syst., vol. 23, pp. 526-534, 2012.

[145] Gui J., Jia W., Zhu L. and Wang S.-L. et al., Locality preserving discriminant projections for face and palmprint recognition," Neurocomputing, vol. 73, pp. 2696-2707, 2010.

[146] Badrinath G., and Gupta P., Palmprint based recognition system using phase-difference information," Futur. Gener. Comput. Syst., vol. 28, no. 1, pp. 287-305, 2012.

[147] Xie S., Yoon S., Yang C., and Park D., "Rule-based fingerprint quality estimation system using the optimal orientation certainty level approach," IEEE international conference on biomedical engineering and informatics, pp. 1–5, 2009.

[148] Yuan L., Mu Z.-C., and Zeng H., "Partially occluded ear recognition based on local features," Journal of University of Science and Technology, vol. 32, no. 4, pp. 530–535, 2010.

[149] Ma X., Jing X., Huang H., and Cui Y. et al., "Palm vein recognition scheme based on an adaptive Gabor filter," IET Biom., vol. 6, no. 5, pp. 325-333, 2017.

[150] Jaswal G., Kaul A. and Nath R., "Multiple feature fusion for unconstrained palm print authentication," Computers and Electrical Engineering, vol. 72, no. 42, pp.53–78, 2018.

[151] Saedi S. and Charkari N.M., "Palmprint authentication based on discrete orthonormal S-transform," Applied Soft Computing, vol. 21, no. 4, pp.341–351, 2014.

[152] Cao X., Yao J., Xu Z., and Meng D., "Hyperspectral Image Classification with Convolutional Neural Network and Active Learning," IEEE Transactions on Geoscience and Remote Sensing, vol. 58, no. 7, pp. 4604-4616, 2020.

[153] Liu Z. -X., Shao W., Ding X., and Ye Z., "GA-Optimized ANN for Modeling of UWB Filters," International Conference on Microwave and Millimeter Wave Technology (ICMMT), pp. 1-2, 2020.

[154] Jiang X., Satapathy S.C., and Yang L. et al., "A Survey on Artificial Intelligence in Chinese Sign Language Recognition," Arab J Sci Eng., vol. 45, pp. 9859–9894, 2020.

[155] He X., "ANN Model Using Gradient Descent to Train Weight Vectors," International Conference on Communications, Information System and Computer Engineering (CISCE), pp. 574-577, 2021.

[156] Canlı H., and Toklu S., "Design and Implementation of a Prediction Approach Using Big Data and Deep Learning Techniques for Parking Occupancy," Arab J Sci Eng., 2021.

[157] Xiong C., Li W., Liu Y., and Wang M., "Multi-Dimensional Edge Features Graph Neural Network on Few-Shot Image Classification," IEEE Signal Processing Letters, vol. 28, pp. 573-577, 2021.

[158] Esfe M. H., Hajmohammad H., Toghraie D., and Rostamian H. et al., "Multi-objective optimization of nanofluid flow in double tube heat exchangers for applications in energy systems," Energy, vol. 137, pp. 160–171, 2017.

[159] Wang D., Tan D., and Liu L., “Particle swarm optimization algorithm: An overview,” Soft Computing, pp. 387–408, 2017.

[160] Jamalia B., Rasekhb M., Jamadic F., and Gandomkara R., “Using PSO-GA algorithm for training artificial neural network to forecast solar space heating system parameters,” Applied Thermal Engineering, vol. 147, pp. 647–660, 2019.

[161] Clerc M., and Kennedy J., “The particle swarm-explosion, stability and convergence in a multidimensional complex space,” IEEE Trans. Evol. Comput., vol. 6, no. 1, pp. 58–73, 2002.

[162] Zhan Z. H., Xiao J., Zhang J., and Chen W.N., “Adaptive control of acceleration coefficients for particle swarm optimization based on clustering analysis,” IEEE Congr. Evol. Comput., Singapore, pp. 3276–3282, 2007.

[163] Kim J., Lee K., and Choe J., “Efficient and robust optimization for well patterns using a PSO algorithm with a CNN-based proxy model,” Journal of Petroleum Science and Engineering, vol. 207,109088, 2021.

[164] Gawanmeh A., Parvin S., and Alwadi A., “A Genetic Algorithmic Method for Scheduling Optimization in Cloud Computing Services,” Arab J Sci Eng., vol. 43, pp. 6709–6718, 2018.

[165] Diederik P., and Kingma J. B., “Adam: A Method for Stochastic Optimization,” ICLR, 2015.

[166] Mahmoodabadi M. J., Mottaghi Z. S., and Bagheri A., “HEPSO: High exploration particle swarm optimization,” Information Sciences, vol. 273, pp. 101–111, 2014.

[167] Jia W., Hu R. X., and Lei Y. K. et al., “Histogram of oriented lines for palmprint recognition,” IEEE Trans. Syst., Man, Cybernetics: Syst., vol. 44, no. 3, pp. 385-395, 2014.

[168] Mokni R., Hassen D., and Monji K., “Combining shape analysis and texture pattern for palmprint identification,” Multimed. Tools Appl., vol. 76, pp. 23981–24008, 2017.

[169] Liao S., Law M., and Chung A., “Dominant local binary patterns for texture classification,” IEEE Trans. Image Process., vol. 18, no. 5, pp. 1107–1118, 2009.

[170] Ojala T., Pietikainen M., and Maenpaa T., “Multiresolution gray-scale and rotation invariant texture classification with local binary patterns,” IEEE. Trans. Pattern Anal. Mach. Intell., vol. 24, no. 7, pp. 971–987, 2002.

[171] Guo Z., Zhang L., and Zhang D., “A completed modeling of local binary pattern operator for texture classification,” IEEE Trans. Image Process., vol. 19, no. 6, pp. 1657–1663, 2010.

[172] Ukil A., Shah V.H., and Deck B., “Fast computation of arctangent functions for embedded applications: a comparative analysis,” IEEE International Symposium on Industrial Electronics, pp. 1206–1211, 2011.

[173] Huang T., Burnett J., and Deczky A., “The importance of phase in image processing filters,” IEEE Trans. Acoust. Speech Signal Process., vol. 23, no. 6, pp. 529–542, 1975.

[174] Oppenheim A.V., and Lim J.S., “The importance of phase in signals,” Proc. IEEE, vol. 69, no. 5, pp. 529–541, 1981.

[175] Kwak K.S. C., and Ventura J. A., “A neural network approach for defect identification and classification on leather fabric,” J. Intell. Manuf., vol. 11, no. 4, pp. 4 85–499, 2000.

[176] Wei P., Liu C., Liu M., and Gao Y. et al., “CNN-based reference comparison method for classifying bare PCB defects,” J. Eng., vol. 16, pp. 1528–1533, 2018.

[177] Liu F., Su L., Fan M., and Yin J. et al., “Using scanning acoustic microscopy and LM-BP algorithm for defect inspection of micro solder bumps,” Microelectron Reliab., vol. 79, pp. 166–174, 2017.

[178] Al-Nima R.R.O., Dlay S. S., and Woo W.L. et al., “A novel biometric approach to generate ROC curve from the probabilistic neural network,” 24th Signal Processing and Communication Application Conference, SIU, pp. 141–144, 2016.

[179] Tarawneh A. S., Chetverikov D., and Hassanat A. B., “Pilot comparative study of different deep features for palmprint identification in low-quality images,” https://arxiv.org/abs/1804.04602, 2018.

[180] Tabejamaat M., and Mousavi A., “Concavityorientation coding for palm print recognition,” Multimed Tools Appl., vol. 76, no. 7, pp. 9387-9403, 2017.

[181] Wang Z., Fan B., and Wu F., “Local intensity order pattern for feature description,” Proc. IEEE ICCV, pp. 603–610, 2011.

[182] Mehta R., and Egiazarian K., “Dominant rotated local binary patterns (DRLBP) for texture classification,” Pattern Recognit. Lett., vol. 71, pp. 16–22, 2016.

[183] Wang X., Girshick R. B., Gupta A., and He K., “Non-local neural networks,” IEEE CVPR, pp. 7794–7803, 2018.

[184] Fernández A., Álvarez M. X., and Bianconi F., “Texture description through histograms of equivalent patterns,” J. Math. Imag. Vis., vol. 45, no. 1, pp. 76–102, 2013.

[185] Song T., Li H., and Meng F. et al., “Noiserobust texture description using local contrast patterns via global measures, IEEE Signal Process. Lett., vol. 21, no. 1, pp. 93–96, 2014.

[186] Buades A., Coll B., and Morel J.-M., “A non-local algorithm for image denoising,” IEEE Comput. Soc. Conf. Comput. Vis. Pattern Recognit. (CVPR), pp. 60–65, 2005.

[187] Fan B., Wu F., and Hu Z., “Aggregating gradient distributions into intensity orders: A novel local image descriptor,” IEEE CVPR, pp. 2377–2384, 2011.

[188] Chakraborty S., Singh S. K., and Chakraborty P., “Local gradient Hexa pattern: A descriptor for face recognition and retrieval,” IEEE Trans Circuits Syst. Video Technol., vol. 28, no. 1, pp. 171–180, 2018.

[189] Wang X., Gong H., Zhang H., and Li B. et al., “Palmprint identification using boosting local binary pattern,” IEEE Int. Conf. Pattern Recognition, vol. 3, pp. 503–506, 2016.

[190] Jabid T., Kabir M.H., and Chae O., “Robust facial expression recognition based on local directional pattern,” ETRI J., vol. 32, no. 5, pp. 784–794, 2010.

[191] ISO/IEC JTC1 SC27 security techniques, ISO/IEC 24745:2011 Information Technology - Security Techniques - Biometric Information Protection, ISO, 2011.

[192] Donahue, and Jeff et al., “Decaf: A deep convolutional activation feature for generic visual recognition,” International conference on machine learning, 2014.

[193] Oquab, and Maxime et al., “Learning and transferring mid-level image representations using convolutional neural networks,” IEEE conference on computer vision and pattern recognition, 2014.

[194] Krizhevsky, Alex, Ilya S., and Geoffrey E. H., “Imagenet classification with deep convolutional neural networks,” Advances in neural information processing systems, 2012.

[195] Liu, Shuying, and Weihong D., “Very deep convolutional neural network-based image classification using small training sample size,” Asian conference on pattern recognition (ACPR), 2015.

[196] Russakovsky, and Olga et al., “Imagenet large scale visual recognition challenge,” International journal of computer vision, vol. 115, no. 3, pp. 211-252, 2015.

[197] Kingma, Diederik P., and Jimmy B., “Adam: A method for stochastic optimization,” vol. 1412, 2014.

[198] Duchi, John, Elad H., and Yoram S., “Adaptive subgradient methods for online learning and stochastic optimization,” Journal of machine learning research, vol. 12, no. 7, pp. 2121-2159, 2011.

[199] Tieleman, Tijmen, and Geoffrey H., “Lecture 6.5-rmsprop: Divide the gradient by a running average of its recent magnitude,” COURSERA: Neural networks for machine learning, vol. 4, no. 2, pp. 26-31, 2012.

[200] Heusel, and Martin et al., “Gans trained by a two time-scale update rule converge to a local nash equilibrium,” Advances in neural information processing systems, 2017.

[201] Srivastava, and Nitish et al., “Dropout: a simple way to prevent neural networks from overfitting,” Journal of machine learning research, vol. 15, no. 1, pp. 1929-1958, 2014.

[202] Ioffe, Sergey, and Christian S., “Batch normalization: Accelerating deep network training by reducing internal covariate shift,” 2015. arXiv preprint arXiv:, 2015, 1502.03167.

[203] Harkeerat K., and Pritee K., “Random Slope method for generation of cancelable biometric features,” Pattern Recognition Letters, vol. 126, pp. 31–40, 2019.

[204] Schneier, Bruce, and Schneier, “On security: cryptanalysis of SHA-1,” Schneier.com, 2005.

[205] Sotirov, and Alexander et al., “MD5 considered harmful today, creating a rogue CA certificate,” 25th Annual Chaos Communication Congress, 2008.

[206] National Institute of Standards and Technology, C. O. R. P. O. R. A. T. E, Federal Information Processing Standards publication, 180 (1993 May 11) specifications for the Secure Hash Standard (SHS), Building in big brother: the cryptographic policy debate. pp. 87-92, 1995.

[207] Bertoni, and Guido et al., “Sponge functions,” Ecrypt Hash Workshop, 2007.

[208] Cappelli R., Ferrara M., and Maltoni D., “Minutia cylinder-code: a new representation and matching technique for fingerprint recognition,” IEEE Trans. Pattern Anal. Mach. Intell., vol. 32, no. 21, pp. 28–41, 2010.

[209] Cho S., and Teoh A. B., “Face template protection via random permutation maxout transform,” Proceedings of Biometrics Engineering and Application, ACM, pp. 21–27, 2017.

[210] Maiorana E., Campisi P., and Neri A., “Bioconvolving: cancelable templates for a multi-biometrics signature recognition system,” IEEE Systems Conference (SysCon), pp. 495–500, 2011.

Candidate's Biography

Poonam Poonia is a PhD scholar of the Birla Institute of Technology and Science, India. She received her M. tech degree from the Dr B. R. Ambedkar National Institute of Technology, India. She obtained her bachelor's degree in Electronics and Communication Engineering from University of Rajasthan, India. Her research interests are biometrics, image processing and signal processing.

Supervisor's Biography

Pawan K. Ajmera is an assistant professor in EEE Department at Birla Institute of Technology and Science, Pilani, India. He received his PhD degree from the Swami Ramanand Teerth Marathwada University, India. His research interest includes multimodal biometrics, signal processing, speech processing and artificial intelligence. He has published many papers in journal of international repute. He is having more than a decade experience in teaching engineering subject at premier institutes of India.